

UNIVERSIDADE CATÓLICA DE BRASÍLIA

PRÓ-REITORIA DE PÓS-GRADUAÇÃO E PESQUISA
STRICTU SENSU EM CIÊNCIAS GENÔMICAS E
BIOTECNOLOGIA

Doutorado

**EFEITO DE MATERIAIS E SUPERFÍCIES NANO-
ESTRUTURADAS EM IMPLANTES OSSEOINTEGRADOS NA
EXPRESSÃO DE GENES DA CASCATA DE
DIFERENCIAÇÃO DE OSTEÓBLASTOS**

Autor: Gustavo Mendonça
Orientador: Prof. Dr. Francisco José Lima Aragão
Co-orientador: Prof. Dr. Lyndon Frederick Cooper

Livros Grátis

<http://www.livrosgratis.com.br>

Milhares de livros grátis para download.

GUSTAVO MENDONÇA

**EFEITO DE MATERIAIS E SUPERFÍCIES NANO-ESTRUTURADAS EM
IMPLANTES OSSEOINTEGRADOS NA EXPRESSÃO DE GENES DA CASCATA
DE DIFERENCIAÇÃO DE OSTEÓBLASTOS**

Tese apresentada ao Programa de Pós-graduação Strictu Sensu em Ciências Genômicas e Biotecnologia da Universidade Católica de Brasília como requisito para obtenção do Título de Doutor em Ciências Genômicas e Biotecnologia.

Orientador: Prof. Dr. Francisco José Lima Aragão.

Co-orientador: Prof. Dr. Lyndon Frederick Cooper.

**Brasília
2008**

M539e Mendonça, Gustavo.

Efeito de materiais e superfícies nano-estruturadas em implantes osseointegrados na expressão de genes da cascata de diferenciação de osteoblastos / Gustavo Mendonça. – 2008.

132 f.: il. ; 30 cm.

Tese (doutorado) – Universidade Católica de Brasília, 2008.

Orientação: Francisco José Lima Aragão.

Co-orientação: Lyndon Frederick Cooper.

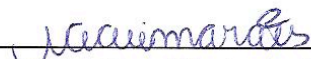
1. Nanotecnologia. 2. Implantes dentários. 3. Tratamento de superfícies (Odontologia). 4. Ossos – Regeneração. I. Aragão, Francisco José Lima, orient. II. Cooper, Lyndon Frederick, co-orient. III. Título.

CDU 620.3:616.314

Tese de autoria de Gustavo Mendonça, intitulada “EFEITO DE MATERIAIS E SUPERFÍCIES NANO-ESTRUTURADAS EM IMPLANTES OSSEOINTEGRADOS NA EXPRESSÃO DE GENES DA CASCATA DE DIFERENCIAÇÃO DE OSTEÓBLASTOS”, apresentada como requisito parcial para obtenção do Título de Doutor em Ciências Genômicas e Biotecnologia da Universidade Católica de Brasília, em 19 de dezembro de 2008, defendida e aprovada pela banca examinadora abaixo assinada:



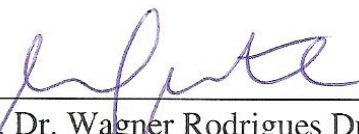
Prof. Dr. Francisco José Lima Aragão
Orientador
Ciências Genômicas e Biotecnologia – UCB



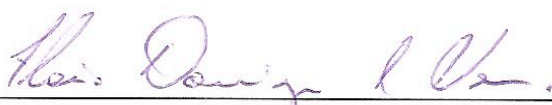
Profa. Dra. Maria do Carmo Machado Guimarães
Curso de Odontologia – UCB



Prof. Dr. Rinaldo Wellerson Pereira
Ciências Genômicas e Biotecnologia – UCB



Prof. Dr. Wagner Rodrigues Duarte
EBO / São Leopoldo Mandic – Brasília



Prof. Dr. Flávio Domingues das Neves
Reabilitação Oral – UFU

A Deus,
Pelo dom da vida, pela minha família e por todos os momentos que me proporcionou.

À Daniela pelo carinho, dedicação e amor que garantiu que esta etapa fosse cumprida, e por todos os momentos que compartilhamos juntos.

Aos meus pais Militão e Necilde, a quem devo tudo o que sou, agradeço pelo incentivo, educação, paciência e sabedoria que me passaram.

Aos meus irmãos Renato e Fabiana, por todos os momentos que passamos juntos.

AGRADECIMENTO ESPECIAL

Aos meus Orientadores, Prof. Dr. Francisco José Lima Aragão e Prof. Dr. Lyndon Frederick Cooper, por terem aberto as portas de seus laboratórios, pelos momentos de dedicação e incentivo e permitirem que este trabalho fosse realizado sob sua orientação e supervisão.

Aos membros de minha família Dr. José Otaviano de Mendonça *“in memoriam”*, Dra. Maria Bernadete Mendonça Rodrigues e Dr. Paulino José de Mendonça *“in memoriam”* que como Cirurgiões-dentistas muito me inspiraram na escolha de minha profissão e também tiveram uma grande influência em minha trajetória até aqui.

AGRADECIMENTOS

À Universidade Católica de Brasília.

À Embrapa Recursos Genéticos e Biotecnologia.

À Universidade da Carolina do Norte.

Aos docentes do Curso de Odontologia da Universidade Católica de Brasília, especialmente aos colegas Luciana, Maurício, Mikaela e Ramos das disciplinas de Oclusão e Prótese.

Aos Professores Doutores Sérgio de Freitas Pedrosa e Daniel Rey de Carvalho, que como diretores do Curso de Odontologia da Universidade Católica de Brasília tornaram possível o cumprimento de minhas atividades como docente do Curso de Odontologia e aluno do Programa de pós-graduação em Ciências Genômicas e Biotecnologia da UCB.

Aos Professor Doutor Ruy Caldas, diretor do Programa de Pós-graduação em Ciências Genômicas e Biotecnologia da Universidade Católica de Brasília, por sempre ter nos ajudado durante todo o desenvolvimento do doutorado.

Aos docentes do Programa de Pós-graduação em Ciências Genômicas e Biotecnologia da Universidade Católica de Brasília, especialmente à Prof. Danielle de Moura Cordeiro.

À Coordenação de Aperfeiçoamento de Pessoal de Nível Superior – CAPES – pela bolsa de doutorado Sandwich que me permitiu expandir meus conhecimentos e vivenciar uma nova experiência na Universidade da Carolina do Norte em Chapel Hill-EUA.

Aos docentes do departamento de Oclusão e Prótese Fixa da Universidade Federal de Uberlândia, especialmente aos Professores Doutor Alfredo Júlio Fernandes Neto e Doutor Flávio Domingues Neves que tiveram um papel muito importante durante a minha formação acadêmica.

Ao Conselho Nacional de Pesquisa – CNPq - pela bolsa de pesquisa do Edital Universal, que permitiu o desenvolvimento deste trabalho.

Aos docentes do departamento de Prótese da Faculdade de Odontologia da Universidade da Carolina do Norte, especialmente à Profa. Ingeborg De Kok e Prof. Sompop Bencharit pela atenção e respeito dedicado durante nossa estadia na UNC.

Ao amigo Prof. Dr. Wagner Rodrigues Duarte que muito me ajudou no desenvolver desta pesquisa.

Ao Prof. Dr. Edson Roberto Leite e aos alunos Luis Gustavo Pagotto Simões, André Luis Araújo do programa de pós-graduação do LIEC - Laboratório Interdisciplinar de Eletroquímica e Cerâmica da Universidade Federal de São Carlos no desenvolvimento dos materiais utilizados nesta pesquisa.

Aos amigos de pós-graduação pelos momentos que passamos juntos e aprendemos uns com os outros.

Aos amigos do Laboratório de Transferência de Genes da Embrapa Recursos Genéticos e Biotecnologia (Embrapa-Cenargen), especialmente à Elsa.

Aos funcionários do Programa de Pós-graduação em Ciências Genômicas e Biotecnologia da Universidade Católica de Brasília, especialmente ao Francisco Fábio Gomes da Costa.

Aos funcionários do Curso de Odontologia da Universidade Católica de Brasília, especialmente a Sylvania e Lucélia.

À Fernanda Beatriz Scalabrin, técnica responsável pelo Laboratório de Cirurgia e Fisiologia Experimental onde realizamos as cirurgias em nossos honrados pacientes (*Ratus norvegicus*).

À Sara Valencia, responsável pelo andamento de todas as atividades no Laboratório de Biologia Óssea e Mineralização da Universidade da Carolina do Norte, e que muito ajudou para que nossos trabalhos no laboratório funcionassem perfeitamente.

À Gidget Jenkins e Martha Taylor do departamento de Prótese da Faculdade de Odontologia da Universidade da Carolina do Norte, por também nos ajudarem em tudo que fosse necessário durante nossa estadia nos Estados Unidos.

À Wallace Ambrose “Research Specialist” do “Dental Research Center” Faculdade de Odontologia da Universidade da Carolina do Norte que ajudou no preparo e análise das amostras para microscopia eletrônica de varredura e histologia.

À Carrie Donley diretora do Chapel Hill Analytical & Nanofabrication Laboratory (CHANL), Instrumentation Facility Institute for Advanced Materials, NanoScience and Technology da Universidade da Carolina do Norte, por disponibilizar a utilização e análise das amostras no microscópio eletrônico de varredura.

Aos amigos que fizemos na Universidade da Carolina do Norte, Gustavo e Grace, Ricardo e Patrícia, Sodsi “Nid” Wirojchanasak e também aos Residentes do Programa de Pós-graduação em prótese Kuang-Han Chang, Juan Li Guo, Ibrahim Duqum, Sorin Uram-Tuculescu, Deepali Jere, Ghadeer Thalji, Carolina Vera-Resendiz, Ming-Yi Chou, Matthew Bryington, Kathryn Conard, William Gates.

À Empresa Neodent Implantes Osseointegrados, pelo apoio no desenvolvimento desta pesquisa e pelo fornecimento dos materiais necessários.

A minha segunda família Mac Tulio e Maria Inez, e também Bruno, Juliana e Flávio, por me acolherem e permitirem que eu trouxesse a Daniela para longe deles e junto comigo em todo o decorrer desta etapa.

A todos os membros de minha família que sempre me apoiaram e cujo exemplos e incentivos também me permitiram chegar até este momento de minha profissão.

A todos que direta ou indiretamente me ajudaram durante todo o decorrer de minha pós-graduação e que permitiram que eu cumprisse mais esta etapa.

RESUMO

MENDONÇA, Gustavo. **Efeito de materiais e superfícies nano-estruturadas em implantes osseointegrados na expressão de genes da cascata de diferenciação de osteoblastos**. 2008. 132p. Tese. Ciências Genômicas e Biotecnologia – Universidade Católica de Brasília, Brasília, 2008

As tendências atuais na terapia com implantes odontológicos têm incluído o uso de implantes com superfícies modificadas utilizando nanotecnologia. Ciência que permite a construção de novos materiais e dispositivos pela manipulação de átomos individuais e moléculas (escala menor do que 100nm). O objetivo deste trabalho foi revisar e avaliar o papel das modificações em escala nanométrica de superfícies de implantes osseointegrados para melhorar o processo de osseointegração. Nanotecnologia oferece a engenheiros e profissionais da área de biologia e saúde novos meios para entender e melhorar funções específicas das células. As várias técnicas utilizadas para adicionar características nanométricas às superfícies de implantes osseointegrados são descritas neste trabalho. Vários trabalhos tem apresentado os efeitos da nanotecnologia na modulação de etapas fundamentais do processo de osseointegração. As vantagens e desvantagens da utilização da nanotecnologia na superfície de implantes também são discutidas nesse trabalho. Posteriormente, em uma série de experimentos *in vitro* e *in vivo*, foi possível avaliar o efeito específico destas modificações em dois diferentes modelos. Como efeitos observados da aplicação de nanoestruturas à superfície dos implantes osseointegrados foi possível verificar-se uma melhor e mais rápida resposta de osseointegração destes materiais, atuando efetivamente na cascata de diferenciação de osteoblastos.

Palavras-chave: Nanotecnologia; Nanotopografia; Implante Dental; Tratamento de Superfície; Regeneração Óssea, Sinalização Celular

ABSTRACT

Current trends in clinical dental implant therapy include use of endosseous dental implant surfaces embellished with nanoscale topographies. Nanotechnology deals with materials with at least one significant dimension less than 100nm. The goal of this study was to consider the role of nanoscale topographic modification of titanium substrates for the purpose of improving osseointegration. Nanotechnology offers engineers and biologists new ways of interacting with relevant biological processes. Moreover, nanotechnology has provided means of understanding and achieving cell specific functions. The various techniques that can impart nanoscale topographic features to titanium endosseous implants are described. Existing data supporting the role of nanotopography suggests that critical steps in osseointegration can be modulated by nanoscale modification of the implant surface. Important distinctions between nanoscale and micron-scale modification of the implant surface are presently considered. The advantages and disadvantages of nanoscale modification of the dental implant surface are discussed. Finally, available data concerning the current dental implant surfaces that utilize nanotopography in clinical dentistry are described. Nanoscale modification of titanium endosseous implant surfaces can alter cellular and tissue responses that may benefit osseointegration and dental implant therapy. In a series of *in vitro* and *in vivo* experiments it was possible to evaluate the effect of this modifications in different study designs. The advantages of the use of nanocues added to the surface of the osseointegrated dental implants allowed to a better and faster osseointegration response of these materials, by acting on the differentiation of the osteoblasts.

Key-words: Nanotopography; Nanotechnology; Dental Implant; Surface Treatment; Bone Regeneration; Cell Signaling.

LISTA DE ABREVIATURAS

ALP – Alkaline phosphatase – Fosfatase alcalina

AFM – Atomic Force Microscope – Microscópio de Força Atômica

BMP – Bone morphogenetic protein – Proteína morfogenética óssea

BSP – Bone sialoprotein – Sialoproteína óssea

EDS/EDX – X-Ray Micro Analysis – Micro-análise de Raios X

mm – milímetro

nm - nanometro

Ncm – Newton centímetro

OCN – Osteocalcina

OPN – Osteopontina

OSX – Osterix

Runx2/CBFA1 – Core binding factor α 1

SEM – Scanning Electron Microscope – Microscópio Eletrônico de Varredura

XPS - X-Ray Photoelectron Spectrometer – Espectrometro de fotoeletron de Raio X

μ m – micrômetro

SUMÁRIO

	Resumo	
	Abstract	
	Lista de Abreviaturas	
Capítulo 1	Introdução	11
Capítulo 2	Artigo 1 – Tecnologia Avançada na Superfície de Implantes Dentários – da micro para a nanotopografia	20
Capítulo 3	Artigo 2 – Efeito do Recobrimento da Superfície de Implante com Alumina Nanoestruturada na Expressão de Genes Relacionados a Osteoblastos e no Contato Osso-Implante <i>in vivo</i>	46
Capítulo 4	Artigo 3 – Efeito da Superfície de Implante Nanoestruturada na Expressão de Genes Relacionados à diferenciação de Osteoblastos e no Contato Osso-Implante <i>in vivo</i>	63
Capítulo 5	Artigo 4 – Nanoestruturas na Superfície de Implantes Alteram a Expressão Gênica em Osteoblastos	78
Capítulo 6	Artigo 5 – Tratamento com H ₂ SO ₄ / H ₂ O ₂ Adiciona Nanoestruturas à Superfície de Implantes e Melhora a Expressão Gênica Específica de Osteoblastos	96
Capítulo 7	Discussão Geral	111
	Referências Bibliográficas	117

Capítulo 1 - Introdução

A nanotecnologia é a aplicação de ciência e engenharia em escala atômica. Ela facilita a construção de novos materiais e dispositivos pela manipulação de átomos individuais e moléculas. A nanotecnologia permite a construção átomo por átomo de minúsculas estruturas (tipicamente 1 – 100nm), as quais têm novas propriedades e grandes aplicações nas ciências da saúde e biotecnologia. Nos implantes osseointegrados o desenvolvimento de superfícies nano-estruturadas poderia aumentar consideravelmente a adesão de células ósseas e também a produção de matriz óssea necessária no processo de mineralização e manutenção do osso que circundará este implante (Gutwein; Webster, 2004; Oh et al., 2005; Price et al., 2003a; Price et al., 2003b; Webster et al., 1999; Webster et al., 2000a; Webster et al., 2001; Webster; Ejiófor, 2004; Webster et al., 2005). Até o presente momento, embora se tenha conhecimento sobre as vantagens das superfícies nano-estruturadas, poucos sistemas de implantes dentários osseointegrados disponíveis comercialmente no mercado tem utilizado essa tecnologia na elaboração de seus produtos (Guo et al., 2007; Mendes et al., 2007).

1.1. Trabalhos de longevidade dos implantes osseointegrados

Nas últimas décadas, tem-se assistido à conquista de um espaço, por parte da implantodontia, no contexto geral da odontologia. Isto se deve ao grande número de dentes perdidos, por cárie, periodontopatias e traumas, além é claro da previsibilidade alcançados por estes tratamentos. A busca de uma prótese que substituísse não só os dentes mas também suas raízes, dando ao paciente maior estabilidade e conforto, sempre foi motivo de trabalhos de implantação, podendo ser observado relatos. Entretanto, o reconhecimento só veio a ocorrer a partir do início dos anos 80, com o aparecimento dos denominados implantes osseointegrados. Até então os trabalhos de longevidade feitos com implantes, mostravam um tratamento cujo sucesso era pouco previsível e os insucessos, seguidos de perda óssea às vezes severa e infecções constantes. Os implantes, tipo parafuso endósseo, agulhados, laminados e sub-periostais, foram os responsáveis pela baixa credibilidade e constantes fracassos na área. Kapur, 1989 e 1991 mostrou em acompanhamento de 5 anos, insucessos de mais de 50%.

Em 1981, Adell et al. apresentaram acompanhamento longitudinal de quinze anos (1965-1980), após exames anuais. Um total de 2.768 implantes Brånemark System instalados em 371 pacientes desdentados. Na maxila, 81% dos implantes e 91% na mandíbula, permaneceram estáveis por um período de cinco a nove anos. A estabilidade

das próteses foi de 89% na maxila e 100% na mandíbula. Observou-se uma perda óssea durante o primeiro ano de uso da prótese da ordem de 1,2mm. Nos anos seguintes, a perda estabilizou-se e foi da ordem de 0,1mm ao ano. Os tecidos moles em torno das fixações mostraram-se clinicamente saudáveis. Concluíram que os resultados clínicos apresentados pelas próteses sobre implantes osseointegrados, preenchem os critérios empregados na avaliação e determinação do sucesso destes implantes, ficando até acima dos mesmos. Em 1986, Albrektsson et al. propuseram critérios para avaliação do sucesso dos implantes. Estes são usados na avaliação da eficácia a longo prazo dos implantes utilizados, incluindo os implantes sub-periosteos, implante de carbono vítreo, implante TCP, parafuso TPS, ITI, IMZ, Core-Vent, implante mandibular trans-ósseo e os implantes osseointegrados Brånemark. Os critérios descritos foram: ausência de mobilidade clínica do implante, quando testado individualmente; ausência de zona radiolúcida ao exame radiográfico; perda óssea vertical anual menor que 0,2mm, após o primeiro ano de função; ausência de sinais e sintomas persistentes e/ou irreversíveis de dor, infecção, neuropatias, parestesia ou violação do canal mandibular; e baseado neste contexto, uma taxa de sucesso de 85% ao final de cinco anos e de 80% após dez anos. Concluíram que se um sistema de implante cumprir estes cinco critérios proverá uma ancoragem previsível para reabilitação em ambos os arcos dentários.

Albrektsson et al. (1988) relataram os trabalhos de 14 centros fora da Universidade de Gotemburgo, cada um com no mínimo três anos de experiência em implantes Nobelpharma, participando de um estudo multicêntrico retrospectivo. O número de implantes instalados foi de 8139. Os resultados de cada implante foram relatados e todas as falhas, independente de quando ocorreram, foram publicadas. Foram seguidos os critérios de sucesso citados por Albrektsson et al. (1986). Na mandíbula, 334 implantes que foram acompanhados por cinco a oito anos, apresentaram somente três falhas, com uma taxa de sucesso de 99,1%. Na maxila, 106 implantes foram acompanhados por cinco a sete anos, com uma taxa de sucesso de 84,9%. Em mandíbulas irradiadas e com enxerto ósseo, 56 implantes foram inseridos e nenhum perdido, durante um acompanhamento de cinco anos. Na maxila irradiada foram colocados 16 implantes com três falhas e em casos de enxerto em maxila foram colocados 71 implantes com 12 falhas. Os autores concluíram que se os implantes forem colocados seguindo corretamente o protocolo de Brånemark, resultará um alto grau de sucesso clínico.

Smith; Zarb (1989) devido a proliferação dos sistemas de implantes osseointegrados, descreveram alguns critérios para o sucesso dos implantes baseados em investigações científicas. Uma revisão da literatura e análise de resultados indicaram que seis critérios são

válidos para determinar o sucesso clínico destes implantes: o implante deve estar imóvel quando avaliado individualmente; não haver radioluscência ao redor do implante; a perda óssea média vertical anual não deve ser maior que 0,2 mm após o primeiro ano de função; ausência de dor, desconforto ou infecção freqüente na região do implante; o tratamento final não deve comprometer a estética; por estes critérios, uma taxa de sucesso de 85% após 5 anos e 80% para 10 anos de observação são os níveis mínimos aceitáveis para o sucesso do tratamento com implantes osseointegrados.

Donlay; Gillette (1991) realizaram uma revisão da literatura sobre a anatomia do periodonto normal e ao redor de implantes. São apresentados os possíveis mecanismos de formação de ligação de células e o efeito das propriedades das superfícies dos implantes. Uma ligação química entre a superfície oxidada do titânio e o epitélio tem sido demonstrado “*in vitro*” e “*in vivo*”. Esta ligação é mediada por uma glicoproteína similar àquela encontrada entre o epitélio e as superfícies dos dentes naturais. Enquanto existem apenas mínimas evidências histológicas naturais, fibras do tecido conjuntivo próximos à superfície do implante podem manter o tecido em aposição justa contra o implante, sem uma absoluta ligação biológica entre o implante e o tecido conjuntivo. Um melhor entendimento dos mecanismos de ligação e dos fatores que aumentam a integridade do selamento biológico entre o implante e os tecidos moles devem permitir um prognóstico melhorado para o funcionamento dos implantes de titânio.

Callan; O’Mahonry; Cobb (1998) relataram que a perda de crista óssea associada com implantes dentários é um fenômeno clínico importante. A ocorrência de tal perda óssea comprometeria o tempo de prognóstico, se extensa, essencialmente levaria à falha. Relativamente poucos estudos têm focalizado as razões da perda de crista óssea em volta dos implantes, embora numerosas explicações para o fenômeno têm sido propostas. Estas investigações retrospectivas examinam o fator causador possível para perdas de crista óssea associada com implante, as quais apenas recentemente têm recebido atenção. A localização da interface implante/intermediário e sua relação com a crista óssea têm fundamental importância nesse sentido. Uma avaliação clínica de 350 implantes individuais em 255 pacientes, indicou o relacionamento direto entre a colocação sub-gengival da interface e a perda de crista óssea. Além do mais, o exame de microscopia eletrônica de 45 falhas de implante mostraram significativo acúmulo de placa na interface implante/intermediário, na interface intermediário/prótese e na interface entre o “colarinho plano, liso,” do implante e uma cobertura pulverizada de plasma na superfície subjacente.

Mendonça et al. (2001) relataram os problemas que ocorreram com pacientes que receberam próteses sobre implantes, buscando determinar as causas e a prevalência destas falhas e insucessos, bem como as melhores formas de tratamento e soluções para estes problemas, realizando um acompanhamento dos pacientes que receberam implantes nos cursos de Aperfeiçoamento em Implantes Odontológicos do Departamento de Reabilitação Oral da Universidade Federal de Uberlândia. Foram acompanhados 86 pacientes que receberam 209 implantes para tratamento de casos totais, parciais e individuais entre os anos de 1996 e 1997 e utilizaram suas próteses por pelo menos um ano. As dificuldades encontradas foram: desaperto e fratura do parafuso de ouro, desaperto do parafuso do intermediário, fratura da porcelana, prótese mal adaptada, adaptação não-passiva, peri-implantite e insatisfação do paciente. Estes problemas foram de pequena incidência, muitos ocorrendo em um mesmo paciente. Quanto aos insucessos, atingiram para os implantes o índice de 3,8% e para as próteses o de 5,2%. Uma análise destes problemas permitiu concluir que um adequado domínio da técnica, bem como uma avaliação dos procedimentos realizados reduziria ainda mais estas complicações, melhorando os resultados obtidos. Comprovando assim, a efetividade e previsibilidade dos implantes osseointegrados.

Um alto índice de falhas nos processo de osseointegração podem ser atribuídas a condições locais, condições biológicas, sistêmicas ou fatores funcionais (Adell et al., 1981; Zarb; Schmitt, 1990). Um controle clínico de todos esses fatores é representado por um plano de tratamento multidisciplinar. Entretanto, é também sabido que estes fatores, bem como fatores relacionados ao profissional são importantes determinantes do sucesso de implantes osseointegrados. Um grande interesse no desenho de implantes tem sido evidente e esforços clínicos para melhorar estes índices de sucesso tem sido direcionados em aumentar a quantidade de tecido ósseo que se forma na interface osso-implante.

1.2. A nanotecnologia melhorando a osseointegração

A nanotecnologia envolve um sistema nos quais os materiais estão em tamanhos na faixa de nanômetros (10^{-9} m) e apresenta a sua utilização na reposição de órgãos e na prevenção e cura de doenças. Embora muitas definições estejam ligadas ao termo “nanomaterial”, esta definição está relacionada aos materiais com topografia com tamanho variando de 1 a 100nm (nano-estruturado), e de acordo com a forma pode ser dividido em sólidos cristalinos com o tamanho dos grãos variando de 1 a 100nm (nanocristais), camadas superficiais únicas ou múltiplas com espessura de 1 a 10nm (nanorevestimentos), pós extremamente finos com partículas variando de 1 a 100nm (nanopós) e fibras também com diâmetro na faixa de 1 a 100nm (nanofibras).

Devido ao fato de também na natureza serem encontradas várias estruturas na escala nanométrica, inclusive no corpo humano (Ayad et al., 1994), é que a nanotecnologia se torna tão importante em termos biológicos. O tecido ósseo é composto de numerosos materiais como colágeno e hidroxiapatita, que se encontram em escala nanométrica, e provem uma adequada estrutura para a interação celular. Embora a confecção de materiais para substituir osso e partes perdidas do corpo não seja recente, a utilização de materiais nano-estruturados em relação aos materiais convencionais é relativamente nova e recente por apresentarem melhores propriedades superficiais (quando comparados aos convencionais) (Klabunde et al., 1996; Wu; DeJong; Rahaman, 1996; Baraton; Chen; Gonçalves, 1997). Por exemplo, um nanomaterial tem um aumento do número de átomos na superfície, partículas na superfície, porosidades nas superfícies, uma maior área de superfície e uma alteração na distribuição de elétrons se comparados aos materiais convencionais, fazendo com que fiquem mais reativos que os materiais convencionais. Os materiais nanoestruturados utilizados em engenharia tecidual podem ser classificados em cerâmicos, metálicos, polímeros e materiais compostos, e cada tipo de material apresenta características distintas e aplicações diferentes.

Em 1999, Webster; Siegel; Bizios demonstraram um aumento da adesão de osteoblastos sobre uma camada de óxido de alumínio (Al_2O_3) e óxido de titânio (TiO_2) em nanopartículas. O tamanho dos grãos era de 23nm para a alumina e 32nm para o óxido de titânio, comparado ao tamanho convencional da alumina (177nm) e óxido de titânio (2,12 μm). Houve um aumento de 46 e 30% na adesão celular à alumina e ao óxido de titânio nanoestruturados, respectivamente após 4 horas, quando comparados aos materiais com partículas convencionais. Este estudo apresentou evidências da capacidade de simular características biológicas de adsorção de proteína e bioatividade das partículas nano-estruturadas de alumina e óxido de titânio.

Webster et al. (2000a) analisaram funções específicas de osteoblastos cultivados sobre superfícies nano-estruturadas de alumina, óxido de titânio e hidroxiapatita, comparadas com os mesmos materiais em tamanhos convencionais. Os autores concluíram que a proliferação dos osteoblastos foi maior em todos os materiais quando apresentavam-se em escala nanométrica quando comparados aos convencionais após três e cinco dias. A síntese de fosfatase alcalina e a deposição de matriz mineral foram significativamente maior nos materiais nano-estruturados do que nos convencionais após 21 e com 28 dias a síntese de fosfatase alcalina foi 36, 22 e 37% maior para alumina, óxido de titânio e hidroxiapatita, respectivamente, quando comparado aos materiais convencionais. O conteúdo de cálcio na

matriz extracelular com 28 dias foi 4, 6 e 2 vezes maior para a alumina, óxido de titânio e hidroxiapatita, respectivamente, quando comparados com os materiais convencionais.

O aumento da adesão de células ósseas em materiais nano-estruturados é também seguido por uma diminuição da afinidade de fibroblastos pela superfície destes materiais (Webster et al., 2000b). Os autores observaram uma redução da afinidade de fibroblastos de 3 para 1 quando comparado com osteoblastos na superfície de alumina. Na superfície convencional a relação entre osteoblastos e fibroblastos foi de 1 para 1.

A função de outros tipos celulares também é importante na remodelação óssea e foi avaliada por Webster et al. (2001). Foi observado um aumento da função osteoclástica medida pela produção de fosfatase ácida resistente a tartaratos (TRAP) e pela formação de poços de reabsorção sobre as superfícies revestidas com alumina, óxido de titânio ou hidroxiapatita. A produção da fosfatase ácida foi mais de duas vezes maior sobre a nanosuperfície do que sobre a superfície convencional de hidroxiapatita. Esta atividade osteoclástica também é importante para a remodelação do tecido ósseo, podendo ser responsável pela manutenção da osseointegração a longo prazo.

Nanotubos de carbono também foram avaliados quanto a sua capacidade de promover adesão de vários tipos celulares (Price et al., 2003a). Tais nanotubos apresentam um aumento significativo na resistência além de possuir a vantagem de serem nanométricos. Quanto a adesão celular foi observado que este material apresentou uma afinidade aumentada para osteoblastos, ao passo que diminuiu a afinidade para fibroblastos, células musculares e condrócitos, tanto na forma de nanotubos de carbono quanto como um composto de policarbonato uretano / nanotubos de carbono.

A modificação da nano-estrutura da alumina também influenciou na adesão de células ósseas. Foi observado um aumento de duas vezes na adesão de osteoblastos apenas modificando a forma da estrutura de alumina de nanopartículas para nanofibras. Demonstrando que não somente o tamanho do material pode ser importante, mas também a forma que ele apresenta para uma melhor relação com as proteínas que irão permitir a adesão celular (Price et al., 2003b).

Outros metais também demonstraram aumentar a adesão celular quando em sua nanofase. Webster; Ejiófor (2004) estudaram a adesão celular sobre metais como Titânio, Ti6Al4V e CoCrMo e observaram um aumento desta adesão nestes metais quando em nanofase ao serem comparados com as conformações convencionais.

A presença de partículas de alumina e óxido de titânio na viabilidade e densidade celular de osteoblastos foi comparado por Gutwein; Webster (2004). Os autores estudaram se o tamanho dessas partículas (nanopartículas ou convencionais) seriam importantes para a viabilidade das células em casos onde fragmentos da camada superficial se soltassem durante o uso ou pelo desgaste de próteses inseridas no tecido ósseo. Foram realizadas análises com cultura de células ($2500 \text{ células/cm}^2$) em um meio contendo 10.000, 1.000 ou $100 \mu\text{g/ml}$ de partículas de alumina de tamanhos convencional ou nano-estruturadas, bem com 10.000, 5.500 e $1000 \mu\text{g/ml}$ de partículas de óxido de titânio também de tamanho convencionais ou nano-estruturados. Após 2 e 6 horas foram analisadas a viabilidade e a densidade celular. Os autores concluíram que houve um melhor resultado das nanopartículas quando comparadas às partículas de tamanho convencional.

Oh et al. (2005) observaram o crescimento de cristais de hidroxiapatita sobre uma superfície de nanotubos de óxido de titânio tratada quimicamente com NaOH. Os nanotubos de óxido de titânio foram feitos por anodização e depois tratado com NaOH, e após o tratamento da superfície foram imersos em um meio semelhante ao plasma sanguíneo. Houve então a nucleação e o crescimento de nanocristais de hidroxiapatita. Foi observado que a formação dos cristais de hidroxiapatita foi acelerada pela composição nano-estruturada do óxido de titânio. No entanto, grande parte destes trabalhos ainda estão em fase experimental, não existindo no mercado odontológico um grande número de material de implantes odontológicos osseointegrados que atualmente use esta tecnologia.

1.3. Outras superfícies de implantes osseointegrados

As superfícies atuais dos implantes osseointegrados são preparadas e/ou modificadas com materiais produzidos em escala micrométrica ou sub-micrométrica (menores do que $1 \mu\text{m}$, mas acima de 100nm), e em muitos casos têm também um tratamento químico da superfície que altera suas propriedades melhorando a adesão celular (Buser et al., 2004; Ellingsen et al., 2004)

Schneider et al. (2003) demonstrou que a utilização de superfícies rugosas pode aumentar a expressão do gene Cbfa1 (regulador da diferenciação de osteoblastos e expressão de genes necessários para o desenvolvimento do fenótipo de mineralização). Neste trabalho, a expressão de Cbfa1 e BSP II foi significativamente maior em superfícies rugosas do que em superfícies com sulcos.

A modificação química da superfície do implante também aumenta a adesão celular e a osseointegração reduzindo o tamanho das porosidades e aumentando a rugosidade da superfície, entretanto, não se pode afirmar se a melhora na adesão celular é devido à rugosidade superficial ou a alguma alteração química destas superfícies. Ellingsen et al. (2004) compararam a superfície de implantes jateados com óxido de titânio e superfícies que além deste jateamento tiveram um tratamento com ácido fluorídrico e observaram uma superfície mais plana e com uma menor rugosidade superficial após o tratamento com o ácido. Esta superfície aumentou o contato osso-implante além de aumentar o torque de remoção dos implantes após três meses.

Em outro trabalho, Buser et al. (2004) também avaliaram superfícies com jateamento e ataque ácido comparadas com uma superfície que passou pelos mesmos procedimentos e foi posteriormente modificada por um procedimento comercial não descrito. Neste trabalho os autores observaram uma aposição óssea mais rápida na superfície modificada quando comparada com a convencional medida pelo contato implante-osso na segunda e quarta semana, entretanto não houveram diferenças na oitava semana.

Em 2005, Araújo et al. avaliaram a colocação de implantes em alvéolos de extração recente em cães. os autores observaram que a superfície SLA não foi capaz de impedir que houvesse uma reabsorção das tábuas ósseas vestibulares e linguais.

Baseado no fato de que as superfícies nanoestruturadas podem modular a resposta celular, a proposta deste trabalho foi desenvolver e testar uma superfície de implante osseointegrado nanoestruturada em termos de efeito na diferenciação de osteoblastos e efeito na formação da interface osso/implante e torque de remoção. Este projeto investigou a hipótese de que a superfície de um implante de TiCp recoberta com uma camada nanoestruturada altera a resposta inicial das células osteogênicas para suportar uma melhor formação óssea na interface osso/implante.

1.4. Delineamento da pesquisa

O objetivo deste trabalho foi estudar *“in vivo”* e *“in vitro”* a expressão diferencial de genes da cascata de diferenciação de osteoblastos em função de distintos materiais e superfícies encontrados nos implantes osseointegrados, com possível redução do período de osseointegração em função da interação célula-implante, baseado na hipótese de que a expressão gênica é controlada em níveis locais na superfície de implantes osseointegrados, para poder explicar os diferentes perfis histológicos de formação óssea e torque de remoção nas diferentes superfícies de implantes.

- 1.4.1.** Desenvolver e caracterizar superfícies de implantes de titânio nano-estruturadas com revestimentos a base de óxido de alumínio, óxido de titânio e óxido de zircônia (Capítulos 3,4,5 e 6);
- 1.4.2.** Comparar a expressão de genes responsáveis pela diferenciação de osteoblastos (*alp*, *bsp*, *ocn*, *opn* e *runx2*) em animais com implantes com revestimentos nano-estruturados, com os implantes de titânio comercialmente puro com superfície lisa e tratados com ataque ácido (Capítulos 4 e 5);
- 1.4.3.** Avaliar o contato implante/osso em animais com implantes com revestimentos nano-estruturados, com os implantes de titânio comercialmente puro com superfície lisa e tratados com ataque ácido, por meio de análise histomorfométrica (Capítulos 3 e 4);
- 1.4.4.** Avaliar o torque de remoção dos implantes com revestimentos nano-estruturados, comparados com os implantes de titânio comercialmente puro com superfície lisa e tratados com ataque ácido (Capítulos 3 e 4);
- 1.4.5.** Avaliar a expressão de genes responsáveis pela diferenciação de osteoblastos (*alp*, *bsp*, *ocn*, *osx*, *opn* e *runx2*) em células ósseas cultivadas sobre a superfície dos implantes com os revestimentos a base de óxido de alumínio, óxido de titânio e óxido de zircônia, e a expressão gênica em células ósseas cultivadas sobre a superfície dos implantes com os revestimentos a base de óxido de alumínio, com os implantes de titânio comercialmente puro com superfície lisa e tratados com ataque ácido, por meio de “PCR arrays” (Capítulo 5);
- 1.4.6.** Avaliar a expressão de genes responsáveis pela diferenciação de osteoblastos (*alp*, *bsp*, *ocn*, *osx*, *opn* e *runx2*) em células ósseas cultivadas sobre a superfície dos implantes nanoestruturados através de tratamento com ataque ácido, comparados com os implantes de titânio comercialmente puro com superfície lisa e jateados (Capítulo 6).

Capítulo 2 – Tecnologia Avançada na Superfície de Implantes Dentários – da micro para a nanotopografia

As tendências atuais na terapia com implantes odontológicos têm incluído o uso de implantes com superfícies modificadas utilizando nanotecnologia. O objetivo deste trabalho foi revisar e avaliar o papel das modificações em escala nanométrica de superfícies de implantes osseointegrados para melhorar o processo de osseointegração. Nanotecnologia oferece a engenheiros e profissionais da área de biologia e saúde novos meios para entender e melhorar funções específicas das células. As várias técnicas utilizadas para adicionar características nanométricas às superfícies de implantes osseointegrados são descritas neste trabalho. Vários trabalhos tem apresentado os efeitos da nanotecnologia na modulação de etapas fundamentais do processo de osseointegração. As vantagens e desvantagens da utilização da nanotecnologia na superfície de implantes também são discutidas nesse trabalho.

Esta revisão da literatura foi proposta e editada diretamente em inglês. Esta revisão está publicada com pequenas modificações no Journal of Biomaterials. Mendonça G, Mendonça DBS, Aragão FJL, Cooper LF. Advancing Dental Implant Surface Technology - From micron- to nano-topography. Biomaterials. 2008 Oct;29(28):3822-35. Este artigo é apresentado em sua versão original na seção Anexo (Artigo I).

Advancing Dental Implant Surface Technology - From micron- to nano-topography

Abstract:

Current trends in clinical dental implant therapy include use of endosseous dental implant surfaces embellished with nanoscale topographies. The goal of this review is to consider the role of nanoscale topographic modification of titanium substrates for the purpose of improving osseointegration. Nanotechnology offers engineers and biologists new ways of interacting with relevant biological processes. Moreover, nanotechnology has provided means of understanding and achieving cell specific functions. The various techniques that can impart nanoscale topographic features to titanium endosseous implants are described. Existing data supporting the role of nanotopography suggests that critical steps in osseointegration can be modulated by nanoscale modification of the implant surface. Important distinctions between nanoscale and micron-scale modification of the implant surface are presently considered. The advantages and disadvantages of nanoscale modification of the dental implant surface are discussed. Finally, available data concerning the current dental implant surfaces that utilize nanotopography in clinical dentistry are described. Nanoscale modification of titanium endosseous implant surfaces can alter cellular and tissue responses that may benefit osseointegration and dental implant therapy.

Key words:

Nanotopography; Dental Implant; Surface treatment; Sol-gel techniques; Bone regeneration; Cell signaling.

Introduction:

Current dental implant success has evolved from modest results of the middle of the past century. Beginning in the late 1960's the focused efforts of PI Branemark led to the detailed microscopic characterization of interfacial bone formation at machined titanium endosseous implants (Branemark et al., 1969; Linder et al., 1983). These concepts of osseointegration focused the profession on a proscribed surgical technique and the biocompatible nature of the machined titanium surface. Bone formation at the endosseous implant surface was considered a positive outcome that was contrasted to fibrous encapsulation, a negative and undesired result (Albrektsson; Sennerby, 1990). The main clinical advantage of osseointegration was the predictable clinical result that occurred when an osseous interface was reproducibly formed and maintained at the titanium surface of load bearing dental implants (Adell et al., 1990).

Over two decades later, osseointegration is widely accepted in clinical dentistry as the basis for dental implant success. The low rate of implant failure in dense bone of the parasymphyseal mandible (Adell et al., 1981; Albrektsson et al., 1988; Goodacre et al., 1999; Zarb; Schmitt, 1990) has not been fully recapitulated by subsequent data from studies involving more challenging clinical situations (Morton et al., 2004; Tolstunov, 2006). Anecdotal reports of difficulty in achieving high rates of implant success in select patient populations (e.g. smokers, diabetics) were supported by initial reports (Jaffin; Berman, 1991; Bain, 1996; Fiorellini et al., 2000). The cause of these failures, while not precisely determined, was largely attributed to a failure in bone formation in support of osseointegration. Challenging osseointegration with new protocols such as immediate placement and immediate loading may require further control of bone formation and osseointegration (Morton et al., 2004).

Failure to achieve osseointegration at a high rate can be attributed to one or more implant, local anatomic, local biologic, systemic or functional factors (Adell et al., 1981; Zarb; Schmitt, 1990). Clinical control of all of these factors is represented by multidisciplinary treatment planning procedures. While it is presently acknowledged that these, as well as clinician-related factors, are important determinants of endosseous implants success, a major interest in implant design factors is evident and clinical efforts to improve implant success have been focused on increasing the amount of bone that forms at the endosseous implant surface.

Implant surface character is one implant design factor affecting the rate and extent of osseointegration (Cooper, 1998; Nanci et al., 1998; Boyan et al., 1993; Schwartz et al., 1992; Stanford et al., 2006). The process of osseointegration is now well described both histologically and at the cellular level. The adhesion of a fibrin blood clot and the population of the implant surface by blood-derived cells and mesenchymal stem cells is orchestrated in a manner that results in osteoid formation and its subsequent mineralization (Masuda et al., 1997; Meyer et al., 2004; Berglundh et al., 2003). A seamless progression of changing cell populations and elaboration and modification of the tissue / implant interface eventually results in bone forming in direct contact with the implant surface. Precisely how much of the implant surface directly contacts bone, how rapidly this bone accrual occurs, and the mechanical nature of the bone / implant connection is influenced by the nature of the implant surface itself (Le Guéhennec et al., 2007).

The character of the implant surface is implicated in this complex process of osseointegration in a number of different ways. Early investigations revealed the

biocompatible nature of the cpTitanium implant (Kasemo, 1983), and revealed some pragmatic advantages for cpTitanium over other suitable materials (Johansson Albrektsson, 1991). Molecular investigations have contributed to defining cellular responses to titanium as “compatible” and advantageous. For example, Suska and colleagues (2005) showed relatively low inflammatory signaling within cells in tissues adjacent to cpTitanium implants and suggested that this is a part of the osseointegration process. During the first 10 – 20 years of applied endosseous implant experience, the concept that cpTitanium implant biocompatibility supported clinical osseointegration success dominated clinical thinking. Subsequently, experiments with surface topography encouraged new considerations of improvements in bone formation at the implant surface.

Micron-scale surface topography

The significance of micro-scale topography, was highlighted in an important report by Buser and colleagues (1991) that compared various surface preparations of cpTitanium to an electropolished surface negative control and a hydroxyapatite coated positive control group. The observation that a micron-scale rough surface prepared by grit blasting and subsequent acid etching was capable of rapid and increased bone accrual reiterated an earlier report that a TiO₂-grit blasted surface also supported more rapid and increased bone accrual at cpTitanium implants (Gotfredsen et al., 1990). These early observations indicated that the cpTitanium surface could be modified to enhance bone accrual and suggested that cpTitanium was not only “bioinert” or “biocompatible”, but could influence cellular activity or tissue responses leading to greater osteogenesis.

At least three different lines of thinking have evolved to better interpret or explain how surface topography at the micron-scale can increase bone to implant contact. One is the biomechanical theory of Hansson and Norton (Hansson; Norton, 1999), the second is the concept of contact osteogenesis (Davies, 2003), and the third is a surface signaling hypothesis supported by many cell culture investigations (Cooper, 1998; Puleo; Nanci, 1999; Schwartz et al., 1999).

Hansson has elegantly described the theoretical interaction of bone with the implant surface and mathematically defined the role of surface roughness at the micron scale within this hypothetical construct (Hansson; Norton, 1999). The result of the theoretical calculations – that an implant surface should be densely covered with pits of approximately 1.5µm depth and 3-5µm diameter – is supported by data collected in a series of studies on implant topography effects on bone to implant contact (Albrektsson; Wennerberg, 2004a; 2004b). There is an appreciation that mechanical interlocking of bone is essential to the improved

performance of endosseous implants. One possible explanation is given by the adaptation of bone to mechanical loading played by the osteocytes acting as mechanosensors (Burger; Klein-Nulend, 1999; Hansson, 2006). Evidence of the important relevance of increased bone to implant contact has been provided by measurement of the physical interaction of micron level rough implants with bone using push out or torque removal assays (Wong et al., 1995; Wennerberg et al., 1997). What has not been fully elucidated is how mechanical signaling in the unmineralized tissue of forming bone and adjacent connective tissue is affected by the implant surface. The bonding of bone to the implant surface is not implicated as a mechanism of enhancing the early physical associations of the implant with bone.

A principal role for fibrin clot stabilization by the implant surface exemplifies one role that microscale surface roughness may play in improved osseointegration (Park et al., 2001). Described is a physical interlocking of fibrin fibers with the surface features which promotes the directed ongrowth of bone forming cells directly at the implant/bone interface. Topographic enhancement may aid in stabilization of fragile extracellular matrix scaffolds for conduction of cells toward and onto the implant surface (contact guidance) (Ricci et al., 2008).

Several investigators have further described surface topography-specific effects on titanium-adherent osteoblastic cell behavior (Schneider et al., 2003; Isa et al., 2006; Ogawa; Nishimura, 2003; Ogawa; Nishimura, 2006). The overriding theme of these investigations is that surface adhesion-mediated control of cell function underscores the positive influences on bone formation. Many investigations have contributed to the understanding that there is a range of micron-level surface topography that enhances the adherent osteoblasts' differentiation and extracellular matrix formation/mineralization (Abron et al., 2001). Together these investigations have shown that increased surface topography effectively enhances extracellular matrix synthesis of adherent cells and provides a faster and more reliable osseointegration response (Ogawa; Nishimura, 2006; Buser et al., 2004; Ellingsen et al., 2004; Gutwein et al., 2004; Oh et al., 2005; Price et al., 2003a; 2003b; Webster et al., 1999; Webster et al., 2000a; Webster et al., 2001a; Webster; Ejiófor, 2004; Webster et al., 2005; Schwartz et al., 2005; Zhao et al., 2005).

A clearly defined role for extracellular matrix proteins-receptors (integrin) has been proposed to transduce topography-specific signals to the adherent cells (Schneider et al., 2003). One possible way that topography may alter cellular differentiation is through imposed changes in cell shape (Dike et al., 1999). Micron level topography effects on increased bone to implant contact are observed in vivo (Buser et al., 1991; García; Reyes, 2005), and in

human clinical histology (Trisi et al., 2003). Limited evidence that integrins are involved in cellular responses to implant surfaces has been obtained using MG63 cell culture studies (Wang et al., 2006).

Micron-scale topographic modification of the cpTitanium surface is accepted in the endosseous dental implant marketplace (Albrektsson; Wennerberg, 2004a; 2004b). The belief that micron level surface topography results in greater accrual of bone at the implant surface is supported by some clinical evidence (Cochran, 1999; Shalabi et al., 2006). Yet, these surfaces have been generally interpreted to be biocompatible devices with limited ability to directly affect the initial fate of surrounding tissues (e.g. impose bone formation or prevent bone resorption).

Today, a growing aspect of endosseous implant surface research is focused on further enhancing the activity of bone forming cells at the tissue implant interface. This desire for “bioactivity” has been addressed using a variety of different approaches. Clearly, cpTitanium surfaces can be modified to direct specific cellular responses such as osteogenesis. More specifically, cpTitanium implant surfaces can be made to direct the osteoinduction of adherent progenitor cells. While one approach is the immobilization of bioactive peptides or growth factors and notably the BMPs (Schliephake et al., 2005; Becker et al., 2006;), other approaches have embraced the use of nanoscale surface engineering to induce intrinsic osteoinductive signaling of the surface adherent cells. The purpose of this review is to explore how nanotechnology applications to the cpTitanium implant surface may provide new opportunities to create endosseous implant surfaces with greater specific control of adherent cell and adjacent tissue fate.

Nanotechnology and Surface Science

Nanotechnology has been defined as “the creation of functional materials, devices and systems through control of matter on the nanometer length scale (1–100nm), and exploitation of novel phenomena and properties (physical, chemical, biological) at that length scale” (National Aeronautics and Space Administration). Nanotechnology involves materials that have a nano-sized topography or are composed of nano-sized materials. These materials have a size range between 1-100nm (10^{-9} m) (Figure 1). Nanotechnology often involves one-dimensional concepts (nanodots, nanowires) or the self-assembly of more complex structures (nanotubes). Materials are also classified according to their form and structure as, nanostructures, nanocrystals, nanocoatings, nanoparticles, and nanofibers (Christenson et al., 2007).

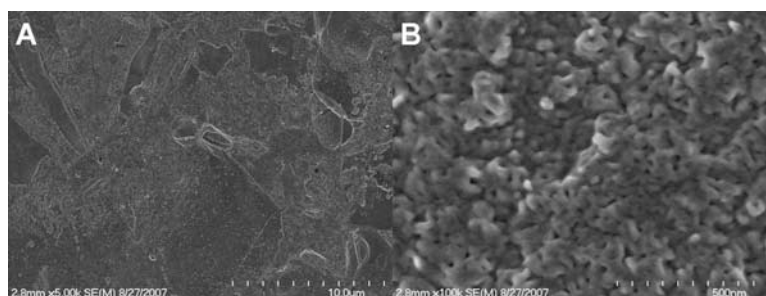


Figure 1 – Nanoscale in perspective. The scanning electron micrograph at 5000x (A) fails to represent true nanoscale features of a titanium implant surface. 100,000x image (B) shows the complex nanoscale surface; here produced by Titania sol-gel deposition.

Application of nanotechnology to the dental implant surface involves a two dimensional association of surface features (across and away from the mean surface plane) (Figure 2). These nanofeatures can be arranged in an organized manner (isotropic) or unorganized manner (anisotropic), often depending on the method of manufacture. Of the surface topographies that have been applied to a dental implant surface, the topography is often characteristically anisotropic. Isotropic features such as nanogrooves or nanopits that are created largely by optical methods are not readily applied to complex screw shaped objects. When these concepts are applied to the endosseous implant surface, implied is the embellishment of the surface with nanometer scale features that lead to novel physicochemical behavior (e.g. bone bonding) or biochemical events (e.g. altered protein adsorption, cell adhesion with changes in cell behavior).

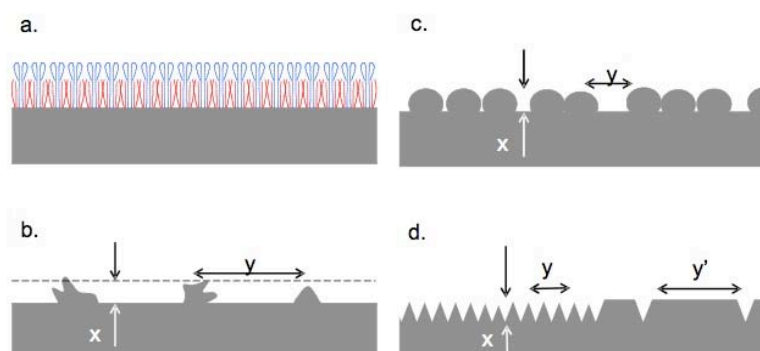


Figure 2 – Nanoscale surface modification. A) self-assembled monolayers (SAM) can change the topography and chemistry of a surface to impart novel physical and/or biochemical properties. B) deposition or chemical modification techniques can apply nanoscale features ($x \leq 100\text{nm}$) in a manner that are distributed in micron scale ($y > 100\text{nm}$). C) other deposition or compaction methods can place nanoscale features in nanoscale distribution. The cell response to surfaces represented by B or C may be different. D) isotropic surfaces can be created in the nanoscale ($x \leq 100\text{nm}$) by subtractive or additive methods. The distribution can be in either the nano (y) or micron (y') scale. It is thought that some nanosurfaces mimic natural cell environments.

Nanoscale modification of the titanium endosseous implant surface may affect both the topography as well as the chemistry of the surface. Specific chemical modification of cpTitanium could be the targeted goal of nanoscale modification. In fact, a complicating feature of nanoscale manipulation of any material is that there are inherent chemical changes of the bulk material surface. Albrektsson and Wennenberg (2004a), divided implant surface quality into three categories: (1) mechanical properties, (2) topographic properties, and (3) physicochemical properties. They indicated that these characteristics are related and by changing any of these groups the others will also be affected. This important observation is likely to be even more relevant to discussions of nanotopographic modifications of the endosseous cpTitanium surface. One frequently encountered limitation to studies comparing nano- and micron-level surface topography is that it can be extremely difficult to isolate chemistry or charge effects induced by the nanotopography. When atomic level control of material assembly is approached, the surface properties are influenced by quantum phenomena that do not govern traditional bulk material behavior (Liu et al., 2006). It is very difficult but important to distinguish distinct topography-specific effects from allied changes in surface energy or chemical reactivity.

Nanotechnology requires novel ways of manipulating matter in the atomic scale. Several approaches are currently prevalent in the experimental application to endosseous implants (Table 1). One approach involves the physical method of compaction of nanoparticles of TiO₂ versus micron level particles to yield surfaces with nanoscale grain boundaries (Webster; Ejiófor, 2004). An advantage of this method is that it conserves the chemistry of the surface among different topographies.

Table 1 - Methods for Creating Nanofeatures on cpTitanium Implants

	Methods	Characteristics
Self assembly of Monolayers		The exposed functional end group could be a molecule with different functions (an osteoinductive or cell adhesive molecule).
Physical approaches	Compaction of nanoparticles Ion Beam Deposition	Conserves the chemistry of the surface among different topographies. Not readily applied over implant surfaces Can impart nanofeatures to the surface based on the material used.
Chemical methods	Acid etching Peroxidation Alkali treatment (NaOH) Anodization	Combined with other methods (sandblasting and/or Peroxidation) can impart nanofeatures to the surface and remove contaminants. Produces a titania gel layer. Both chemical and topography changes are imparted. Produces a sodium titanate gel layer allowing hydroxyapatite deposition. Both chemical and topography changes are imparted. Can impart nanofeatures to the surface creating a new oxide layer (based on the material used).
Nanoparticle Deposition	Sol-Gel (colloidal particle adsorption) Discrete crystalline deposition	Creates a thin-film of controlled chemical characteristics. Atomic-scale interactions display strong physical interactions. Superimposes a nanoscale surface topographical complexity on the surface.
Lithography and contact printing technique		Many different shapes and materials can be applied over the surface. Approaches are labor intensive and require considerable development prior to clinical translation and application on implant surface.

Second is the process of molecular self-assembly. Self-assembled monolayers (SAMs) are formed by the spontaneous chemisorption and vertical close-packed positioning of molecules onto some specific substrata, exposing only the end-chain group(s) at the interface (Scotchford et al., 2002). The exposed functional end group could be an osteoinductive or cell adhesive molecule. An example of this is the use of cell adhesive peptide domains (RGD domains) appended to SAMs composed of polyethylene Glycol (PEG) and applied to the Titanium implant surfaces (Germanier et al., 2006).

A third method is the chemical treatment of different surfaces to expose reactive groups on the material surface and create nanoscale topography. This is popular among current dental implant investigators. NaOH-treatment catalyzes the production of titanium nanostructures outward from the titanium surface (Zhou et al., 2007). Treatment with a NaOH solution produces a sodium titanate gel layer on the Ti surface while H₂O₂ produces a titania gel layer. The NaOH treatment creates a gel-like layer over the material allowing hydroxyapatite deposition. This behavior has also been seen with other metals such as Zirconium and Aluminum (Kim et al., 2000; Wang et al., 2001; Uchida et al., 2002). Titanium oxide nanotubes chemically treated with NaOH accelerated HA crystal growth in a simulated body fluid (SBF) (Oh et al., 2005). The kinetics of HA formation is significantly accelerated by the presence of the nanostructure associated to the NaOH treatment. Both chemical and topography changes are imparted.

Chemical treatments (Peroxidation (H_2O_2) or acid oxidation, such as Hydrofluoric acid) have also been used to create nanotopography (Nanci et al., 1998; Wang et al., 2001; Uchida et al., 2002). The use of H_2O_2 with acid etching has been shown to create novel nanostructures of amorphous titanium oxide on the implant surface (Wang et al., 2002). It was found that the treatment of the implant surface with $\text{H}_2\text{O}_2/\text{HCl}$ increased the adsorption of RGD peptides onto the surface followed by passivated surfaces (30% HNO_3) and heat-treated surfaces (Mante et al., 2004). These surface treatments also increased the mineralization in the same order. Treatment with hydrofluoric acid also creates discrete nanostructures on TiO_2 grit blasted surfaces (Ellingsen et al., 2006). Several cell culture studies (Isa et al., 2006; Cooper et al., 2006; Guo et al., 2007), preclinical investigations (Ellingsen et al., 2004; Berglundh et al., 2007), and clinical studies (Stanford et al., 2006) support the observation that hydrofluoric acid treatment of TiO_2 grit blasted titanium implants is associated with rapid bone accrual at the implant surface. Complex chemical changes induced by these methods may require careful inspection.

The deposition of nanoparticles onto the titanium surface represents a fourth approach to imparting nanofeatures to a titanium dental implant (Ben-Nissan; Choi, 2006). Sol-gel transformation techniques achieve deposition of nanometer scale calcium phosphate accretions to the implant surface (Liu et al., 2001; Kim et al., 2004). Alumina, titania, zirconia and other materials can also be applied (Lee et al., 2006). Owing to their resultant atomic-scale interactions, the accretions display strong physical interactions (Ben-Nissan; Choi, 2006; Piveteau et al., 2000; Arias et al., 2003; Choi; Ben-Nissan, 2007). In a modified approach, Nishimura and colleagues (2007) recently demonstrated a directed approach to assembly of CaPO_4 nanofeatures on dual acid etched cpTitanium implant surfaces. The deposition of discrete 20-40nm nanoparticles on an acid etched titanium surface led to increased mechanical interlocking with bone and the early healing of bone at the endosseous implant surface in a rat model.

One of the main concerns related to coating the implant surface is the risk of coating detachment and toxicity of related debris. This question was addressed by Gutwein and Webster (2004) who evaluated the relationship of particle size and cell viability and proliferation compared to micron-particles. Nanoparticles of titania and alumina had less negative impact in cell viability and proliferation. There may be an advantage to nanoscale modification of surfaces using sol-gel coating methods. The quantum interaction of high electron density at the atomic level can enforce high bond strength between the substrate and nanoscale coating. Examples of this have been reported for the calcium phosphate

(CaP) / Discrete crystalline deposition (DCD) sol-gel coating of Ti alloy implant surfaces (Mendes et al., 2007).

A fifth approach to creating nanoscale topography on Titanium is the use of optical methods (typically lithography) reliant on wavelength specific dimensions to achieve the appropriate nanoscale modification (Zhou et al., 2007). These approaches are labor-intensive methods that require considerable development prior to clinical translation. The present use of lasers to promote micron level groove on an implant surface can produce micron level, not nanoscale, modification of the implant surface (Ricci et al., 2000). Another method of depositing nanoscale material on to the implant surface involves ion beam deposition (e.g. Hydroxyapatite) (Coelho; Suzuki, 2005). All are relevant to the endosseous dental implant surface and experimental examples of each can be identified.

Nanotopography has been shown to influence cell adhesion, proliferation, differentiation, and cell specific adhesion. Related changes in chemistry and nanostructure impart important chemical changes and permit biomimetic relationships between alloplastic surfaces and tissues. It is speculated that alloplastic nanosurfaces possess topographic elements scaled to naturally occurring substrates.

Biomimetics and Nanotechnology:

The recapitulation of natural cellular environments can be achieved at the nanoscale. Nanoscale modification of an implant surface could contribute to the mimicry of cellular environments to favor the process of rapid bone accrual. For example, cell adhesion to basement membranes is an often-cited example of nanoscale biomimetics. The structure of the epithelial basement membrane contains pores approximating 70–100nm (Brody et al., 2006). It is suggested that the surface roughness of bone is approximately 32nm making it within the nanoscale range of current nanotechnology investigations (Lim et al., 2005; Palin et al., 2005; Hansen et al., 2007; Lim et al., 2007). These in vivo examples further exemplify an anisotropic arrangement of nanofeatures. Intentionally placing molecular structures at such resolution on an endosseous implant may be achieved with anisotropic arrangements. The result may be changes in physical properties including enhanced magnetic, catalytic, optical, electrical, mechanical, and biological properties when compared to conventional formulations of the same material (Park et al., 2005).

Nanotopography Alters Cellular Responses

Surface nanotopography appears to affect cell interactions at surfaces and alter cell behavior when compared to conventional sized topography (Figure 3) (Klabunde et al., 1996; Wu et al., 1996; Baraton et al., 1997). Different physical relationships exist between cells and nano- versus cell and micron-scale surface features. Nanotopography specific effects on cellular behavior have been demonstrated using a wide range of different cell types including epithelial cells, fibroblasts, myocytes and osteoblasts. Nanostructured surfaces possess unique properties that alter cell adhesion by direct (cell – surface interactions) and indirect (affecting protein – surface interactions) mechanisms. Evidence has been gathered using several models and surface systems (Tables 2 and 3).

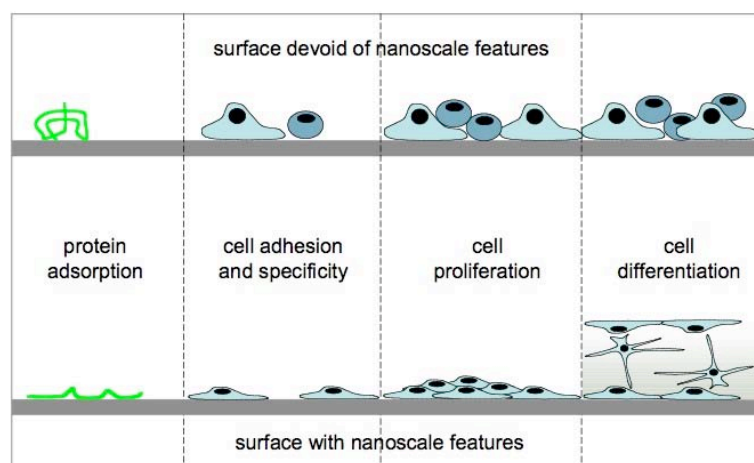


Figure 3 – Depiction of broad range of nanoscale topography effects observed in cellular protein adsorption is altered by nanoscale modification of bulk material. Both cell specificity and extent of cell adhesion is altered. Depending on the nano-architecture cell spreading may be increased or decreased. By presently undefined mechanisms, cell proliferation appears to be enhanced by nanoscale topography. For osteoblast, several investigators have shown nanoscale topography enhances osteoblast differentiation.

Table 2 - Reported Osteoblast responses to Nanosurfaces – In vitro

Size / nanofeature	Cell response	Material / fabrication	Cell culture model	Ref.
14, 29, 45 nm nanopits	Change in Signaling	poly(l-lactic acid) and polystyrene (50/50 w/w) / polymer demixing	hFOB	(Lim et al., 2007)
Ion beam coating thickness ~60 nm SG Coating thickness of 70 nm	Change in Signaling	Ti6Al4V / Ion Beam implantation of Zn or Mg or SG coating with HA	human bone-derived cells	(Zreiqat et al., 2005)
12 nn ridges / 0.2 – 2 mm separation	Changes in cell cytoskeleton	Ti / PLD	Osteoblast – rat calvaria	(Monsees et al., 2005)
Pits with 120 nm Ø, spacing of 300 nm in orthogonal or hexagonal arrangement.	Changes in cell cytoskeleton	PMMA / EBL in Silica	hMSCs	(Hart et al., 2005)
Pits with 120 nm Ø. The pitch between the pits was 300 nm. Hexagonal and square pit arrangements.	Changes in cell cytoskeleton - Restriction of spreading – Filopodia	PMMA / ELB in poly(carbonate)	hMSCs	(Hart et al., 2007)
Alumina (23-nm average Ø), titania (32-nm average Ø)	Decreased Apoptosis	Particles diluted in growth media at concentrations of 10,000, 1000, and 100 mg/ml as well as 10,000, 5500, and 1000 mg/ml	Human osteoblasts	(Gutwein; Webster, 2004)
RMS roughness values from 0.5 to 13nm.	Decreased proliferation	Gradients of polymer crystallinity were fabricated on films of poly(l-lactic acid) / gradient in annealing temperature.	Osteoblast – MC3T3-E1	(Washburn et al., 2004)
0.5–2.4 µm – Ti 0.5–1.4 µm – Ti6Al4V 0.2–0.4 µm – Co28Cr6Mo	Increased Adhesion	Ti, Ti6Al4V, and CoCrMo alloys / compaction	Human osteoblasts	(Webster; Ejiófor, 2004)
7 – 40 nm	Increased Adhesion	nobium oxidation of cpTi / sol–gel coating	Osteoblast – MC3T3-E1	(Eisenbarth et al., 2007)
HA, Ti-coated HA annealed in air, and Ti coated HA annealed in N2+H2 possessed Sq of 5, 32, and 28 nm, respectively.	Increased Adhesion	HA / compaction / Ti coating (CaTiO3)	Human osteoblasts	(Webster et al., 2003)
Nanograined / Not shown	Increased Adhesion	HA, TCP, or CaTiO3 / compaction	Human Osteoblasts	(Ergun et al., 2007)
nm HA and HA functionalized with RGD	Increased Adhesion	Sintering	Human osteoblasts	(Balasundaram et al., 2006)
Alumina (23-nm Ø diameter), titania (32-nm Ø diameter)	Increased Adhesion	Titania or Alumina powders / compaction	Osteoblasts from neonatal rat calvaria	(Webster et al., 2001a)
Alumina (24 and 45 nm average Ø), titania (39 and 97 nm average Ø) and HA (67-nm) powders.	Increased Adhesion	Titania, Alumina or HA powders / compaction	Osteoblasts from neonatal rat calvaria.	(Webster et al., 2000b)
Nanotubes of 3.4±0.3 nm	Increased Adhesion	cpTi coated with helical rosette nanotubes featuring lysine side chains (HRN-K1)	human fetal osteoblast	(Chun et al., 2005)
Self-assembled nanowires 50-100 wide	Increased Adhesion	Ti Mesh / NaOH treatment	MSCs and Mice	(Dong et al., 2007)
Alumina nanofibers with 2 nm in Ø and ~50 nm in length alumina nanospherical grain size (<100 nm) powder	Increased Adhesion - Ca deposition	Alumina grain or nanofibers / compaction	Human osteoblasts	(Price et al., 2003a)
5-50 nm pores	Increased Adhesion – Ca deposition	Ti6Al4V / H2SO4/H2O2 70/30% followed by coating of TiO2	Osteoblast – MC3T3-E1	(Advincula et al., 2006)
Nanophase titania (32-nm average Ø) powders.	Increased Adhesion – Ca deposition	PLGA mixed with titania (in various proportions) / cured in air	Human osteoblasts	(Webster; Smith, 2005)
11- 85 nm	Increased Adhesion - Differentiation	Polystyrene-polybromostyrene / polymer demixing	hFOB	(Lim et al., 2005)
	Increased Adhesion – Differentiation – Ca deposition	nanophase titania/ (PLGA) composites	Human osteoblasts	(Liu et al., 2006)

~ 100 nm / nanotubes	Increased Adhesion – Proliferation - Differentiation	titania / anodization	primary rat bone marrow MSCs	(Popat et al., 2007a)
~ 100 nm / nanopores	Increased Adhesion – Proliferation - Differentiation - Ca deposition	alumina sheets / anodization	primary murine bone marrow MSCs	(Popat et al., 2007b)
~100nm features on Ti	Increased Differentiation	cpTi / TiO ₂ Blasting / HF treatment	Osteoblast – MC3T3-E1 and Ratus novergicus	(Guo et al., 2007)
10 - ___ nm	Increased Differentiation	PMMA / Colloidal lithography and polymer demixing	primary human osteoprogenitors	(Dalby et al., 2006)
20 – 50 nm surface features	Increased Differentiation	cpTi and Ti6Al4V / oxidation with H ₂ SO ₄ /H ₂ O ₂	primary rat calvaria derived osteoblasts	(Oliveira; Nanci, 2004)
Elongated HA nanocrystals, with a mean length of about 100 nm.	Increased Differentiation	Ti13Nb13Zr / mechanomaking process or Ti6Al4V followed by HF/HNO ₃ acid etch CaP coating	hMSCs	(Bigi et al., 2007)
Parallel ridges/channels (microstructured) / nanostructured HA (100 nm).	Increased Differentiation	Photolithography / nanostructured HAP (biomimetic) on silicon microstructures	Saos-2 and MG-63 cell lines	(Tan et al., 2004)
Alumina nanofibers with 2 nm in Ø and ~50 nm in length	Increased Differentiation - Ca deposition	Alumina nanofibers / compaction / Sintered at 400oC, 600oC, 800oC, 1000oC, or 1200oC	Human osteoblast	(Webster et al., 2005)
20 – 50 nm surface features	Increased Differentiation – Ca deposition	cpTi / oxidation with H ₂ SO ₄ /H ₂ O ₂	primary rat calvaria derived osteoblasts	(Oliveira et al., 2007)
Alumina (24-nm average Ø), titania (39-nm average Ø) and HA (67-nm) powders.	Increased Differentiation – Ca deposition	Titania, Alumina or HA powders / compaction	Osteoblasts from neonatal rat calvaria	(Webster et al., 2000a)
island height of about 90 nm	Increased Filopodia	Polystyrene and polybromostyrene/ Polymer demixing	Human Bone marrow cells	(Berry et al., 2006)
Nanofibers (60-100 nm)	Increased Osteoblast Specificity	Carbon nanofibers / compaction	Human osteoblasts	(Price et al., 2003b; Price et al., 2004)
Alumina (23-nm average Ø), titania (49-nm average Ø) and HA (67-nm) powders.	Increased Osteoblast Specificity	PLA or PMMA powder mixed with titania, alumina or HA (in various proportions) / compaction	Neonatal rat calvaria osteoblasts.	(McManus et al., 2005)
Nanophase titania (32-nm average Ø) powders.	Increased Osteoblast Specificity	PLGA mixed with titania (in various proportions) / cured in air	Rat skin fibroblasts	(Kay et al., 2002)
~ 160 nm pores	Increased Proliferation	Alumina / EBE	Human osteoblasts	(Briggs et al., 2004)
AAT texture showed micropores and an overlapped nanometric net of filaments	Increased Proliferation	cpTi / alkali etching process with CaP solution (biomimetic)	Osteoblast-like MG63	(Chiesa et al., 2007)

cpTi – Commercially pure Titanium; EBL – Electron beam lithography; EBE – Electron beam evaporation; HF – Hidrofluoric acid treatment; PLD – Pulsed laser deposition; PMMA – Polimethyl methacrilate; SG – Sol-gel; Ti – Titanium.

Table 3 - Reported Osteoblast responses to Nanosurfaces – In vivo

size / nanofeature	Tissue response	material / fabrication	Animal / cell culture model	ref.
3µm CaP coating	Elimination of tissue fibrous encapsulation and foreign body giant cell response	PLGA / CaP coated with CaP	Ratus novergicus	(Lickorish et al., 2007)
8nm diameter and 100nm length	Enhanced bone formation	PLGA mixed with Ti nanotubes	Ratus novergicus	(Kubota et al., 2004)
AAT texture showed micropores and an overlapped nanometric net of filaments	Increased Bone-to-implant contact	cpTi / alkali etching process with CaP solution (biomimetic)	Sheep	(Chiesa et al., 2007)
Not shown	Increased Bone-to-implant contact	cpTi / HA - Ion Beam Assisted Deposition (IBAD)	Rabbit	(Jung et al., 2001)
~100nm features on Ti	Increased Bone-to-implant contact	cpTi / TiO ₂ Blasting / HF treatment	Dog	(Berglundh et al., 2007)
~100nm features on Ti	Increased Differentiation	cpTi / TiO ₂ Blasting / HF treatment	Ratus novergicus	(Guo et al., 2007)
Not shown	Increased osseoactivity	cpTi / HA - Ion Beam Assisted Deposition (IBAD)	Dog	(Coelho; Suzuki, 2005)
discrete deposition of HA nanoparticles (20–40 nm) on Ti substrate	Increased Push-out test resistance	cpTi / dual acid etch / coated with CaP by DCD	Ratus novergicus	(Nishimura et al., 2007)
Not shown	Increased removal torque – Bone-to-implant contact – Bone volume	cpTi / Sandblast / HA - Ion Beam Assisted Deposition (IBAD)	Rabbit	(Park et al., 2005)
20–100 nm range of the features (HA)	Increased tensile test resistance	cpTi and Ti6Al4V / acid etch / coated with CaP by DCD	Ratus novergicus	(Mendes et al., 2007)

Protein/surface interactions - Surface Wettability

The changes in initial protein – surface interaction are believed to control osteoblast adhesion (Balasundaram et al., 2006). This is a critical aspect of the osseointegration process. When implants come into contact with a biological environment, protein adsorption (e.g. plasma fibronectin) that occurs immediately will mediate subsequent cell attachment and proliferation. Cell binding to protein domains of adhesive extracellular matrix proteins involves receptors termed integrin receptors that transmit signals through a collection of proteins on the cytoplasmic face of the contact, termed focal contacts (Fath et al., 1989). Surface effects are often mediated through integrins that bind the RGD motif in cell attachment proteins (Tosatti et al., 2004). The RGD motif of cell adhesive proteins such as fibronectin or vitronectin are important in mediating cell adhesion of osteoblasts and other cells to synthetic material surfaces (Sinha; Tuan, 1996). Nanofeatures could alter the conformation of these RGD containing proteins, a phenomenon known to affect cell adhesion and behavior (Cavalcanti-Adam et al., 2007).

Changing the surface energy or wettability of a biomaterial represents a classical approach to altering cell interactions with the surface. Extracellular matrix protein adsorption onto surfaces (to subsequently modulate cell adhesion) is dramatically affected by surface energy. Interestingly, many studies of self-assembled monolayers (SAM) have demonstrated

that hydrophobic groups are more likely to adsorb albumin and that albumin is not replaced by ECM proteins, blocking cell adhesion. Hydrophobic surfaces adsorbed fibrinogen (Rodrigues et al., 2006), while hydrophilic surfaces allowed an interchange of adsorbed albumin by ECM proteins (Arima et al., 2007).

Nanoscale topography is a powerful way of altering protein interactions with a surface. Webster and colleagues (Webster et al., 2000b; Webster et al., 2001a) observed an increased vitronectin adsorption on nanostructured surfaces when compared to conventional surfaces. They also found an increased osteoblast adhesion when compared to other cell types, such as fibroblasts, on the nanosurfaces (Webster et al., 2000a). Another study suggested higher adsorption of fibronectin on hydrophilic SAMs surfaces with greater focal adhesion formation (integrin binding) evident in the osteoblast cells adhered to the hydrophilic SAM treated surfaces (Scotchford et al., 2002). Lim and colleagues (Lim et al., 2005) more directly related protein adsorption, cell adhesion and the active process of attachment by measurement of increased focal adhesion kinase (FAK) activity. In a study using SAMs biofunctionalized with RGD, Cavalcanti-Adam and colleagues (2007) also found that the spacing among the nanofeatures modulate focal adhesion (FA) formation; cells cultured on a 58nm nanopattern formed normal FA, whereas those plated on a 108nm nanopattern failed to develop FA. Surface roughness at the nanoscale is an important determinant of protein interactions that ultimately direct cell activity in control of tissue formation at implant surfaces (Park; Webster, 2005).

Cell adhesion, spreading and motility

Irrespective of the surface - adsorbed proteins, cells are remarkable in their ability to sense nanostructure (Figure 4). Nanofeatures of a surface affect both cell adhesion and cell motility. Both of these cell traits are attributed, in part, to the function of integrins. Underlying substratum topography influences cell behaviors by both direct and indirect interactions (Brunette, 1988). Indirect interactions are enacted by the interposed adherent proteins described above. Direct interactions involving the integrin receptors with the surface may also transmit signals to control adhesion, spreading and motility.

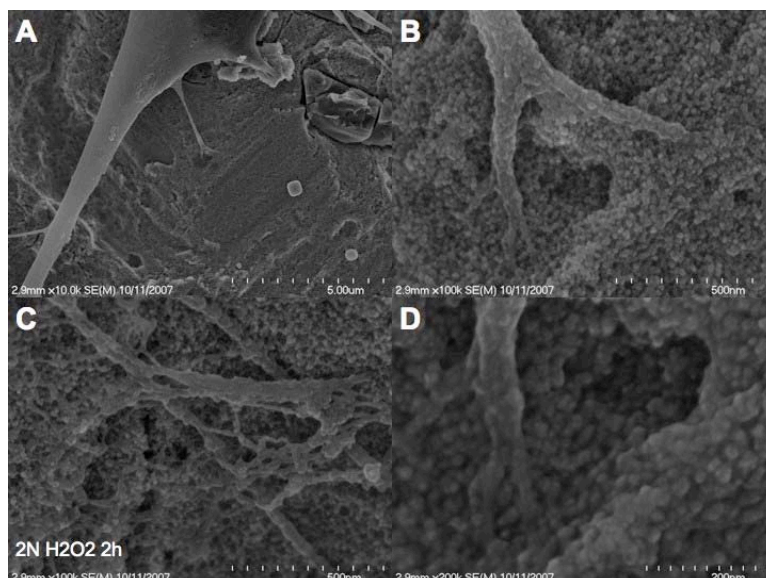


Figure 4 – Nanoscale cell interactions. There is apparent affinity of cells for nanoscale features. Here, 20-40 nm features produced by H₂O₂/H₂SO₄ treatment are interactive points for lamellipodia of spreading cells. The cause and effect relationship is a current point of investigation. A = 10,000x image of adherent cell. B and C represent 100,000x images of the same adherent cell. D = 200,000x magnification of the cell with nanofeatures.

Nanofeatures of an alloplastic surface may have unique attributes affecting cell interactions. Both the dimension and the density of the nanofeatures affect cell behavior (Cavalcanti-Adam et al., 2007). In a well-controlled investigation of Titanium nanostructure, Andersson and colleagues (2003) compared cell morphology and cytokine production on titanium substrates with 15mm wide and 185nm deep grooves versus Ti substrates with 100nm high, 168nm diameter hemispherical nanopillars. The cells appeared partially aligned to the grooves and had a cytokine release similar to that found from cells on flat surfaces. Cells on hemispherical pillars had a smaller area and had more membrane projections compared to cells on grooves. Morphological changes correlated with diminished protein secretion. It has been suggested that 70-100nm features of an implant surface are scaled to function directly with the focal adhesion of cells.

Cells respond differently to the scale of roughness. Osteoprogenitor cell adhesion was enhanced on poly-L-lactide (PLLA) and polystyrene (PS) surface with nano-scale and micro-scale roughness compared to smooth surfaces. OCT-1 osteoblast-like cells grew along the surface with two different nanoscale surfaces (PLLA) and grew inside micron-scale pits of PS (Wan et al., 2005). Similar conclusions were made when comparing nano- and micron-scale grain boundary effects on osteoblast cell adhesion and proliferation (Webster; Ejiófor, 2004). Some greater details of the relationship between surface nanofeatures and cell adhesion are emerging. Teixeira and colleagues (2003) demonstrated that when cells bridge

sub-micron-scale patterns, integrin binding was limited to substrate-adsorbed proteins on the top of the ridges. Geometrical constraints imposed by topographic features smaller than focal adhesion architecture (approximately 300nm) actually confine the cell attachment apparatus to the top of the topographic feature. Therefore, on the nanoscale patterns, integrin occupancy within a focal adhesion may be spatially segregated whereas on microscale ridges there are no constraints on integrin-ligand binding. While the current understanding of nanotopography effects on adherent osteoblast behavior requires further clarification, nanotopography may work at a linear scale that facilitates the mechanotransduction signaling mechanisms of the adherent osteoblast.

Several investigations demonstrate that cell spreading is restricted on nanoscale surfaces. For example, Dalby and co-workers (Dalby et al., 2006) investigated primary human osteoblast cell behavior on nanopitted surfaces. High pit density reduced cell spreading and ordered arrays of nanopits were effective in this regard. Randomization of the pits led to more cell spreading.

Nanotopography presents an opportunity to modulate cell adhesion and spreading both positively and negatively. When Lim and co-workers (2005) compared osteoblast adhesion on PLLA substrates with 3–45nm nanofeatures they demonstrated that cell adhesion was positively affected by nanotopography and interdependent on substratum surface characteristics of topography and surface chemistry. Lim and colleagues (2007) further demonstrated that 14–29nm pits favorably supported adherent cell integrin signaling when compared to 45nm pits. In contrast, Cai and co-workers (2006) found no major differences in Fibronectin adsorption or cell proliferation on 2 versus 20nm titanium films. There may be cell-type specific responses to nanofeatures of a given surface.

Teixeira and colleagues (2006) have also shown that, depending on cell culture conditions, corneal cell integrins aligned either parallel to or perpendicular with the isotropic nanofeatures. Cellular responses to nanoscale and submicron topographic cues are context dependent. Given the relatively anisotropic nature of natural cellular substrates, the significance of such findings remains to be defined. Nonetheless, these and other studies show that cell adhesion through integrins is sensitive to nanoscale features.

Cells adherent to nanotopographies may possess altered motility. Recent reports demonstrated that fibroblast and MSCs motility varied remarkably across a small range of nanostructures (Alsberg et al., 2006; Dalby et al., 2007). Hansen and colleagues (2007) cultured MC3T3-E1 osteoblastic cells on nanotopographic surfaces (11–38nm high islands).

Using AFM, they measured relatively higher cellular modulus values for cells on surfaces with nanofeatures compared with cells on flat control surfaces. They concluded that nanoscale topography affects the actual mechanical properties of the individual cell. This may be attributed to the resultant integrin-based remodeling of the cytoskeleton or more complex biophysical changes in the cell membrane. The ability to control cell motility or spreading may be valuable in future engineering of the implant-bone-mucosa interface or the mucosa-epithelial interface at the dental implant abutment.

Proliferation

Apparently, nanoscale features can increase adherent cell proliferation. Zhao and co-workers (2006) used three different approaches (electrochemical machining, anodization and chemical etching) to produce reproducible submicron-scale structures on Ti surfaces and observed an inverse relationship between cell proliferation and cell differentiation with the diminishing scale of surface features. Webster and colleagues (2000a) also observed increased osteoblast proliferation on the nanoscale (alumina, titania and hydroxyapatite) materials tested.

It is not fully understood how nanostructured surfaces modulate the adherent osteoblast response. At the simplest of levels, the proliferation rate of adherent cells has been measured as an index of cytocompatibility. Suggested is the concept that surface-to-cell signaling result in increased rate of proliferation. The mechanism(s) affecting this process is not defined, however, it can be speculated that many of the events associated with adhesion can affect signaling pathways that control proliferation. One example is the cross talk between integrin-signaling and the predominant MAP kinase pathways affecting cell proliferation (Schwartz et al., 2002).

Selectivity of adhesion

An interesting feature of nanoscale topographic surfaces is the selectivity of cell adhesion. Several investigators have demonstrated the relative diminution of fibroblast adhesion compared to osteoblast adhesion when nano- and micron- structured surfaces were evaluated (McManus et al., 2005; Price et al., 2003a). For example, on nano-sized materials, the affinity ratio between osteoblasts and fibroblasts was 3 to 1. In the conventional materials the ratio was 1 to 1 (Webster et al., 2000a). Similar results with other cell types such as smooth muscle cells and chondrocytes have been reported (Price et al., 2004). This could have important implications in specification of tissue responses at bone and mucosal surfaces of the dental implant/abutment assembly.

Bacterial adhesion and proliferation is also diminished on nanophase materials (Colon et al., 2006). Decreased bacterial colonization on nanostructured TiO₂ and ZnO is observed even though these surfaces promote osteoblast adhesion and differentiation. These initial observations imply that further development of the implant and the implant abutment surface can be explored in terms of biofilm accumulation and peri-implantitis.

The function of other cell types on nanostructured surfaces has also been addressed by Webster and co-workers (2001b). They measured on nanoscale surface an increase in osteoclast function measured by tartrate resistant acid phosphatase (TRAP) synthesis and formation of resorption pits. The TRAP synthesis on nanophase hydroxyapatite was more than twice that measured on conventional hydroxyapatite. This increased osteoclastic activity may be important for the formation and maintenance of healthy new bone juxtaposed to a dental implant.

Differentiation

In addition to supporting osteoblast-specific adhesion and adherent cellular proliferation, it is important to the process of osseointegration that the adherent mesenchymal cells differentiate rapidly along the osteoblast lineage. Early indications of nanoscale topography advantages were reported by Webster (1999). They revealed that alkaline phosphatase synthesis and calcium mineral content increased in cell layers formed on nano-sized materials after 21 and 28 days.

To date few studies have evaluated the gene expression pattern indicative of differentiation of osteoblasts on nanostructured surfaces. Immunolabeled osteopontin and BSP were found in higher concentration in nanostructured surfaces (Oliveira, Nanci, 2004). Isa and co-workers (2006) compared adherent palatal mesenchyme cell differentiation when cultured on a hydrophilic micron-scale topography cpTi surface or a nanoscale cpTi surface. Both surfaces supported osteoblastic differentiation, however, Runx2 expression (the key transcription factor controlling osteoblast differentiation) was increased on the nanoscale surface only. A recent in vitro and in vivo study has also demonstrated the upregulation in Runx2 expression (Guo et al., 2007). Also, many other genes are upregulated in nanostructured surfaces as a response to Runx2 levels, such as, BSP, OPN, OCN (Figure 5).

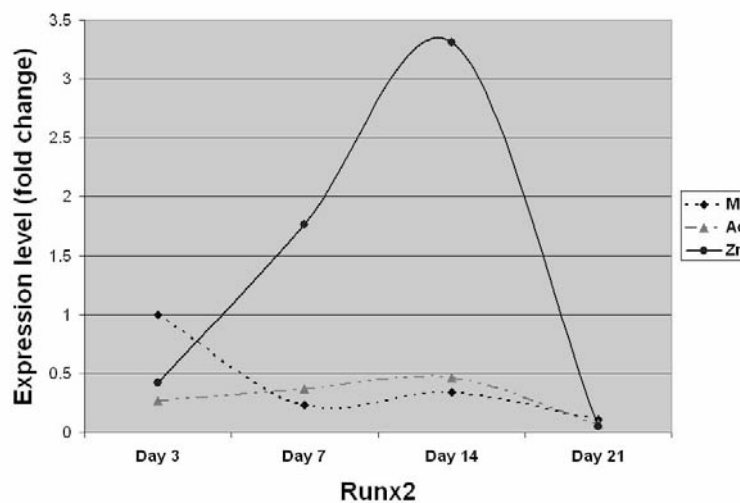


Figure 5 – Effect on surface treatment (topography) on osteoblast differentiation. Osteoblasts were cultured on titanium disks treated by machining ($R_a=86.52\text{nm}$), acid etching to provide a micron-rough surface ($R_a=388.40$), and with Zirconia sol-gel deposition ($R_a=89.71\text{nm}$) to produce a nanoscale topography with pore sizes ranging from 20-40nm. During the 21 days, expression of the key osteoblast differentiation factor, Runx2, was determined by real-time PCR. The results are plotted as fold change in expression level (compared to day 3 machined surface) versus culture duration (days). The marked elevation in Runx2 levels for the nanoscale surface reflects data for other nanoscale surfaces (Guo et al, 2007). M – Machined surface. Ac – Acid etched surface. Zr – Nanozirconia surface.

Increased bone formation was measured for nanoscale rough implant surfaces in animal models (Meirelles et al., 2007). In a series of studies the same group found early bone formation and increased torque removal when implant surfaces were added with nano hydroxyapatite or titania (Meirelles, 2007).

Nanotechnology alters surface reactivity

Nanoscale modification of the implant surface may alter the endosseous implants surface reactivity. Existing reports suggest that little bone bonding occurs at endosseous titanium implants, particularly during the early phases of bone formation (Davies, 2007). Nanoscale modifications of topography appear to change the chemical reactivity of bulk materials (Tasker et al., 2007). Ellingsen (2000) demonstrated that the calcium phosphate precipitation on grit blasted titanium was dramatically altered by HF surface treatment that creates nanoscale topographic surface features. When the physical interaction of such titanium disks with bone were measured by a pull-off test, bonding of bone to the HF treated titanium surface was evident (Ellingsen; Lyngstadaas, 2003). Bone bonding may be a benefit attributed to titanium implants through nanoscale surface modification.

Biomimetic features of nanoscale modifications to the endosseous surface tissue – implant interface also address molecular (not cellular) interactions with tissues. Davies (Davies, 2003; Davies, 2007) described the formation of bone/implant bonding at solid surfaces as a four-stage process comprising: the adsorption of non-collagenous bone proteins to the solid surface. Critical to the process is the initiation of mineralization by the adsorbed proteins and incipient surface directed mineralization. In a recent study, Mendes and colleagues (2007) concluded that the traditional “bioactive” lithomorphous materials such as CAPs and bioactive glasses are not obligatory to promote bone-bonding, but rather that a surface should have a sub-micron surface complexity into which the bony cement line matrix can be deposited, and with which it can interact. Nanoscale topography may provide biomimetic surfaces that support hydroxyapatite mineral formation (Ward; Webster, 2006), and related organic phase guidance of bone mineralization (Zhu et al., 2005).

The relative value of nanoscale and micron scale roughness

The development of an implant-bone interface may be influenced by both nanoscale and micron scale parameters of topography. The role of surface parameters (both bulk chemistry and topography) requires consideration of molecular (ionic and biomolecular) interactions with the surface, cell adhesion phenomenon and local biomechanical features of the established interface. It is clear that nanoscale modification will affect the chemical reactivity of an endosseous implant surface and alter the ionic and biomolecular interactions with the surface. Proposed changes include enhanced wettability, altered protein adsorption, and potential mineralization phenomenon. Changes in wettability and altered protein adsorption lead to altered cell adhesion, likely involving both integrin and non-integrin receptors. The potential for mineralization and epitaxial crystal growth in support of early bone bonding could dramatically alter the biomechanical environment of the healing implant in favor of stability.

Various reports support the concept that nanotopography enhances osteoblastic differentiation which could also promote stability and favorably alter the biomechanical environment for healing (See Tables 2 and 3). However, initial clinical stability may require additional considerations of micron-scale topography and overall implant design. The pioneering investigations of Meirelles and co-workers (Meirelles et al., 2007; Meirelles, 2007) suggest that nanometer-scale topography alone is not sufficient to assure robust osseointegration. Investigations that have isolated nanometer-scale topography as an experimental variable in osseointegration have required additional consideration of endosseous implant stability. It is possible that micron level roughness is of additional value

to the process of osseointegration. The theoretical consideration of how forming tissues interlock with micron-level topographic elements (Davies 2003), and how mechanical stimulation of forming tissues is imparted by such topographic elements (Hansson; Norton, 1999) represent ideas that may not be fully displaced by the introduction of nanotopographic modification to the endosseous implant surface.

Nanostructured surfaces for implant dentistry

There are many different methods to impart nanoscale features to the implant surface (see table 1). Several of these methods have already been used to modify implants available commercially. Others are advancing through the research and development process.

As indicated above, positive bone responses occur at nanostructured surfaces tested *in vitro* and *in vivo*. Presently, only a few nanoscale surface topography modifications have been used to enhance bone responses at clinical dental implants. The OsseoSpeed surface (Astra Tech AB, Mölndal, Sweden) possesses nanostructured features created by TiO₂ blasting followed by a proprietary hydrofluoric acid treatment (Abramson et al., 2001; Cooper et al., 2006). Across a micron rough titanium surface, 50–100nm surface accretions of Titanium oxide are observed by SEM analysis (Figure 6). Greater osteoblastic gene expression (Runx2, Osterix, Alkaline Phosphatase and Bone Sialoprotein) was measured in cells adherent to the nanoscale HF treated surface compared to the micron scale surface (Guo et al., 2007). This nanotopography is associated with the elevated levels of gene expression that indicate rapid osteoblastic differentiation. Most recent investigations show that this nanoscale surface modification promotes high levels of IGF-2 and BMP2 and BMP6 expression by adherent human mesenchymal stem cells for prolonged periods of time in culture.

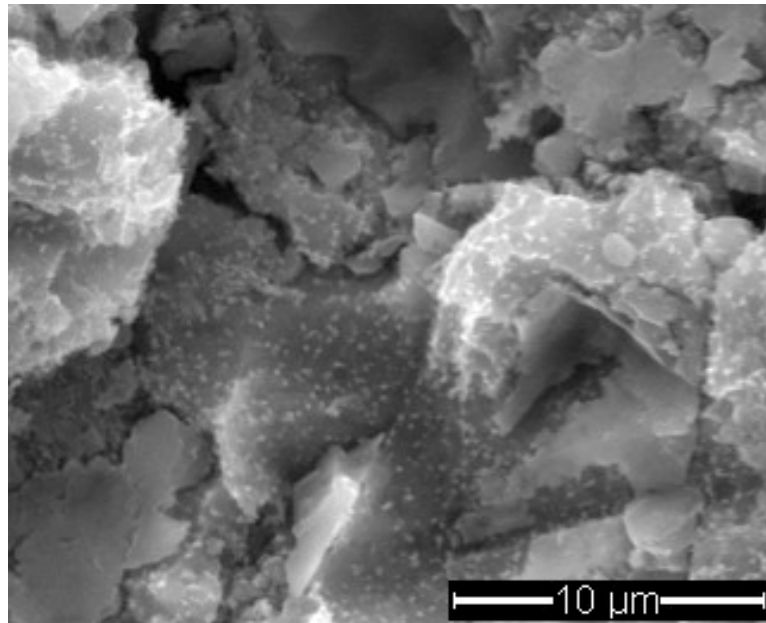


Figure 6 – Scanning Electron Microscopic evaluation of an OsseoSpeed implant. 2,500x magnification of the TiO₂ grit blasted and HF treated implant surface. Note that the TiO₂ grit-blasted surface is randomly covered with surface features of approximately 100nm imparted by the HF etching.

Other studies concerning this nanoscale surface modification have demonstrated an increased bone formation, torque removal value (Ellingsen et al., 2004). In the rabbit tibia model of osseointegration, histomorphometric evaluations demonstrated higher bone-to-implant contact for the nanoscale OsseoSpeed implants compared to the micronscale TiOBlast implants (Astra Tech AB, Molndal, Sweden) at 1 month (35%±14 vs 26%±8) and 3 months (39%±11 vs 31%±6) after placement. Berglundh and colleagues (Berglundh et al., 2007) used a gap model of osseointegration in the canine mandible to demonstrate the amount of new bone that formed in the voids within the first 2 weeks of healing was greater for HF-modified (OsseoSpeed) implants than at TiOBlast implants and concluded that the nanoscale surface promotes osseointegration in the early phase of healing following implant installation.

Clinical evaluation of this implant surface preceded clinical launch and a report of the first data was provided in 2006 (Stanford et al., 2006). 634 patients received 1860 OsseoSpeed™ implants. The initial report indicated 4% surfaces had signs of inflammation (BOP) with plaque present on 12% of sites. 21 patients have lost a total of 25 implants (15 in maxilla and 10 in mandible) for a CISR of 98.7% from placement. Evaluation of this

effectiveness trial performed in more than 100 practices is ongoing. High success in challenging situations such as immediate placement and loading was also reported (Oxby et al., 2006).

Another nanoscale surface implant presently available in the clinical marketplace involves a CaP nanoparticle modification of a minimally rough titanium alloy implant (NanoTite, 3i Implant Innovations, Palm Beach Gardens, FL). The surface has been described as being created by a particulate sol-gel deposition method using discrete crystalline deposition (DCD) of calcium phosphate (CaP) (nominal crystal size 20nm) with surface coverage of approx. 50%. The suggested nanofeature size of the tightly adherent adsorbed CaP/DCD crystal is 50–100 nm. Mendes and co-workers (2007) measured bone ingrowth for implants modified using this technology in a rat tibia model using a well defined bone chamber model. The extend of bone ingrowth was 26.95% and 29.73% for cpTi and Ti alloy modified surfaces compared to the 12.01% cpTi and 16.97% Ti alloy chambers. In a related presentation, Mendes and colleagues (2007) showed bone bonding behavior; DCD, surfaces had statistically greater tensile detachment force (e.g.; 11.30 N nanoscale DCD vs. 1.90 N control).

The nanoscale CaP surface created by DCD (Nanotite, 3i) was further evaluated (Orsini et al., 2007). The histologic evaluation of clinical implants revealed bone to implant contact of $19\% \pm 14.2\%$ and $32.2\% \pm 18.5\%$ for the Osseotite (3i) control and the Nanotite (3i) experimental implants, respectively. Other clinical studies are ongoing to determine the safety and performance of this implant with nanoscale topography. For example, Goene and co-workers (2007) observed greater bone formation at 4 and 8 weeks and concluded that the addition of a nanometer-scale calcium phosphate treatment to a dual acid-etched implant surface appeared to increase the extent of bone development after 4 and 8 weeks of healing. The authors suggest that this rapid accrual of bone at the implant expedites the implant healing period and supports early loading protocols.

Ion Beam Assisted Deposition (IBAD) has also been used to create a commercially available dental implant surface (Coelho; Suzuki, 2005). This technique creates a thin-film over the implant surface by deposition of the chemical element of interest. In one available study, the bone formation (measured by tetracycline labeling quantification) was higher in the experimental group than in the control group (sand-blasted/acid-etched) after two (13.56% vs 24.04%) and four weeks (14.22% vs 27.39%) (Coelho; Suzuki, 2005). An example of this type of surface modification is presented on the Nanotite surface of Bicon Implants (Nanotite,

Bicon Inc. Boston, MA). These very different chemical and physical approaches all impart nanoscale features to existing endosseous cpTitanium implant surfaces.

These initial reports of nanoscale topography implants provide insight into potential advantages for dental implant therapy. High implant survival rates have been reported. The high survival in effectiveness trials involving the HF modified TiO₂ grit blasted surface implant and in challenging clinical examinations may reflect greater control of initial bone formation due to the rapid differentiation of osteoblastic cells observed in laboratory studies. The potential impact of bone bonding measured in preclinical studies requires further study; however, the possible advantages of bone bonding behavior at a titanium surface could have clinical merit. How nanoscale topography and nanotechnology may be used to enhance the tissue-abutment interface remains largely unexplored. It should be noted that the currently available implants differ in their micron-level topography, in their design and in their bulk material composition. It may be difficult to derive specific conclusions from the aggregate data regarding nanoscale surface topography alone. However, for each example of current nanoscale implant surfaces of available implants, cell culture, histological, and clinical data suggests that nanoscale surfaces offer incremental advantages to clinical problems where rapid bone accrual at the implant surface provide solutions.

Conclusions

Nanoscale modification can alter the chemistry and/or topography of the implant surface. Different methods have been described to modify or to embellish titanium substrates with nanoscale features. Such changes alter the implant surface interaction with ions, biomolecules and cells. These interactions can favorably influence molecular and cellular activities and alter the process of osseointegration. Cell culture studies reveal that there exists a range of nanoscale topography that promotes the osteoinductive molecular program for adherent osteoprogenitor cells. Additionally, nanoscale alterations may promote bone-bonding behavior at the titanium-bone interface. Nanoscale modification of titanium endosseous implant surfaces enhances interfacial bone formation measured as bone-to-implant contact. At this moment, both a hydrofluoric acid modified titanium endosseous implant with nanoscale features and two calcium phosphate nanofeature-modified titanium implants are available for clinical use. The potential risks and benefits of manipulating biomaterial interfaces at the nanoscale will be defined by long-term clinical evaluation of such endosseous devices.

Capítulo 3 - Efeito do Recobrimento da Superfície de Implante com Alumina Nanoestruturada na Expressão de Genes Relacionados a Osteoblastos e no Contato Osso-Implante *in vivo*

Novas superfícies de implantes têm sido desenvolvidas e podem ter papel importante no sucesso e manutenção da osseointegração. Vários estudos têm sido feitos para entender a relação entre a superfície de implantes osseointegrados e os osteoblastos. Outra ciência que tem emergido nos dias atuais é a nanotecnologia, que trabalha com partículas em escala atômica, construindo o que se deseja átomo por átomo e isto pode ser importante para a adsorção de proteínas e adesão de células ósseas. O uso da nanotecnologia para alterar a superfície de implantes dentários pode melhorar os resultados clínicos da osseointegração. Este estudo investigou a influência de uma superfície de implante com recobrimento nanoestruturado de óxido de alumínio na diferenciação de osteoblastos, no contato osso-implante e nos valores de torque de remoção. Neste capítulo é apresentada uma pesquisa com a inserção de implantes recobertos com Alumina nanoestruturada em tibia de *Ratus norvegicus*. Todas as superfícies foram caracterizadas química e fisicamente (Microscopia de força atômica - AFM, microscopia eletrônica de varredura – MEV, e micro-análise de Raios X – EDS). Após a inserção, estes implantes foram removidos com 3, 7, 14 e 21 dias, com a medição do torque de remoção. O tecido ósseo ao redor destes implantes foi removido para análise de expressão gênica. Avaliação topográfica e química revelaram diferentes características entre as superfícies. Os valores de rugosidade (S_a nm) foram para as superfícies M:Ac: Al₂O₃ de 86,5:388,4:61,2. Na cultura de células os níveis de expressão de BSP e OCN foram 4,5 e 5,8 vezes maiores na superfícies Al₂O₃. Os níveis de Runx2 também estavam elevados (2x) comparados à superfície usinada (M). Após 56 dias, os valores médios de torque de remoção (Ncm) foram 13,9±1,3, 10,4±3,9 e 9,7±1,4 para Al₂O₃, Ac, e M respectivamente ($p=0.02$ – Kruskal-Wallis). Maior área de contato osso-implante foi observado para a superfície Al₂O₃ comparado ao Ac (dia 56, $p=0,05$) e Al₂O₃ comparada à M (dia 56, $p=0.05$). Os resultados obtidos permitiram concluir que a adição de nanoestruturas a base de Al₂O₃ ao implante de Titânio comercialmente puro (cpTi) promoveu uma diferenciação de células-tronco mesenquimais em osteoblastos. Uma maior expressão de genes relacionados à cascata de diferenciação de osteoblastos foi observado em tecidos adjacentes aos implantes recobertos com Al₂O₃. Foi também observado um aumento associado no contato osso-implante e torque de remoção para esta mesma superfície.

Este capítulo foi aceito para publicação com pequenas modificações no International Journal of Oral and Maxillofacial Implants. Mendonça G, Mendonça DBS, Simões LGP, Araújo AL, Leite ER, Duarte WR, Cooper LF, Aragão FJL. Nanostructured alumina coated implant surface effect on the osteoblast-related gene expression and bone-to-implant contact in vivo. Int J Oral Maxillofac Implants. *In press*.

Nanostructured alumina coated implant surface effect on the osteoblast-related gene expression and bone-to-implant contact in vivo

Abstract

Purpose: The use of nanotechnology to enhance endosseous implant surfaces may improve the clinical control of interfacial osteoblast biology. This study investigated the influence of a nanostructured coated implant surface on osteoblast differentiation and its effects in bone-to-implant contact (BIC) and removal torque values. **Methods:** Titanium disks (6.0x1.0mm) were machined (M) or machined and subsequently treated by acid etching (Ac) or by dipping in an aluminum oxide solution (Al₂O₃). Surfaces were characterized by scanning electron microscopy (SEM), atomic force microscopy (AFM), and X-ray microanalysis (EDX). For the in vitro experiment, rat mesenchymal stem cells (rMSCs) were grown in osteogenic supplements on the disks surfaces for 3 days. Real time PCR was used to measure BSP, OCN, OPN and RUNX-2 mRNA levels. For the in vivo experiment, titanium implants (1.6 x 4.0mm) were placed in rat tibia and harvested after 3-21 days for measurement of bone specific mRNA levels by real-time PCR. Removal torque and bone-implant contact were measured 3-56 days after placement. **Results:** Topographical and chemical evaluation revealed different surface characteristics: average height deviation (S_a nm) values for M:Ac:Al₂O₃ implants were 86.5:388.4:61.2. In cell culture, BSP and OCN levels were 4.5- fold and 5.8-fold greater on the Al₂O₃ surfaces. Runx2 levels were almost 2-fold increased compared to M. In vivo, bone specific mRNAs were all increased on Al₂O₃ adherent cells. Runx2 mRNA levels on Al₂O₃ were increased 2.5 – 3.0-fold compared to M and Ac at 3 – 21 days. At 56 days, mean torque removal (Ncm) was 13.9±1.3, 10.4±3.9 and 9.7±1.4 for Al₂O₃, Ac, and M respectively ($p=0.02$ – Kruskal-Wallis test). Higher bone-to-implant contact was measured for the Al₂O₃ versus Ac (day 56, $p=0.05$) and Al₂O₃ versus M surface implants (day 56, $p=0.05$). **Conclusion:** Nanostructured Al₂O₃ topographic features applied to machined cpTi implants promoted mesenchymal stem cell commitment to the osteoblast phenotype. Greater bone-specific gene expression was observed in tissues adjacent to Al₂O₃ implants and associated increases in bone to implant contact and torque removal were noted. Nanostructured Alumina may directly influence cell behavior to enhance osseointegration.

Key words:

Nanotechnology, Implant surface, Surface treatment, Alumina, Sol-gel coating, Nanostructured surface.

Introduction

In the last ten years, many implant surfaces have been developed beyond the machined cpTitanium surface and are available in the market place. The apparent goal of implant surface improvement has been to improve the bone-implant contact and to decrease healing time. This result is largely attributed to increased osteoblastic activity at dental implant surfaces. Nanotechnology represents a new spectrum of possible surface modification techniques for the implant surface (Christenson et al., 2007; Price et al., 2003a; Price et al., 2003b; Webster et al., 1999; Webster et al., 2000a; Webster et al., 2000b; Webster et al., 2001a). Nanostructured surfaces may increase bone cells differentiation, adhesion and bone matrix production, all of which are mandatory in the process of interfacial bone formation, and also be important in the long term response of the surrounding bone (Webster et al., 1999; Webster et al., 2000a; Webster et al., 2000b; Price et al., 2003a; Price et al., 2003b; Schneider et al., 2003; Gutwein; Webster, 2004; Webster; Ejiogor, 2004; Oh et al., 2005; Webster et al., 2005; Isa et al., 2006; Guo et al., 2007).

Nanosurface topographic features are defined to be approximately 100 nm in scale. This is contrasted to current implant surfaces with micron scale roughness with features of approximately 1 – 2 μ m (Albrektsson; Wennerberg, 2004a). The many potential advantages of nanoscale topographic modification reflect the actual atom-size resolution and quantum behavior of the material (Christenson et al., 2007; Webster et al., 1999). Nanotechnology often involves one-dimensional concepts (nanodots, nanowires) or the self assembly of more complex structures (nanotubes). Materials are also classified according to their form and structure as, nanostructures, nanocrystals, nanocoatings, nanoparticles, and nanofibers (Christenson et al., 2007). Additionally, the surface features may represent biomimetic features resembling the architecture of bone matrix or basement membrane (Teixeira et al., 2003). Cell adhesion and function can be influenced by alteration of adsorbed proteins to the modified surface (indirect) or possibly by interaction of the cell with atomic scale features of the surface itself (direct). Nanostructured surfaces improve protein adsorption, such as vitronectin that affects cell adhesion (Webster et al., 2000b; Webster et al., 2001b), and they can induce MSC to express osteoblast differentiation genes even in the absence of other inductive media (Dalby et al., 2007). This may positively influence osteoblastic cells adhesion and differentiation.

The deposition of nanoparticles onto the titanium surface represents one of many approaches to imparting nanofeatures to a titanium dental implant. They offer the possibility of modifying the surface of surgical-grade materials to achieve improvement in performance,

reliability and biocompatibility (Ben-Nissan; Choi, 2006). Several investigations have applied sol-gel transformation techniques to achieve deposition of nanometer scale calcium phosphate, Alumina, Titania, Zirconia and other materials to the implant surface (Kim et al., 2004; Lee et al., 2006). The advantages of sol-gel coating include homogenous and pure product owing to mix in the molecular scale, reduced firing temperatures and it is easily applied to complex shapes with a range of coatings techniques (Ben-Nissan; Choi, 2006). Owing to their resultant atomic-scale interactions, the accretions display strong physical interactions (Piveteau et al., 2000; Arias et al., 2003; Ben-Nissan; Choi, 2006; Choi; Ben-Nissan, 2007).

Osseointegrated implants are very predictable in diverse situations, such as the treatment of edentulism or of partially dentate or single missing teeth, both using delayed and immediate loading strategies (Adell et al., 1981; Adell et al., 1990; Cooper et al., 2007). However, in poor bone quality conditions, these outcome may become unpredictable (Neves et al., 2006). By changing the implant surface and the rate at which bone accumulates around the implant, improved clinical responses may be obtained in poor bone quality situations (Cooper et al., 1998; Puleo; Nanci, 1999; Abron et al., 2001; Schneider et al., 2003; Buser et al., 2004; Isa et al., 2006; Cooper et al., 2006; Guo et al., 2007).

Based on the hypothesis that nanostructured surfaces can modulate adherent cellular responses, the aim of this study was to investigate the response of a novel nanostructured cpTitanium implant surface at the level of osteoblast differentiation and at the level of interfacial bone formation by measurement of bone-to-implant contact and removal torque values. This project investigated the hypothesis that nanostructured cpTitanium endosseous implant surfaces alter initial osteoinductive responses of adherent cells to support the accrual of interfacial bone mass.

Materials and Methods

Implants and Disks Preparation

Commercially pure grade IV titanium disks (6.0x1.0 mm) were initially prepared by machining (turning). One third of the disks were subsequently treated by dual acid etching (Neodent Implante Osteointegravel Ltda., Curitiba, PR, Brazil), and one third by coating with an aluminum oxide (Al_2O_3) nanocoating. The coated surfaces were prepared by dip coating the entire disk/implant in an Aluminum containing solution. This solution was prepared using the polymeric method (Pechini, 1967) (Nanox SA, São Carlos, SP, Brazil). The disks were divided into three groups: machined (M), acid etched (Ac), and Alumina nanocoating (Al_2O_3).

Threaded implants for the rat tibia were fabricated from commercially pure grade IV titanium (1.6x4.0 mm) by turning (Neodent Implante Osteointegravel). One third of the implants were acid etched and the other one third were coated with aluminum oxide. All implants and disks were subsequently cleaned and sterilized according to standard procedures for manufacture of dental implants.

Surface Analysis

The surface of the disks was examined by a high-resolution scanning electron microscope (Supra 35, Carl Zeiss, Oberkochen, Germany) to identify the presence of nanofeatures. Atomic force microscopy (Nanoscope IIIA atomic force microscope, Digital Instruments, Santa Barbara, CA, United States) was performed to characterize the roughness parameter of these surfaces. AFM analysis was performed in Tapping-Mode. A measurement area of 50x50 μm was used. The images were corrected with a third order least mean square fit (SPIPTM, Image Metrology, Denmark). AFM observations were made at three different points on the disks surfaces (3 disks per group), and average values were calculated for the following parameters: Sa (nm) - the arithmetic average height deviation from a mean plane; Sq (nm) - the root mean square parameter; Sdr (%) - the developed surface ratio; and Sci - core fluid retention index (Wennerberg; Albrektsson, 2000). The chemical composition of the surfaces was analyzed by X-ray microanalysis (EDX) in a Zeiss DSM 940A (Carl Zeiss, Oberkochen, Germany) scanning electron microscope outfitted with an Oxford INCA X-sight microanalysis system (Oxford Instruments, the United. Kingdom).

In vitro - Cell Culture

Bone marrow cells were isolated from the femurs of 8-week-old Sprague Dawley rats and maintained using α -Modified Eagle's Media (MEM) and 10% fetal bovine serum (FBS). At 80% confluence in 100mm dishes, cells were detached by trypsin-EDTA treatment. 50,000 cells in 50 μl of media were plated onto 6 mm titanium disks for 4 hours. After initial cell attachment, additional culture media was added. Osteoblastic differentiation was initiated 24 hours after plating of cells onto the titanium disks by changing culture media to differentiation media containing 10^{-8}M dexamethasone, 50nM ascorbic acid and 2.5 μM beta-glycerophosphate. At the 3rd day of the differentiation period the cells were detached from the disks and the RNA was isolated for molecular analysis.

In vitro - RNA isolation and analysis

For evaluation of mRNA expression in cells adherent to titanium disks. Titanium disks were removed from the culture dishes and rinsed twice with cold phosphate buffered saline (PBS). Adherent cells on each disk were lysed using Trizol (Invitrogen, Carlsbad, CA) and

the lysates were collected by pipetting and centrifugation. Total RNA in the cell lysates was isolated using the Trizol protocol and collected by ethanol precipitation. Total RNA was quantified using UV spectrophotometry. From each total RNA sample, cDNA was generated using SuperScript reverse transcriptase (Invitrogen, Carlsbad, CA) in a standard 20 μ L reaction. All cDNAs were subjected to polymerase chain reaction (PCR) for GAPDH mRNA as a test of RNA integrity and cDNA synthesis. Subsequently, equal volumes of cDNA were used to program real time PCR reactions specific for mRNAs encoding BSP, OCN, OPN and RUNX-2. Reactions were performed using TaqMan Universal PCR Master Mix (Applied Biosystems, Foster City, CA) and thermocycling in an ABI 7200 real time thermocycler (Applied Biosystems, Foster City, CA). Relative mRNA abundance was determined by the $2^{-\Delta\Delta Ct}$ method and reported as fold induction. GAPDH abundance was used for normalization.

In vivo - Animal Surgery

A rat tibia model of osseointegration was used (Masuda et al., 1997). All procedures were performed according to a University of Brasilia approved protocol. Male Wistar rats (12-week-old) were purchased and acclimated for 7 days prior to initiation of studies. Anesthesia was achieved using ketamine / xylazine (80-100 mg/kg and 10-20 mg/kg respectively) and supplemental local anesthesia was obtained using lidocaine 2% with epinephrine (1:100:000). Each surgical site was shaved, prepared using betadine scrub and then isolated for implant placement by a full thickness myocutaneous flap. Implants were placed distal to the tibial diaphysis using a stepwise drilling procedure performed with dental drills and using sterile saline irrigation. Implants were placed into the osteotomies by a self-tapping procedure. The sites were closed using resorbable sutures. Buprenorphine (0.01 – 0.05 mg/kg) was administered as post-surgical analgesia and 5 mg/kg of ketoprofen subcutaneously 24 hours post-operatively. Animals were evaluated continuously following surgery and ambulation using the implanted limbs was the defined criteria for immediate recovery. The animals were sedated and euthanized with an overdose of thiopental.

For the molecular analysis, two implants were placed in each tibia to provide sufficient RNA for each experimental sample. The first implant was inserted 7mm away from the knee joint and the second implant was 5mm distal to the first one. The time points for molecular analyses were 3, 7, 14 and 21 days after implant placement. For every time point, three rats were used for each implant surface (n =3 rats / time point).

For removal torque analysis, two implants were placed in each tibia. The implants were inserted as described above. The time points for removal torque analysis were 3, 7, 14, 21 and 56 days after implant placement. For every time point, three rats were used for each

implant surface (n =3 rats / time point). After sacrifice, implant resistance to torque was measured using a torque-gauged wrench (1200ATG-NS; Tochnichi, Tokyo, Japan).

For the histological analysis, one implant was placed in each tibia. The implant was inserted 7 mm away from the knee joint. The time points for histological analyses were 7, 21 and 56 days after implant placement. For every time point, three rats were used for each implant surface (n =3 rats / time point). The tibias were removed and fixed in 4% phosphate-buffered formalin (pH 7.0), for 10 days, and then transferred to a solution of 70% ethanol until processing. The specimens were dehydrated in increasing concentrations of ethanol up to 100%, infiltrated and embedded in methylmethacrylate resin (London Resin Company, Berkshire, England), according to the technique described by Donath & Breuner (1982). The final histomorphometry sections were approximately 50 µm thick and stained with Toluidine Blue for optic microscopic analysis.

In vivo - RNA isolation and analysis

Immediately following sacrifice, the implants were unscrewed and the surrounding bone tissue removed with a 2.0 mm trephine. The tissues were kept frozen in liquid nitrogen until the RNA isolation procedure. Tissue was ground with mortar and pestle in liquid nitrogen. Total RNA in the cell lysates was isolated using the Trizol (Invitrogen, Carlsbad, CA) according to the manufacturer's protocol and collected by ethanol precipitation. Total RNA was quantified using UV spectrophotometry. From each total RNA sample, cDNA was generated using SuperScript reverse transcriptase (Invitrogen) in a standard 20 µL reaction. All cDNAs were subjected to polymerase chain reaction (PCR) for GAPDH mRNA as a test of RNA integrity and cDNA synthesis. Subsequently, equal volumes of cDNA were used to program real time PCR reactions specific for mRNAs encoding ALP, BSP, OCN, OPN and RUNX-2 as described above. GAPDH abundance was used for normalization.

Histomorphometry

Longitudinal histological sections from each implant were captured through a video camera Sony (Sony Corp, Tokyo, Japan) joined to a light microscope. The images were analyzed through the Bioquant Nova (Bioquant Image Analysis Corporation, Nashville, TN), where the percentages of bone-to-implant contact (BIC) were determined. Through linear measurements, the percentages of mineralized bone in direct contact with the implant surface were determined (Masuda et al., 1997).

Statistical analyses

Descriptive statistics were calculated using SPSS. The roughness parameter (S_a) was compared by one-way ANOVA followed by Tukey Test. Comparison of Torque removal values and histomorphometric measurements on implants in vivo was performed by Kruskal-Wallis test. For all statistical analysis significance level was set at $p \leq 0.05$.

Results

Surface analysis

SEM and AFM evaluation reveal marked topographic differences among the M, Ac, and Al_2O_3 surfaces. For the Al_2O_3 implants (Figure 1), at 50,000x and 100,000x magnification a nanoscale topography is distributed on the entire surface with features of approximately 20 nm in diameter (nanopores). For the Machined and Acid etched surfaces the images are shown in Figure 2 and there is no evidence, or just a few, nanofeatures on the surface at 50,000x and 100,000x.

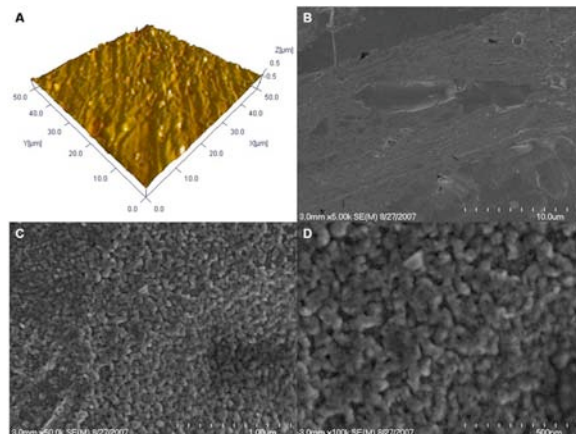


Figure 1 – AFM and SEM evaluation of the Aluminum oxide coated implant surface. A- Surface roughness (AFM). B, C and D- SEM images at low and high magnification. At 50,000x and 100,000x magnification the nanofeatures of the surface are evident (C and D).

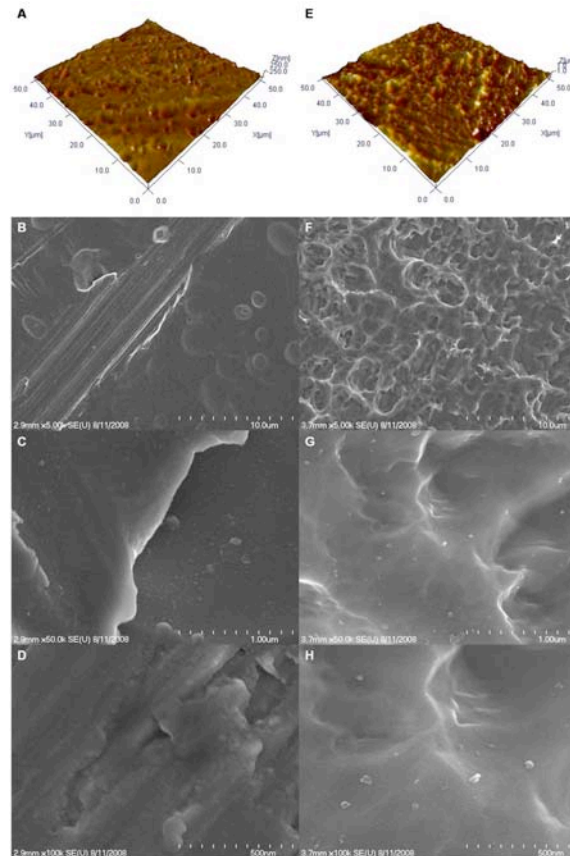


Figure 2 – AFM and SEM evaluation of the Machined and Acid etched implant surface. A- Surface roughness (AFM) for Machined. B, C and D- SEM images at low and high magnification for the Machined surface. E- Surface roughness (AFM) for Acid etched. F, G and H- SEM images at low and high magnification for Acid etched surface. At 50,000x and 100,000x magnification a very few nanofeatures are observed (D and H).

Surface roughness parameters were obtained from the AFM analysis and are described in Table 1. The roughness profile is shown in figures 1 and 2. AFM images and resultant values for Al₂O₃ coated surfaces were reduced compared to machined surfaces and resulted from the coating process. At higher resolution, nanoscale features were evident on the coated surfaces.

Table 1 - Roughness parameters - Atomic force microscopy surface characterization (50 x 50 μ m), mean \pm SD.

	M	Ac	Al ₂ O ₃
Sa (nm)	86.52 \pm 6.75 ^{*D}	388.40 \pm 16.02 ^{*C}	61.19 \pm 1.81 ^{*A}
Sq (nm)	111.10 \pm 11.29	488.51 \pm 18.18	80.80 \pm 1.76
Sdr (%)	0.58 \pm 0.27	13.65 \pm 0.32	0.81 \pm 0.01
Sci	1.37 \pm 0.04	1.88 \pm 0.02	1.28 \pm 0.10

*Means were significantly different at $p \leq 0.05$.

The chemical analysis showed the general composition of the three implant surfaces (Figure 3). The chemical composition of the M surface was essentially Titanium and traces of

small contaminants from machining process (Figure 3 A). The Ac surface presented Titanium with no traces of other contaminants (Figure 3 B). The Al₂O₃ surfaces were traces of Titanium, Aluminum and Oxygen (Figure 3 C). For the Al₂O₃ implant surface, the EDX surface scanning showed that Aluminum and Oxygen was distributed over the entire implant surface (Figure 4).

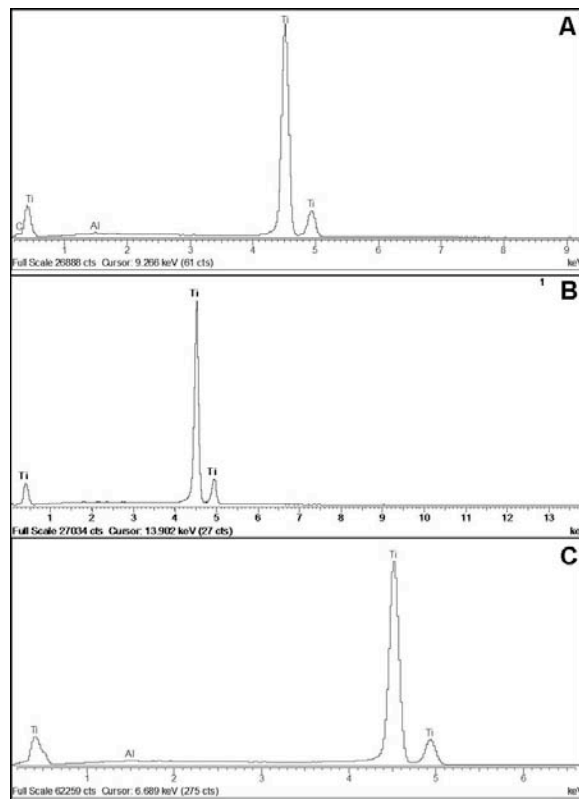


Figure 3- X-ray microanalysis (EDX) of the chemical composition of the implant surface. A- Machined. B- Acid etched. C- Aluminum oxide coated.

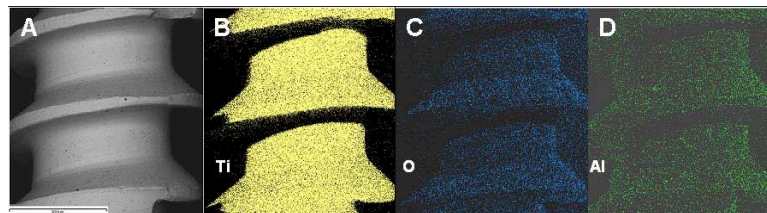


Figure 4- X-ray microanalysis (EDX) of the Aluminum oxide coated implant. A- SEM image of the implant. B, C and D- Scanning of the surface demonstrate the presence of titanium (B), oxygen (C) and aluminum (D) covering the surface.

Gene expression analysis

Surface modifications using Ac and Al₂O₃ had different effects on osteoblastic gene expression. To verify the influence of surface nanotopography on the initial behavior of the adherent cells, the expression of key osteogenic mRNAs was evaluated 3 days after plating of cells onto the three different implant surfaces. The expression level for rat stromal cells

adherent to the Al₂O₃ surface was at least 2 fold higher than the machined surface for BSP, OPN, OCN and RUNX-2 (Figure 5).

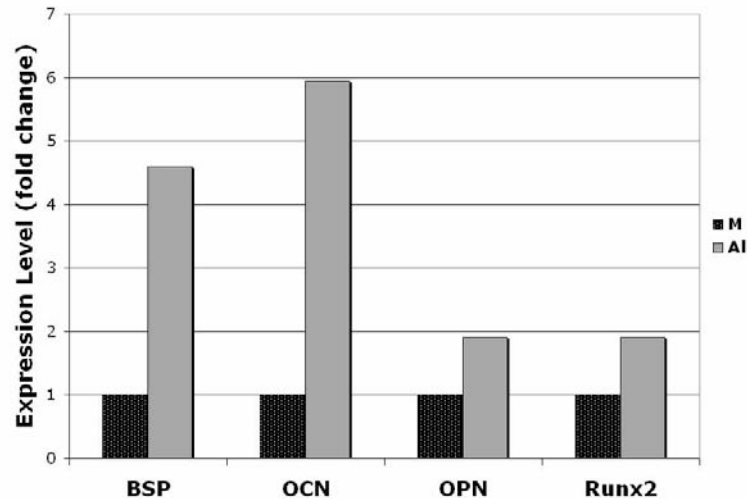


Figure 5 - Adherent rMSCs bone-specific mRNA expression. Total RNA was isolated from cells 3 days of culture on M, Ac, and Al₂O₃ treated Titanium disks. Expression levels for bone sialoprotein (BSP), osteocalcin (OCN), osteopontin (OPN) and Runx2 are shown as -fold change in mRNA levels ($2^{-\Delta\Delta C_t}$ method; baseline = day 0 undifferentiated cells).

When osteoblastic gene expression was measured in bone surrounding endosseous implants harvested following placement in rat tibia, osteoblast-specific mRNA levels were greater in bone surrounding Al₂O₃ versus M implants. For example, ALP expression levels were increased in Al₂O₃ adherent cells after 3 days. For Ac implants, ALP mRNA levels in bone surrounding implants increased only after day 14. The relative expression of ALP was further delayed in bone surrounding M implants, with expression being elevated after 21 days. ALP levels were highest on Al₂O₃ surfaces at all time points (Figure 6). Osteopontin levels for the Al₂O₃ surface were upregulated at day 14 up to day 21 (Figure 6c).

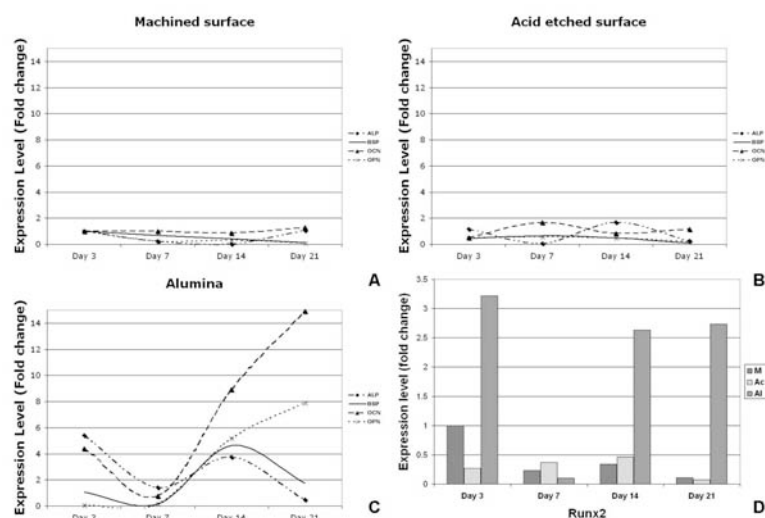


Figure 6 – Bone-specific mRNA expression in bone tissue adjacent to M, Ac or Al₂O₃ implants. Total RNA was isolated from peri-implant bone tissues after 3, 7, 14 and 21 days. Expression levels (fold change) for ALP, BSP, OCN, OPN are compared for Machined, Acid etched and Aluminum oxide coated implants, in A, B and C, respectively. D, the RNA levels for Runx2 in peri-implant bone tissues surrounding Machined, Acid etched and Aluminum oxide coated implants are compared as fold change 3 – 21 days following implant placement. The results are shown as fold change ($2^{-\Delta\Delta C_t}$ method).

Further evidence of differential osteoblastic activity in bone surrounding the various implants was provided by measurement of BSP expression. BSP levels were 8-fold increased 14 days for bone derived from tibia with Al₂O₃ implants. This level persisted for 21 days. In contrast, BSP mRNA levels were not elevated on Ac or M implant samples. (Figure 6).

Osteocalcin mRNAs were also evaluated in the bone around dental implants in this study. OCN levels were increased after 3 days in bone samples derived from tibia with the Al₂O₃ implants. These levels further increased at day 14 with the highest levels being attained at day 21. For samples involving both the Ac and M implants, modest increases were noted even after 21 days (Figure 6).

Runx2 mRNAs from bone among the three different implant types was also compared. The levels of Runx2 in bone samples from Al₂O₃ implants were elevated on days 3, 14 and 21. No present explanation is available for the absence of expression among the day 7 implant data (Figure 6d).

Removal torque

The mean removal torque for all surfaces was similar up to day 21, and then higher for the Al₂O₃ implant group thereafter. The mean removal torque after 56 days was 13.9 ± 1.3 Ncm, 10.4 ± 3.9 Ncm, and 9.7 ± 1.4 Ncm for the Al₂O₃, Ac, and M implant groups, respectively. There were significant differences between the Al₂O₃ and Acid etched ($p=0.02$) groups and between the Al₂O₃ and Machined ($p=0.01$) groups at day 56 (Figure 7).

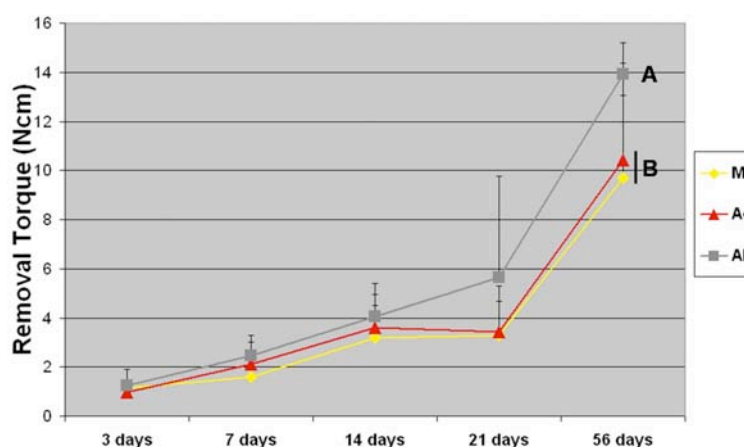


Figure 7 – Removal torque values for Machined, Acid Etched and Aluminum Oxide treated Titanium implants. Removal torque was measured for 6 implants / surface / timepoint. (*= $p<0.05$ compared to Machined day 56 – Kruskal-Wallis test).

Histomorphometric analysis

The histomorphometric analysis revealed a higher bone-to-implant contact for the Al₂O₃ implant group. A more rapid accrual of interfacial bone was suggested by the increase in BIC from day 7 to 21 compared to M and Ac implant groups. There were significant differences between the Al₂O₃ and Acid etched groups and between the Al₂O₃ and Machined groups at days 21 ($p=0.05$) and 56 ($p=0.05$) (Figure 8). There were also significant differences between Acid etched and Machined groups at 21 ($p=0.05$) and 56 days ($p=0.05$) (Figure 8 and 9).

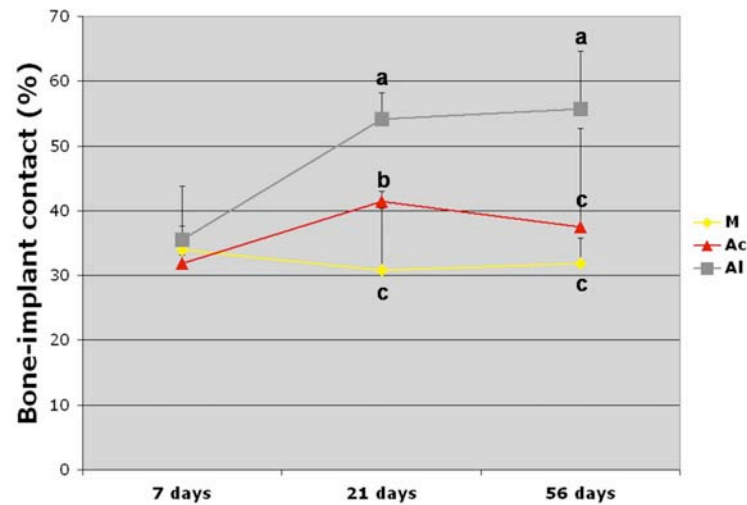


Figure 8 – Bone-to-implant contact for Machined, Acid Etched and Alumina Oxide treated Titanium implants. Histomorphometric measurement of bone to implant contact was calculated for 3 implants / surface / timepoint. The mean percent of bone to implant contact is shown. Different letters mean statistically significant differences ($p < 0.05$ – Kruskal-Wallis test).

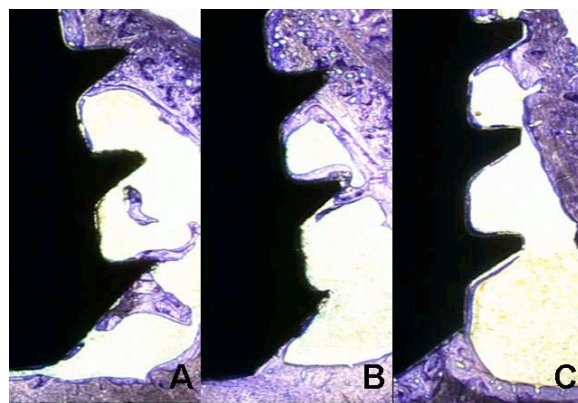


Figure 9 - Histological representation of the bone-to-implant contact developed after 56 days at the implants placed in this rat tibia model. Machined (A), Acid etched (B) and Aluminum oxide coated (C) implants. (toluidine blue; original magnification x6.25).

Discussion

The effects of nanostructured topography on adherent osteoblast responses regarding differentiation and mineralization have been addressed in several previous *in vitro* studies (Webster et al., 1999; Webster et al., 2000a). *In vivo* studies have been performed in only a few investigations (Ellingsen et al., 2004; Guo et al., 2007; Meirelles et al., 2008a). The mechanism by which nanotopography improves osteoblast response at endosseous titanium implants is not fully appreciated. This study employed the rat model to gain insight into the potential differences that occur during the osseointegration process at an Aluminum oxide coated titanium implant with defined nanometer-scale features versus implants with

defined machined and acid etched surfaces devoid of intentionally arrayed nanoscale features. The *in vivo* molecular data, the histomorphometry and the removal torque data suggest that, when compared with machined or acid etched cpTitanium implant surfaces, the nanoscale Alumina coated implant surface supported greater osteoblastic differentiation, osteoblast-specific gene expression, related bone accrual and mechanical interaction with surrounding bone.

This study sought to evaluate a sol-gel deposited nanocoating of Alumina on cpTitanium endosseous implant behavior with cells and tissues. The main limitation of this investigation involves the superimposition of a nanoscale topography (Al₂O₃ coating) on a micron scale structure (machined titanium). While the machined surface served as one control and an acid etched surface provided insight into cellular responses to increased micron scale surface features, the present investigation did not experimentally segregate nanoscale feature effects from potential influences of micron scale topography. Webster and colleagues al (1999; 2000a), presented positive effects of nanostructured Alumina, Titania and Hydroxyapatite when compared to the same materials in micron scale. This strongly implicates the nanostructures in control of osteoblast function. The present investigation also did not segregate potential effects of surface chemistry, a situation commonly encountered in such studies (Webster et al., 2000a; Webster et al., 2001a; Oh et al., 2005). Other recent studies have shown that the size and characteristics of the features may be more important than chemical composition effects alone (Mendes et al., 2007; Meirelles et al., 2008b). Despite these limitations, the data indicates that superimposition of nanoscale topographic features using Al₂O₃ coating on machined Titanium endosseous implants increased the osteogenic behavior of cells and resulting bone to implant contact. The measured cell behavior suggests that changes in topography affected osteogenesis of adherent and neighboring cells.

The comparison presented offers insight into the influence of the addition of nanoscale topography to implant surface design. The machined surface is well represented among clinical dentistry and supporting literature. The acid etched surface used here is akin to some of the acid etched dental implant surfaces currently promoted to enhance bone to implant contact and dental implant clinical performance. The modest molecular changes in gene expression that occurred at the acid etched surface are not inconsistent with the minimally rough micron level architecture (Albrektsson; Wennerberg, 2004a). The machined surface offers a baseline for comparison. Alumina has been used as implant treatment material for many years (Shishido et al., 2003; Murphy et al., 2006), and more recently,

together with nanotechnology, it has again been applied to improving biocompatible tissue responses. It may be possible to pursue clinical translation of this technology.

One issue that need to be addressed is related to the fact that some studies have shown a probable cause / effect between Alumina particles (as used for sandblasting or a contaminating) and adverse effects in bone cells (Canabarro et al., 2008). Other investigators found no relation between Alumina particles and bone-to-implant contact (Piattelli et al., 2003). Whether or not this is true, sol-gel derived coating have an ability to form a physically and chemically uniform and durable coating over the surface and the low temperatures used during the processing avoid decomposition of the coating material (Ben-Nissan; Choi, 2006). Studies addressing the effects of nano- versus micron- sized particles have demonstrated a less cytotoxic effect of nano-sized Alumina and Titania when compared to micron-sized same material (Gutwein; Webster, 2004).

The removal torque analysis showed similar low values for all three surfaces at day 3, 7 and 14. This is consistent with the early responses of bone tissue to surgical intervention. However, from day 21 up to day 56, the Al₂O₃ implants presented a higher increase in torque removal and BIC values compared to M and Ac implants. Statistically significant differences in removal torque values were revealed only after 56 days. Although after 21 days a marked separation between Al₂O₃ removal torque values and M and Ac are noted (Figure 7). This parallels the emergence of significantly greater bone accrual at the Al₂O₃ implants after 21 days. Suggested is a relationship between torque removal and bone to implant contact. The torque removal analysis in this study appears to be related to the other results obtained in this study and also with other papers that used the same analysis (Narai; Nagahata, 2003). The acknowledgement of increased bone to implant contact had occurred in the same time frame as increased torque removal suggests that the surface nanofeatures influenced bone accrual predominantly and potential physicochemical interactions with surrounding bone (bone bonding) secondarily. Comprehensive proof that one surface parameter (nanoscale features alone) affected the bone bonding behavior of the implant requires isolation of individual variables. This cannot be fully accomplished using the complex (nano/micron) topographic character of the implant design under current study.

Enhanced bone accrual was measured directly (Figure 9) and indirect suggestions for the underlying cellular processes was provided by demonstration of increased levels and accelerated expression of bone specific genes. Notable among this data set is the expression of the key osteoinductive transcription factor Runx2. Elevated Runx2 expression is characteristic of osteoblast differentiation (Harada; Rodan, 2003), and its early expression

has been observed in other in vitro studies of titanium implant surfaces with nanoscale features (Guo et al., 2007). In a recent study, Dalby and colleagues (2007) demonstrated that in the presence of nanofeatures, MSCs are able to initiate and display some osteogenic markers even without cell culture induction of the cells along the osteoblast pathway. In this report, similar in vitro measurements of the rat bone marrow derived MSCs showed at 3 days an increase in Runx2 mRNA levels as well as concomitant increases in BSP, OCN, OPN levels by cells adherent to Al₂O₃, but not M or Ac disks (Figure 5).

This in vitro data of incipient cell – implant surface interactions reflects the in vivo analysis of gene expression events that occurred in the bone adjacent to the different implants. As in cell culture, the Al₂O₃ implants in vivo supported early and elevated and sustained RUNX2 expression. In this study it is suggested that an early expression of Runx2 might have played an important role in the results seen with the other genes expression levels (Figure 6). The Runx2 elevations will increase the expression of other bone related genes such as Alkaline phosphatase, Collagen type I, Osteocalcin, and Osteopontin (Harada et al., 1999). The enhancement of RUNX2 expression could represent a fundamental aspect of stromal cell behavior at Al₂O₃ nanoscale topography. Other studies of cellular responses to nanofeatures superimposed on implant surfaces demonstrate similar elevations of RUNX2 (Isa et al., 2006; Guo et al., 2007) relative to cells adherent to surfaces with micron scale roughness only. It is not clear yet how nanotopography improves osteoblast response, but it is clear it has an important role in cell differentiation (Webster et al., 2000a; Guo et al., 2007; Dalby et al., 2007). A systematic investigation of how nanoscale topography of a given bulk chemistry affects the processes underscoring the result of osseointegration is indicated.

Conclusion

Modification of machined cpTitanium surfaces by application of a nanoscale Al₂O₃ coating (20 – 100 nm features) improved mesenchymal stem cell differentiation in the osteoblastic pathway in vitro and in vivo. Similarly, greater bone-specific gene expression was measured in tissues adjacent to Al₂O₃ implants versus machined and acid etched implants both in vitro and in vivo. Associated increases in torque removal values and bone to implant contact were also observed for the Al₂O₃ implants. Nanostructured aluminum oxide coating applied to a machined cpTitanium endosseous implants may directly influence cell behavior to enhance osseointegration.

Capítulo 4 - Efeito da Superfície de Implante Nanoestruturada na Expressão de Genes Relacionados à diferenciação de Osteoblastos e no Contato Osso-Implante *in vivo*

Neste capítulo, a nanotecnologia para alterar a superfície de implantes dentários foi utilizada para produzir um recobrimento nanométrico a base de óxido de titânio ou óxido de zircônio. Este estudo investigou a influência destas superfícies de implante com recobrimento nanoestruturado na diferenciação de osteoblastos, no contato osso-implante e nos valores de torque de remoção. Estes implantes recobertos com uma camada nanoestruturada a base de óxido de titânio ou óxido de zircônio foram inseridos em tibia de *Ratus norvegicus*. Todas as superfícies foram caracterizadas química e fisicamente (Microscopia de força atômica - AFM, microscopia eletrônica de varredura – MEV, e micro-análise de Raios X – EDS). Após a inserção, estes implantes foram removidos com 3, 7, 14 e 21 dias, com a medição do torque de remoção. O tecido ósseo ao redor destes implantes foi removido para análise de expressão gênica. Os níveis de mRNA para as superfícies nanoestruturadas estavam aumentados quando comparados a superfície usinada (M). Após 56 dias, os valores médios de torque de remoção (Ncm) foram: $11,6 \pm 2,5$, $11,3 \pm 2,4$, $11,1 \pm 3,5$, $9,7 \pm 1,4$ para An, Ru, Zr, e M, respectivamente. Maior BIC (%) foi observado para todas as superfícies nanoestruturadas comparadas a usinada (M) após 21 e 56 dias. $65,77 \pm 6,49$, $51,81 \pm 7,20$, $51,49 \pm 6,46$, $31,88 \pm 3,84$, para Zr, An, Ru, e M após 56 dias, respectivamente ($n=3$, $p<0.05$; Kruskal-Wallis). Os resultados obtidos permitiram concluir que a adição de nanoestruturas a base de TiO_2 e ZrO_2 aos implantes de Titânio comercialmente puro (cpTi) promoveram uma diferenciação de células-tronco mesenquimais em osteoblastos. Uma maior expressão de genes relacionados à cascata de diferenciação de osteoblastos também foi observado em tecidos adjacentes aos implantes recobertos com TiO_2 e ZrO_2 , especialmente à superfície ZrO_2 . Tendo sido novamente observado um aumento associado no contato osso-implante e torque de remoção para esta mesma superfície.

Este capítulo foi submetido para publicação com pequenas modificações. Gustavo Mendonça, Daniela Baccelli Silveira Mendonça, Luis Gustavo Pagotto Simões, André Luis Araújo, Edson Roberto Leite, Wagner Rodrigues Duarte, Lyndon F. Cooper, Francisco J. L. Aragão.

Nanostructured implant surface effect on the osteoblasts gene expression and bone-to-implant contact in vivo

Purpose: The aim of this study was to investigate the response of a nanostructured implant surface at the level of osteoblast differentiation and its effects in bone-to-implant contact (BIC) and removal-torque values (RTV). **Methods:** Commercially pure grade IV titanium implants (1.6x4.0 mm) were machined or machined and subsequently treated by dipping in an oxide resin solution. The surfaces were divided into four groups: machined (M), and nanostructured: titania-anatase (An), titania-rutile (Ru), and zirconia (Zr). Surfaces were examined by scanning electron microscopy (SEM), atomic force microscopy (AFM), and by X-ray microanalysis (EDX). Implants for all the surfaces were inserted in rat tibia and harvested from 0-21 days for measurement of Alkaline Phosphatase (ALP), Bone Sialoprotein (BSP), Osteocalcin (OCN), Osteopontin (OPN), and RUNX-2 mRNA levels by real time PCR; from 0-56 days for RTV; and from 0–56 days for BIC. **Results:** mRNA levels on all nanostructured surfaces were increased compared to M. At 56 days, the mean RTV in Ncm was 11.6 ± 2.5 , 11.3 ± 2.4 , 11.1 ± 3.5 , 9.7 ± 1.4 for An, Ru, Zr, and M, respectively. Higher BIC (%) was measured for the all nanostructured surfaces versus M at 21 and 56 days. 65.77 ± 6.49 , 51.81 ± 7.20 , 51.49 ± 6.46 , 31.88 ± 3.84 , for Zr, An, Ru, and M at 56 days, respectively ($n=3$, $p<0.05$; Kruskal-Wallis test). **Conclusion:** Nanostructured topographic features composed of TiO_2 or ZrO_2 applied to machined cpTi implant promoted greater mesenchymal stem cell commitment to the osteoblast phenotype and associated increased BIC and physical association with bone.

Key-words:

Titanium oxide, Zirconia oxide, Nanostructured, Implant surface.

Introduction

Advances in materials science and biotechnology have led to many improves in implant and bone regeneration therapy (Buser et al., 2004; Cooper et al., 2006; Guo et al., 2007). Modifying the implant surface is one way of improving bone-to-implant contact and the host response to a better and more reliable osseointegration process (Buser et al., 2004; Cooper et al., 2006; Guo et al., 2007). Implant surface technology has experienced many advances during the last two decades. In the last ten years many novel implant surfaces have been developed and became available in the market. Nanotechnology allows the manipulation of materials at the atom level creating a surface that is more interactive to the molecules and structures that are related to the host cells. Many studies have demonstrated the effect of nanotechnology by means of improved cell attachment, proliferation, differentiation, and in the case of bone cells, the deposition and mineralization of the bone matrix (Webster et al., 1999; Webster et al., 2000a; Webster et al., 2000b; Webster et al., 2001a; Price et al., 2003a; Price et al., 2003b; Mendes et al., 2007; Guo et al., 2007).

Deposition of nanoparticles onto the titanium surface represents one of many approaches to imparting nanofeatures to a titanium dental implant (Mendonca et al., 2008). Sol-gel techniques achieve deposition of nanometer scale accretions to the implant surface (Kim et al., 2004; Lee et al., 2006). Alumina, titania, zirconia, hidroxyapatite, and other materials can be applied using this technique (Ben-Nissan; Choi, 2006). Owing to their resultant atomic-scale interactions, the accretions display strong physical interactions with the underlying surface (Ben-Nissan; Choi, 2006; Piveteau et al., 2000; Arias et al., 2003).

The exact mechanism by which nanostructured surfaces allow this improved cell response is still not fully understood. Some studies have demonstrated an increase in protein adsorption on the surface when nanostructures are present (Webster et al., 2001a). Another studies have shown an upregulation in osteoblast specific genes that drives the osteoblastic pathway (Guo et al., 2007; Isa et al., 2006). Imparting nanofeatures to the surface can create a hydrophilic surface that helps protein adsorption and increased cell adhesion (Webster et al., 2001a).

The outcomes of osseointegrated implants have been very predictable in many different situation, such as fully, partially or single edentulism not only in delayed healing but also in immediate loading (Adell et al., 1981; Adell et al., 1990; Cooper et al., 2007). However, in poor bone quality conditions, theses outcomes may become unpredictable (Neves et al., 2006). By changing the implant surface, the way bone heals around the

implant can be modified and this can assure a better bone-to-implant contact in poor bone quality situations. Based on the fact that Titanium implant surfaces imparted with nanofeatures can modulate adherent cellular responses, the aim of this study was to investigate the response of three different nanostructured cpTitanium implant surfaces at the level of osteoblast differentiation and at the level of interfacial bone formation by measuring gene expression, removal torque values and bone-to-implant contact.

Materials and Methods

Implant Design and Surface Analysis

Commercially pure grade IV titanium disks (6.0x1.0 mm) were prepared by machining (Neodent Implante Osseointegrável, Curitiba, PR, Brazil). Other disks were subsequently treated by coating with a Titanium or Zirconium oxide (TiO₂ or ZrO₂) nanocoating. The coated surfaces were prepared by dip coating the implant in a Titanium or Zirconium containing solution. The disks were divided into four groups: machined (M), Titania-Anatase (An), Titania-Rutile (Ru), and Zirconia nanocoating (Zr). The surface of the disks was examined by a high-resolution scanning electron microscope (Supra 35, Carl Zeiss, Oberkochen, Germany) and atomic force microscopy (Nanoscope IIIA atomic force microscope (Digital Instruments, Santa Barbara, CA, United States). Observations were made at three different points on the disks surfaces, and average values were calculated. The chemical composition of the surfaces was analyzed by X-ray microanalysis (EDX) in a Zeiss DSM 940A (Carl Zeiss, Oberkochen, Germany) scanning electron microscope outfitted with an Oxford INCA X-sight microanalysis system (Oxford Instruments, the United. Kingdom).

Threaded implants for the rat tibia were fabricated from commercially pure grade IV titanium (1.6x4.0 mm). The implants were kept as machined or treated as described above by dip coating the implant in a Titanium or Zirconium containing solution. All implants and disks were subsequently cleaned and sterilized according to standard procedures for manufacture of dental implants.

Animal Surgery

A rat tibia model of osseointegration was used (Masuda et al., 1997). All procedures were performed according to a University of Brasília approved protocol. Male Wistar rats (12-week-old) were purchased and acclimated for 7 days prior to initiation of studies. Anesthesia was achieved using ketamine / xylazine (80-100 mg/kg and 10-20 mg/kg respectively) and supplemental local anesthesia was obtained using lidocaine 2% with epinephrine (1:100:000). Each surgical site was shaved, prepared using betadine scrub and then isolated

for implant placement by a full thickness myocutaneous flap. Implants were placed distal to the tibial diaphysis using a stepwise drilling procedure performed with dental drills and using sterile saline irrigation. Implants were placed into the osteotomies by a self-tapping procedure. The sites were closed using resorbable sutures. Buprenorphine (0.01 – 0.05 mg/kg) was administered as post-surgical analgesia and 5 mg/kg of ketoprofen subcutaneously 24 hours post-operatively. Animals were evaluated continuously following surgery and ambulation using the implanted limbs was the defined criteria for immediate recovery. The animals were sedated and euthanized with an overdose of thiopental.

For the molecular analysis, two implants were placed in each tibia to provide sufficient RNA for each experimental sample. The first implant was inserted 7mm away from the knee joint and the second implant was 5mm distal to the first one. The time points for molecular analyses were 3, 7, 14 and 21 days after implant placement. For every time point, three rats were used for each implant surface (n =3 rats).

For removal torque analysis, two implants were placed in each tibia. The implants were inserted as described above. The time points for removal torque analysis were 7, 21 and 56 days after implant placement. For every time point, three rats were used for each implant surface (n =3 rats; 6 implants). After sacrifice, implant resistance to torque was measured using a torque-gauged wrench (1200ATG-NS; Tochnichi, Tokyo, Japan).

For the histological analysis, one implant was placed in each tibia. The implant was inserted 7 mm away from the knee joint. The time points for histological analyses were 7, 21 and 56 days after implant placement. For every time point, three rats were used for each implant surface (n =3 rats; 3 implants). The tibias were removed and fixed in 4% phosphate-buffered formalin (pH 7.0), for 10 days, and then transferred to a solution of 70% ethanol until processing. The specimens were dehydrated in increasing concentrations of ethanol up to 100%, infiltrated and embedded in methylmethacrylate resin (London Resin Company, Berkshire, England), according to the technique described by Donath; Breuner (1982). The sections were prepared for histomorphometry and stained with Toluidine Blue for optic microscopic analysis.

RNA isolation and analysis

Immediately following sacrifice, the implants were unscrewed and the surrounding bone tissue removed with a 2.0 mm trephine. The tissues were kept frozen in liquid nitrogen until the RNA isolation procedure. Tissue was ground with mortar and pestle in liquid nitrogen. Total RNA in the cell lysates was isolated using the Trizol (Invitrogen, Carlsbad, CA)

according to the manufacturer's protocol and collected by ethanol precipitation. Total RNA was quantified using UV spectrophotometry. From each total RNA sample, cDNA was generated using SuperScript reverse transcriptase (Invitrogen, Carlsbad, CA) in a standard 20 μ L reaction. All cDNAs were subjected to polymerase chain reaction (PCR) for GAPDH mRNA as a test of RNA integrity and cDNA synthesis. Subsequently, equal volumes of cDNA were used to program real time PCR reactions specific for mRNAs encoding ALP, BSP, OCN, OPN and RUNX-2. Reactions were performed using TaqMan Universal PCR Master Mix (Applied Biosystems, Foster City, CA) and thermocycling in an ABI 7200 real time thermocycler (Applied Biosystems, Foster City, CA). Relative mRNA abundance was determined by the $2^{-\Delta\Delta Ct}$ method and reported as fold induction. GAPDH abundance was used for normalization.

Histomorphometry

Longitudinal histological sections from each implant were captured through a video camera Sony (Sony Corp, Tokyo, Japan) joined to a light microscope. The images were analyzed through the Bioquant Nova (Bioquant Image Analysis Corporation, Nashville, TN), where the percentages of bone-to-implant contact (BIC) were determined. Through linear measurements, the percentages of mineralized bone in direct contact with the implant surface were determined (Masuda et al., 1997).

Statistical analyses

Descriptive statistics were calculated using SPSS. Comparison of Torque removal values and histomorphometric measurements on implants in vivo was performed by Kruskal-Wallis test. For all statistical analysis significance level was set at $p \leq 0.05$.

Results

Surface analysis

SEM and AFM evaluation reveal marked topographic differences among M, and nanostructured surfaces. For the An, Ru and Zr implants (Figure 1-4) at 5,000x magnification the coating is visible (change in morphology compared to machined surface). At 50,000x and 100,000x magnification nanoscale topography is distributed on the surface with features of approximately 20 nm in diameter (Figure 2-4). For the Machined (Figure 1) there is no evidence of nanofeatures on the surface at 50,000x or 100,000x magnification.

Surface roughness parameters were obtained from the AFM analysis (Table 1). The roughness profile of each surface is shown in figures 1 to 4. Differences between machined

surface and all nanostructured surfaces were evident demonstrating that the coating was able to cover the original machined surface creating a new topography.

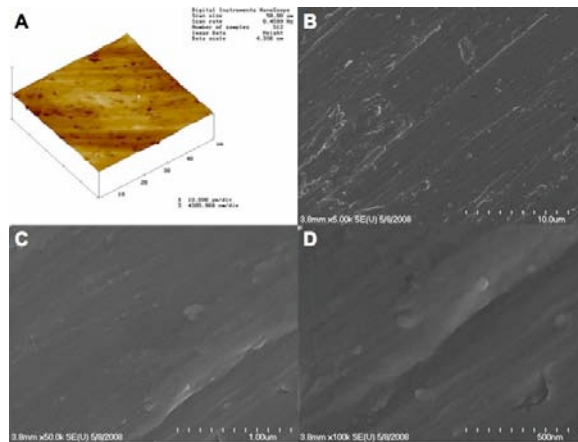


Figure 1 – AFM and SEM evaluation of the Machined implant surface. A- Surface roughness (AFM) for Machined. B, C and D- SEM images at low and high magnification for the Machined surface. At 50,000x and 100,000x magnification nanostructures are not observed (C and D).

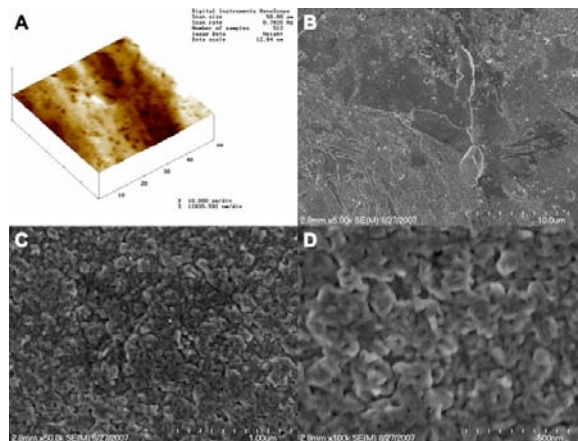


Figure 2 – AFM and SEM evaluation of the Titania - Anatase coated implant surface. A- Surface roughness (AFM). B, C and D- SEM images at low and high magnification. At 50,000x and 100,000x magnification the nanostructures of the surface are evident (C and D).

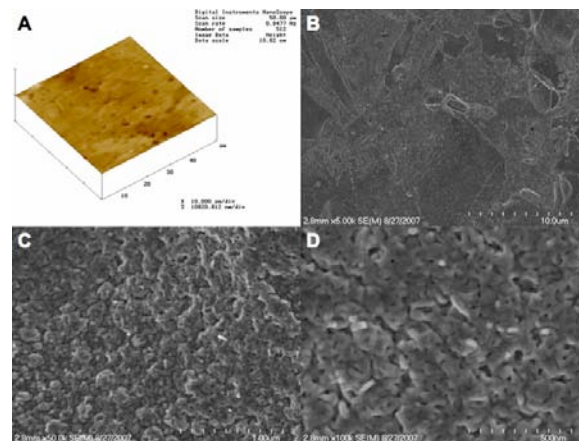


Figure 3 – AFM and SEM evaluation of the Titania - Rutile coated implant surface. A- Surface roughness (AFM). B, C and D- SEM images at low and high magnification. At 50,000x and 100,000x magnification the nanostructures of the surface are evident (C and D).

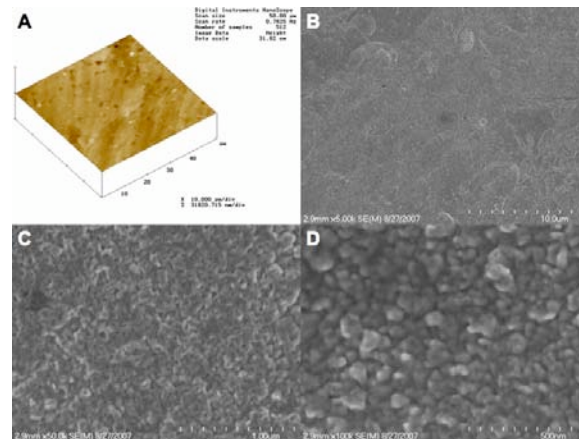


Figure 4 – AFM and SEM evaluation of the Zirconia coated implant surface. A- Surface roughness (AFM). B, C and D- SEM images at low and high magnification. At 50,000x and 100,000x magnification the nanostructures of the surface are evident (C and D).

Table 1 – Roughness parameters of the surfaces.

	Roughness Parameters			
	M	An	Ru	Zr
Sa (nm)	86.52* ^b	162.21* ^c	60.08* ^a	89.71* ^b
Sq (nm)	111.10	204.34	81.22	109.25
Rp (µm)	0.49	0.91	0.36	0.23

*Means were significantly different at $p \leq 0.05$.

The chemical analysis (EDX) showed the general composition of the implant surfaces (Figure 5). The chemical composition of the M surface was essentially Titanium and traces of small contaminants from machining process (Figure 5a). The An and Ru surfaces were composed of Titanium and Oxygen (Figure 5b and 5c). The Zr surfaces presented traces of Titanium, Zirconium and Oxygen (Figure 5d). For the nanostructured implant surface, the

EDX surface scanning showed that the expected material was distributed over the entire implant surface (Figure 6).

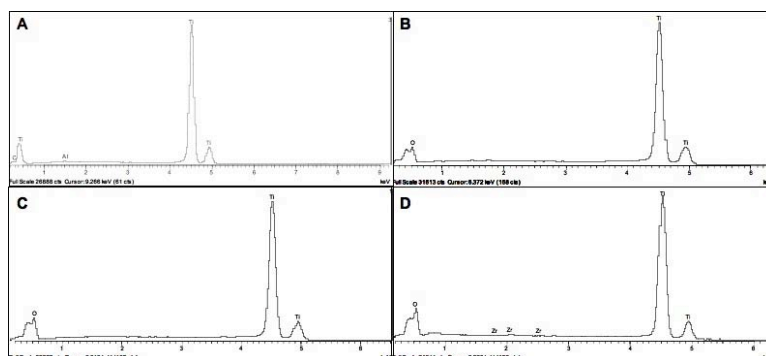


Figure 5- X-ray microanalysis (EDX) of the chemical composition of the implant surface. A- Machined. B- Anatase. C- Rutile. D- Zirconia.

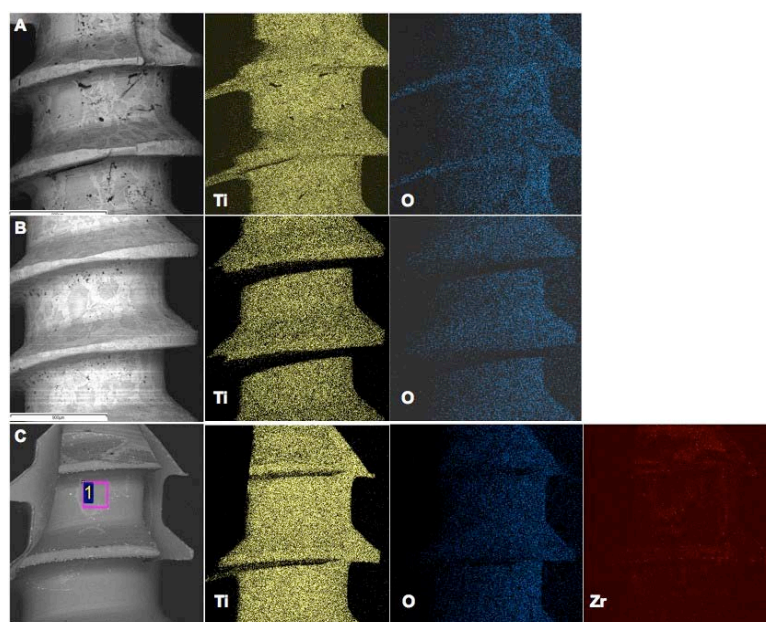


Figure 6- X-ray microanalysis (EDX) of the Titanium and Zirconium oxide coated implants. A, B and C- SEM image of the implants. Ti, O and Zr - Scanning of the surface demonstrate the presence of titanium (Ti), oxygen (O) and zirconium (Zr) on the surfaces.

Gene expression analysis

Surface modifications had different effects on osteoblast gene expression. When osteoblastic gene expression was measured in the bone surrounding endosseous implants harvested following placement in rat tibia, osteoblast-specific mRNA levels were greater in bone surrounding all nanostructured surfaces versus M implants.

For example, ALP expression levels were increased in An adherent cells after 3 and 7 days (up to 4-fold increase). For Ru and Zr the ALP levels increased after 14 days, 2-fold increase

for Ru and more than 4-fold increase for Zr. The relative expression of ALP was further delayed in bone surrounding M implants, with expression being elevated after 21 days.

BSP mRNA levels derived from rat tibia also demonstrated evidence of increased differentiation on Zr surface after 14 days with up to 2-fold increase. An and Ru surfaces showed just a slight increase at day 7 and day 14, respectively. In contrast, BSP mRNA levels were not elevated on M implant samples. (Figure 7).

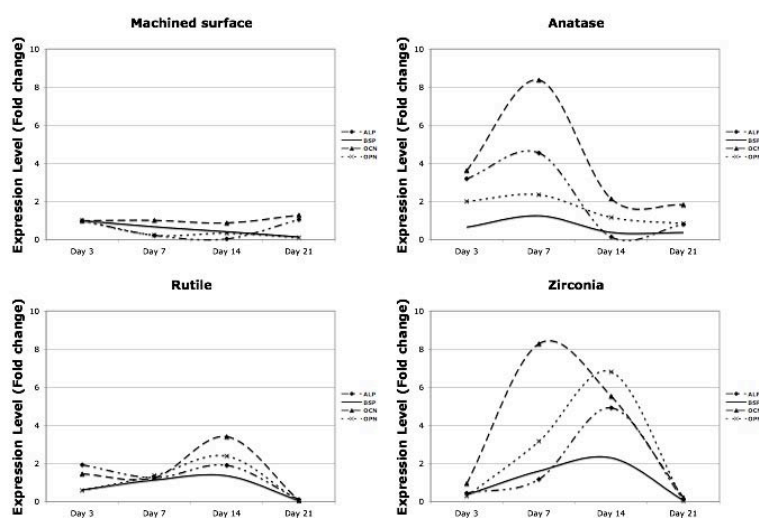


Figure 7 – Bone-specific mRNA expression in bone tissue adjacent to M, An, Ru or Zr implants. Total RNA was isolated from peri-implant bone tissues after 3, 7, 14 and 21 days. Expression levels (fold change) for ALP, BSP, OCN, OPN are compared to Machined day 3 for Machined, Anatase, Rutile and Zirconia coated implants, A, B, C and D, respectively, 3 – 21 days following implant placement ($2^{-\Delta\Delta Ct}$ method).

For Osteocalcin, mRNA levels were also evaluated in the bone around dental implants in this study. For An, OCN levels were increased after 3 days (3.5-fold), these levels further increased at day 7 (8-fold) and kept around 2-fold at days 14 and 21. For Ru, OCN levels reached up to 3.5-fold increase at day 14. OCN levels for Zr also reached 8-fold increase at day 7 and 5.5-fold at day 14. For samples involving M implants, mRNA levels kept steady even after 21 days (Figure 7).

Osteopontin levels were up-regulated for An surfaces at day 3 and 7 (2-fold), and at day 14 for Ru (2-fold). Zr surface presented an increase of 3-fold at day 7 and up to 7-fold at day 14. Levels of Runx2 in bone samples from An implants were elevated on day 3 (1.5-fold) and then decreased (Figure 8). Zr implants showed an increase of 3-fold for Runx2 mRNA expression level at day 14. For Ru, no change on Runx2 levels were observed compared to Machined at day 3. Compared to M day 7 and M day 14 the level of Runx2 for Ru were at least 2-fold higher at each time-point; however (Figure 8).

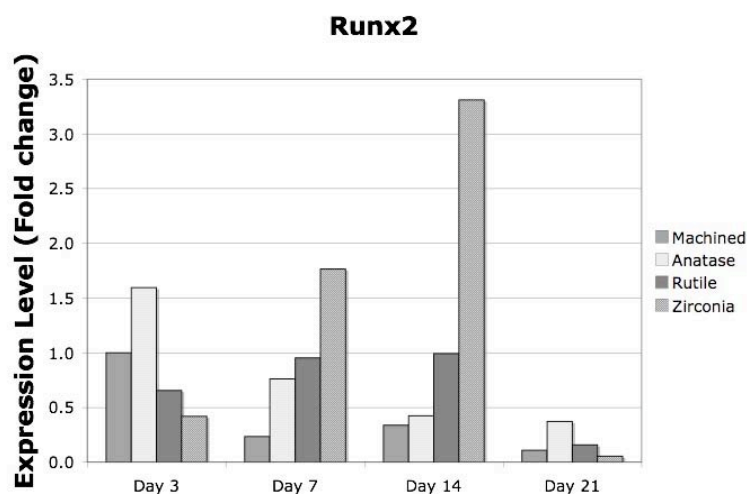


Figure 8 –The RNA levels for Runx2 in peri-implant bone tissues surrounding Machined, Anatase, Rutile and Zirconia coated implants are compared as fold change 3 – 21 days following implant placement. The results are shown as fold change ($2^{-\Delta\Delta Ct}$ method).

Removal torque and Histomorphometric analysis

The mean removal torque for all surfaces was similar at day 7, and then higher for the Ru implant group at day 21. After 56 days, the mean removal torque was 11.6 ± 2.5 , 11.3 ± 2.4 , 11.1 ± 3.5 , 9.7 ± 1.4 for An, Ru, Zr, and M implant groups, respectively (Figure 9). The histomorphometric analysis revealed a higher bone-to-implant contact for all nanostructured surfaces versus M at 21 and 56 days. A more rapid accrual of interfacial bone was suggested by the increase in BIC from day 7 to 21 compared to M implant groups. There were significant differences between all nanostructured (An, Ru and Zr) and Machined groups at days 21 ($p < 0.05$). At 56 days the BIC were 65.77 ± 6.49 , 51.81 ± 7.20 , 51.49 ± 6.46 , 31.88 ± 3.84 , for Zr, An, Ru, and M, respectively ($n=3$, $p < 0.05$; Kruskal-Wallis test) (Figure 10). No statistically significant differences were found among the nanostructured implants regarding the BIC. For the Removal torque values, no statistically significant differences were observed between the groups at the same time-point; however, all the nanostructured surfaces presented a higher RTV compared to Machined at day 56 (Figure 9).

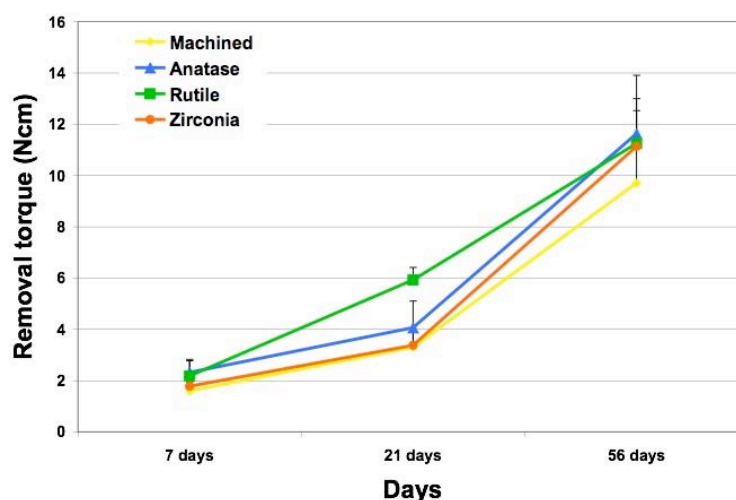


Figure 9 – Removal torque values for Machined, Anatase, Rutile and Zirconia coated implants. Removal torque was measured for 6 implants / surface / timepoint.

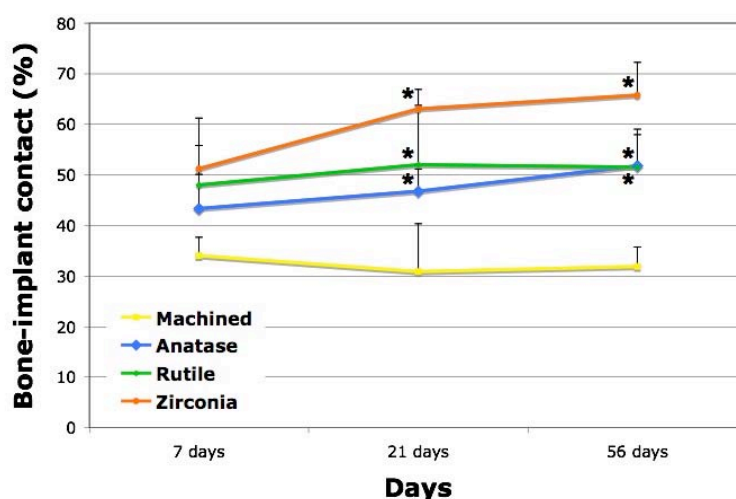


Figure 10 – Bone-to-implant contact for Machined, Anatase, Rutile and Zirconia coated implants. Histomorphometric measurement of bone to implant contact was calculated for 3 implants / surface / timepoint. The mean percent of bone to implant contact is shown (7 – 56 days; * $p < 0.05$).

Discussion

AFM and SEM evaluation demonstrated a marked difference between a machined implant surface and implant surfaces that were accrued with a coating that imparted nanofeatures to the surface. In this study, a machined implant was coated with three different coating materials, based on Titanium or Zirconium. The difference between the two TiO_2 coatings is regarding to its crystallographic form. In the last few years, Zirconia ceramics have also been used as implant material because of its biocompatibility and mechanical properties that make them suitable as materials for dental implants (Gahlert et al., 2007;

Oliva et al., 2007; Wenz et al., 2008). Little is known about how surface modification influences the stability and bone tissue response to zirconia implants, and how a Titanium implant modified with a Zirconia coating would behave.

One of the main concerns related to coating the implant surface is the risk of coating detachment and toxicity of related debris. This question was addressed by Gutwein and Webster (2004) who evaluated the relationship of particle size and cell viability and proliferation compared to micron-particles. Nanoparticles of titania and alumina had less negative impact in cell viability and proliferation. However, owing to their resultant atomic-scale interactions, the accretions display strong physical interactions with the underlying surface.

The roughness (S_a) values as measured by the AFM for the nanostructured and machined surfaces were below 100nm, except for the An group. The features for the An coated implants were composed of small pores of around 20nm similar to Ru and Zr; however (Figures 2-4). The mean roughness is just one parameter used to classify the surfaces. The chemical composition and characteristics of the coatings were evaluated by SEM and EDX analysis revealing that the material of interest was deposited evenly on the surface of the implants.

Very few *in vivo* studies have been performed to investigate the effects of a nanostructured implant surface on osseointegration (Ellingsen et al., 2004; Guo et al., 2007; Meirelles et al., 2008). On the other hand, the effects of nanostructured topography on adherent osteoblast responses regarding differentiation and mineralization have been addressed in several *in vitro* studies (Webster et al., 1999; Webster et al., 2000a). All these studies corroborate the effects of imparted nanotopography on osteoblast behavior and osseointegration process. This study employed the rat model to gain insight into the potential differences that occur during the osseointegration process at Titanium or Zirconium oxide coated titanium implant of defined nanometer-scale topography versus implants with defined machined topography. Together, the *in vivo* molecular data, the histomorphometry and the removal torque data suggest that, when compared with machined cpTitanium implant surfaces, the nanoscale Zirconia or Titania coated implant surfaces supported greater osteoblastic differentiation, osteoblast-specific gene expression, related bone accrual and mechanical interaction with surrounding bone.

The surface-specific gene expression obtained at each time point demonstrated a higher level at Runx2 expression for Zr surface. Runx2 is a key transcription gene in

osteoblast differentiation and an increase in its levels may be related to the effect of nanostructured surfaces on osteoblast (Harada et al., 1999; Harada; Rodan, 2003). Some authors have also shown an increase in Runx2 levels on Osseospeed implant surface (another nanostructured surface) (Guo et al., 2007; Isa et al., 2006). In this study the Runx2 mRNA levels for Zr and Ru surface increased up to day 14, and for An the levels started higher and decreased after that. This behavior may be related to the different chemical composition of each surface.

Dalby and co-workers (2007) demonstrated that the presence of nanofeatures could initiate, in MSCs, the expression of some osteogenic markers even without cell culture induction of the cells along the osteoblast pathway. In this report, *in vivo* measurements of mRNA levels in bone surrounding the various implants showed an increase in Runx2 mRNA levels as well as concomitant increases in ALP, BSP, OCN, OPN levels to Zr, Ru and An, but not M (Figure 7 and 8). Runx2 elevations will increase the expression of other bone related genes such as Alkaline phosphatase, Collagen type I, Osteocalcin, and Osteopontin.

ALP, BSP, OCN and OPN are marked genes of osteoblast differentiation and expressed at various time-points related to stage of cell commitment (Cooper, 1998). In this study, An surface presented an increase in ALP, OCN and OPN at day 7 (Figure 7) followed by a higher peak of Runx2 expression at day 3 (Figure 8). The same pattern is noted to Ru and Zr, although they are both one time-point shifted (to day 7 and 14).

For the removal torque analysis similar low values were observed for all surfaces at day 7. This is consistent with the early responses of bone tissue to surgical intervention. At day 21 up to day 56, the Ru implants presented a higher increase in removal torque values compared to M implants. An presented a slight increase at day 21 and the highest value of all surfaces at day 56. Zr only increased the RTV at day 56. All this behavior may be related to the chemical composition of the surfaces. Statistically significant differences in removal torque values were not revealed in this study, however all nanostructured surfaces presented higher removal torque values than M at day 56 (Figure 9).

The removal torque values are in accordance with the other results in this paper and may be correlated to a significantly greater bone accrual at the Nanostructured implants after 21 days. Suggested is a relationship between torque removal and bone to implant contact. The torque removal analysis in this study appears to be related to the other results obtained in this study and also with other papers that used the same analysis (Narai; Nagahata, 2003). Although the increase in BIC and the gene expression pattern did not led to a

statistically significant difference in the RTV it may be related to the challenges of the animal model used in this study. The acknowledgement of increased bone to implant contact had occurred in the same time frame as increased torque removal and suggests that the surface nanofeatures influenced bone accrual predominantly and potential physicochemical interactions with surrounding bone (bone bonding) secondarily. While this cannot be fully excluded without direct comparisons among similar materials with different nanotopographies, the results suggest that this Nanostructured surfaces (An, Ru and Zr) promoted greater physical interaction of the implant with bone through a process of enhanced bone accrual.

According to our results, it is not clear yet how nanotopography improves osteoblast response, but it is clear it has an important role in cell differentiation. A systematic investigation of how nanoscale topography of a given bulk chemistry affects the processes underscoring the result of osseointegration is indicated.

Conclusion

Nanostructured topographic features composed of TiO_2 or ZrO_2 applied to machined cpTi implant promoted greater mesenchymal stem cell commitment to the osteoblast phenotype and associated increase in BIC and physical association with bone. However, more studies are necessary to evaluate the long-term effects of such surface modifications on implant stability and osseointegration.

Capítulo 5 - Nanoestruturas na Superfície de Implantes Alteram a Expressão Gênica em Osteoblastos

O efeito do tratamento de superfícies na melhora e na qualidade da osseointegração já foi comprovado em vários trabalhos científicos. Vários estudos têm sido realizados para entender a relação entre a superfície de implantes osseointegrados e os osteoblastos. O uso da nanotecnologia no desenvolvimento de novas superfícies pode ajudar na compreensão deste mecanismo como uma nova ferramenta de estudo da interação entre as células e a superfície de implantes. Neste capítulo, células-tronco mesenquimais humanas foram cultivadas sobre as superfícies nanoestruturadas a base de óxido de titânio, óxido de alumínio e óxido de zircônia (apresentadas nos Capítulos 3 e 4). Todas as superfícies foram novamente caracterizadas química e fisicamente (Microscopia de força atômica - AFM, microscopia eletrônica de varredura – MEV, e espectroscopia de fluorescência – XPS). Após 3, 7, 14 e 28 dias as células foram removidas para isolar o RNA. O perfil de expressão gênica de alguns genes relacionadas à cascata de diferenciação de osteoblastos foi obtido, e a partir desta análise preliminar selecionou-se a superfície de óxido de alumínio como apresentando o melhor resultado. Esta superfície foi então utilizada em um estudo mais amplo, no qual um arranjo de PCR (“polimerase chain reaction”) baseado em 84 genes relacionados à mineralização e osteoblastos foi obtido para esta superfície. Uma melhor resposta de todas as superfícies nanoestruturadas foi observada, quando comparado à superfície controle. A superfície recoberta com óxido de alumínio mudou drasticamente o perfil de expressão gênica das células-tronco mesenquimais humanas, demonstrando que esta superfície pode levar a uma melhor e mais rápida resposta de osseointegração.

Este capítulo foi aceito para publicação com pequenas modificações no *Biomaterials*. Mendonça G, Mendonça DBS, Simões LGP, Araújo AL, Leite ER, Duarte WR, Cooper LF, Aragão FJL. The effects of implant surface nanoscale features on osteoblast-specific gene expression. *Biomaterials*. *In press*.

The effects of implant surface nanoscale features on osteoblast-specific gene expression

Abstract:

Purpose: Nanotechnology has been used to enhance implant surfaces and further improve the clinical results of osseointegrated implants. This study investigated the influence of nanostructured coated implant surfaces on osteoblast differentiation. The hypothesis is that a nanostructured-coated surface could alter the initial osteoinductive responses of cells to increase the osteoblast differentiation. **Methods:** Titanium disks (20.0x1.0mm) were machined (M) or machined and subsequently treated by acid etching (Ac) or by dipping in titanium (TiO₂), aluminum (Al₂O₃), or zirconium (ZrO₂) oxide solution. Surfaces were characterized by scanning electron microscopy (SEM), atomic force microscopy (AFM) and analyzed by X-Ray Photoelectron Spectrometer (XPS). Human Mesenchymal Stem Cells (hMSCs) were cultured on the disks. The data points analyzed were 3, 7, 14 and 28 days. Real Time PCR was used to measure the mRNA levels of ALP, BSP, Runx2, OCN, OPG, and OSX and a panel of 84 genes (PCR array). The housekeeping gene GAPDH was used as a control. Descriptive statistics were calculated using Microsoft Excel. T-test was performed for comparison of mRNA levels compared to M surfaces (p<0.05). **Results:** Topographical and chemical evaluation revealed different surface characteristics. Bone specific mRNAs were increased on nanostructured-coated surfaces compared to Ac and M surface at day 14. For OSX, An (2-fold), Ru (3.5-fold), Al (4-fold) and Zr (3-fold). OSX expression levels for M and Ac approximated baseline levels. ALP mRNAs relative levels for An, Al and Zr presented the highest level at day 28 (around 4-fold increase). At day 14 and 28 the BSP relative mRNAs expression was significantly up regulated for all nanostructured surfaces (up to 45-fold increase for Al). The PCR array of 84 osteogenic specific genes shown an up-regulation on Al₂O₃ coated implants when compared to M. **Conclusion:** An improved response of nanostructured-coated implant surfaces with an increase in OSX and BSP expression was observed. Furthermore, we demonstrated that the nanostructured surface coated with aluminum oxide significantly changed the hMSCs gene expression pattern towards an up regulation in osteoblast differentiation. These surfaces may be able to improve the osseointegration response providing a faster and more reliable bone to implant contact.

Key words:

Titanium oxide; Aluminum oxide; Zirconium oxide; Nanotopography; Dental Implant; Surface treatment; Bone regeneration.

Introduction

Novel implant surfaces have been developed in the last decade and in a concentrated effort to provide bone in a faster and improved osseointegration process (Ellingsen et al., 2004; Buser et al., 2004; Coelho; Suzuki, 2005; Guo et al., 2007; Mendes et al., 2007; Le Guéhennec et al., 2007; Mendonça et al., 2008). The mechanisms involved in this faster and improved osseointegration are yet to be fully determined. Many studies have focused on the analysis of surface characteristics and chemical composition as a way to control bone healing around dental implants (Kasemo, 1983; Nanci et al., 1998; Davies, 2003; Albrektsson; Wennerberg, 2004a; Albrektsson; Wennerberg, 2004b; Schwartz et al., 2005; Cooper et al., 2007; Christenson et al., 2007). Surfaces with imparted microtopography improve cell attachment and differentiation (Buser et al., 1991; Ogawa; Nishimura, 2003). Suggested is the signaled alteration in adherent cell gene expression. Several investigators have revealed that nanoscale topography also changes cell adhesion and osteoblastic differentiation (Dalby et al., 2007; Dalby et al., 2008). Novel research studies have now focused on the role of nanotopography and how nanotechnology can further improve the cell / implant interface (Webster et al., 1999; Webster et al., 2000a; Webster et al., 2001a; Price et al., 2003a; Guo et al., 2007; Mendes et al., 2007).

Nanotechnology can not only control the size of the features that are imparted to the implant surface at an atomic level (Oh et al., 2005) but it also controls the chemical composition of these surfaces (Guo et al., 2007). Different chemical elements can be added to the implant surface and also molecules can be applied and covalently bonded to the implant (Scotchford et al., 2002). In several studies the benefits of using nanotechnology on dental implants have been proved *in vitro* and *in vivo* (Webster et al., 1999; Webster et al., 2000a; Webster et al., 2001a; Price et al., 2003a; Ellingsen et al., 2004; Guo et al., 2007; Mendes et al., 2007). These studies used several animal and cell culture models to help understand the role of nanocues on directing osteoblast differentiation. One of the mechanisms may be related to an increased protein adsorption onto the surface, including vitronectin and fibronectin (Webster et al., 2001a). Another mechanisms is related to an increased expression of bone-related transcription factors such as Runx2 and Osterix (Osx) that can drive mesenchymal stem cells differentiation over the osteoblastic pathway (Isa et al., 2006; Guo et al., 2007).

In this work, titanium disks coated with nanostructured films of each aluminum, titanium or zirconium presented an increased expression of Osx and Bone sialoprotein (BSP) over a 28-day period of culture of adherent hMSCs. Detailed evaluation of nanoscale

aluminum oxide coated implant led to an increased expression of 33 osteogenesis-related genes. These genes are associated with osteoblastic differentiation.

The aim of this study was to investigate the behavior of human mesenchymal stem cells (hMSCs) cultured on nanostructured titanium implants for up to 28 days. We also evaluated the gene expression profile of these cells by PCR array. The hypothesis was that the nanostructured surface can modulate the gene expression and control the osteoblast differentiation compared to machined implant surfaces.

Materials and Methods

Surfaces preparation

Commercially pure grade IV titanium disks (20.0x1.0 mm) were prepared by machining (Neodent Implante Osteointegrável, Curitiba, PR, Brazil), and cleaned by sonicating in acetone and distilled water three times for 15 min each. Subsequently, the disks were treated by coating with a titanium (TiO_2), zirconium (ZrO_2), or aluminum oxide (Al_2O_3) nanocoating. The coated surfaces were prepared by dip coating the disks in a Titanium, Zirconium or Aluminum containing solution. This solution was prepared using the polymeric method (Pechini, 1967) in a controlled temperature. Another set of disks was machined only and composed the Machined (M) group. These disks were cleaned by sonicating three times in distilled water for 15 min each, and then were passivated with 30% HNO_3 for 15 min. A sixth group was composed of disks that after machining were grit-blasted with 100 μm aluminum oxide particles, and cleaned by sonicating three times in water for 15 min each, followed by immersion in HCl solution (Fisher Scientific, Inc., Pittsburgh, PA) overnight, and then passivated with 30% HNO_3 for 15 min. The disks were divided into six groups: machined (M), acid etched (Ac), Titania-Anatase (An), Titania-Rutile (Ru), Alumina (Al), and Zirconia (Zr) nanocoating.

Surfaces analysis

The surface of the disks were examined by high-resolution scanning electron microscopy (Field Emission Scanning Electron Microscope (FEG-SEM), Hitachi S-4700) and atomic force microscopy (Nanoscope IIIA atomic force microscope, Digital Instruments, Santa Barbara, CA, United States). Observations were made at three different points on the disks surfaces, and average values were calculated. XPS spectra were recorded on a Kratos Axis Ultra spectrometer with a concentric hemispherical analyzer and a delay line detector. Monochromatic Al Ka x-rays were used at 150 W, and the chamber base pressure was less than 10^{-8} torr. Survey spectra were obtained at a pass energy of 80 eV and a step size of 1

eV, while high resolution elemental scans were taken at a pass energy of 20 eV and a step size of 0.1 eV. All spectra were corrected for the adventitious C 1s peak at 284.6eV.

Cell Culture

Human mesenchymal stem cells (hMSCs) P2 were purchased (Lonza) and cultured in accordance with published protocols. Growth media included Dulbecco's modified eagle medium Low glucose (LG-DMEM) (Gibco) supplemented with 10% fetal bovine serum (FBS) and antibiotic/antimycotic (penicillin/streptomycin/amphotericin B, Sigma). Osteogenic media includes LG-DMEM (Gibco, #11885) supplemented with 10% FBS and antibiotic/antimycotic and the osteogenic supplements 10^{-7} M dexamethasone (Sigma), 10mM glycerophosphate (Sigma G9891) and 0.2mM ascorbic acid (Sigma). Passage 2 cells were plated at low density and grown until nearly confluent. Cells were subsequently passaged onto prepared titanium disks using 100,000 cells in 250 μ l of growth media. The formed meniscus was left undisturbed to permit cell attachment over 4 hours and subsequently additional growth media was applied. Following overnight incubation, cultures were carefully rinsed and osteogenic media was placed in culture dishes. This represented the starting time point (T = 0). The osteogenic media was replaced every third day. Disks with adherent cell and forming tissue layers were collected on day 3, 7, 14, and 28.

RNA isolation and quantification

For evaluation of mRNA expression in cells adherent to titanium disks. Titanium disks were removed from the culture dishes and rinsed twice with cold phosphate buffered saline (PBS). Adherent cells on each disk were lysed using Trizol (Invitrogen, Carlsbad, CA) and lysates were collected by pipetting and centrifugation. Total RNA in the cell lysates was isolated using the Trizol according to the manufacturer's protocol and collected by ethanol precipitation. Total RNA was quantified using UV spectrophotometry.

Real-time RT-PCR Analysis

From each total RNA sample, cDNA was generated using RT² First Strand Kit reverse transcriptase (Superarray, Frederick, MD) in a standard 20 μ L reaction using 1 μ g of the total RNA. All cDNAs were subjected to polymerase chain reaction (PCR) for GAPDH mRNA as a test of RNA integrity and cDNA synthesis. Subsequently, equal volumes of cDNA were used to program real time PCR reactions specific for mRNAs encoding ALP, BSP, Runx2, OCN, OPN, and OSX. Reactions were performed using a customized RT² Profiler™ PCR Arrays (CAPH-0398) (Superarray, Frederick, MD) and thermocycling in an ABI 7200 real time thermocycler (Applied Biosystems, Foster City, CA). Relative mRNA abundance was

determined by the $2^{-\Delta\Delta C_t}$ method and reported as fold induction. GAPDH abundance was used for normalization.

The data points analyzed were 3, 7, 14 and 28 days. Real Time PCR was used to measure the mRNA levels of ALP, BSP, Runx2, OCN, OPN, and OSX. The housekeeping gene GAPDH was used as a control.

The effects of nanostructured alumina on the osteoblast-specific gene expression were further evaluated for 3, 7 and 14 days, by means of an array of osteogenesis-related genes using human osteogenesis RT² Profiler PCR array (PAHS-0026A - SuperArray Bioscience, Frederick, MD) according to the manufacturer's instructions, and compared to the Machined surface. In brief, cDNA was prepared from 1µg total RNA by using a RT² PCR array first strand kit (Superarray, Frederick, MD). A total volume of 25µl of PCR mixture, which included 12.5µl of RT² Real-Time SYBR Green/ROX PCR master mix from SuperArray Bioscience (containing HotStart DNA polymerase, SYBR Green dye, and the ROX reference dye), 11.5µl of double-distilled H₂O, and 1µl of template cDNA, was loaded in each well of the PCR array. PCR amplification was conducted with an initial 10-min step at 95°C followed by 40 cycles of 95°C for 15 s and 60°C for 1 min). The fluorescent signal from SYBR Green was detected immediately after the extension step of each cycle, and the cycle at which the product was first detectable was recorded as the cycle threshold. Data were imported into an Excel database and analyzed using the comparative cycle threshold method with normalization of the raw data to housekeeping genes including b2M, hypoxanthine phosphoribosyltransferase 1, ribosomal protein L13a, GAPDH, and ACTB (b-actin).

Statistical analysis

Descriptive statistics were calculated using SPSS. The roughness parameter (Sa) was compared by one-way ANOVA followed by Tukey Test. For the gene expression analysis, descriptive statistics were calculated using Microsoft Excel. T-test was performed for comparison of mRNA levels compared to M surface day 3. For all statistical analysis significance level was set at $P < .05$.

Results

Surface analysis

The surfaces in this study presented different characteristics related to the nanoscale level. At low resolution, scanning electron micrographs suggest the conservation of the surface characteristics between Machined and the nanostructured surfaces (M and An, Ru, Al and Zr) (Figures 1-6). At high resolution, it reveals the presence of 20 – 30nm

nanofeatures on all four nanostructured surfaces (An, Ru, Al and Zr) (Figures 1-6). At high resolution, there are little nanotopographic features on the M and Ac surface (Figures 1-6).

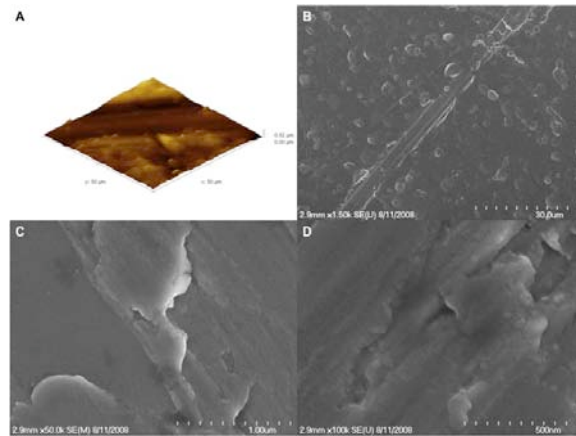


Figure 1 – AFM and SEM evaluation of the Machined implant surface. A- Surface roughness (AFM) for Machined. B, C and D- SEM images at low and high magnification for the Machined surface. At 50,000x and 100,000x magnification a very few nanofeatures are observed (C and D).

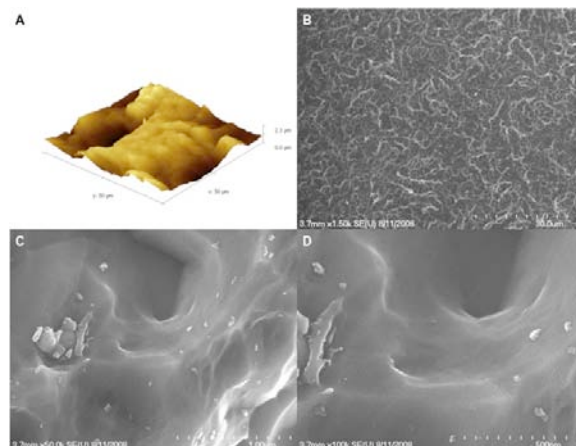


Figure 2 – AFM and SEM evaluation of the Acid etched implant surface. A- Surface roughness (AFM) for Acid etched. B, C and D- SEM images at low and high magnification. At 50,000x and 100,000x magnification a very few nanofeatures are observed (C and D).

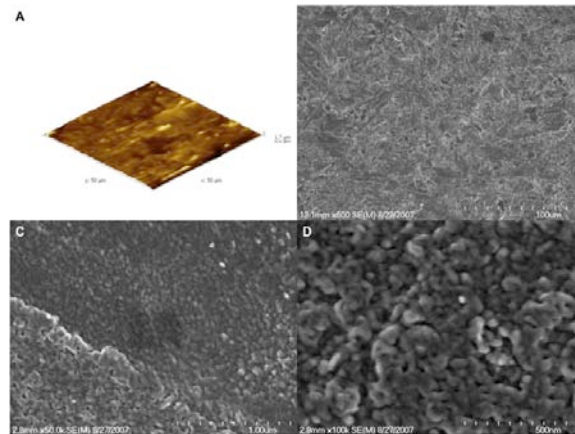


Figure 3 – AFM and SEM evaluation of the Anatase coated implant surface. A- Surface roughness (AFM). B, C and D- SEM images at low and high magnification. At 50,000x and 100,000x magnification the nanofeatures of the surface are evident (C and D).

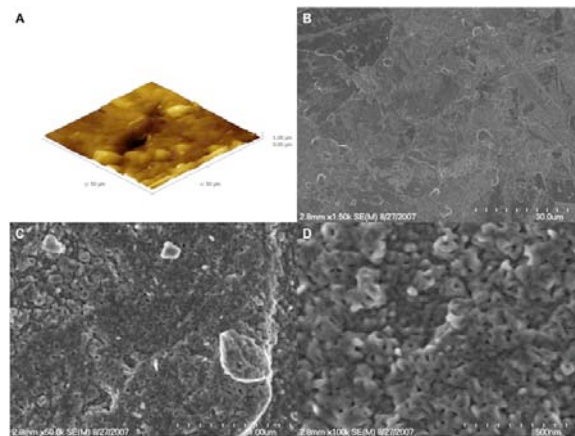


Figure 4 – AFM and SEM evaluation of the Rutile coated implant surface. A- Surface roughness (AFM). B, C and D- SEM images at low and high magnification. At 50,000x and 100,000x magnification the nanofeatures of the surface are evident (C and D).

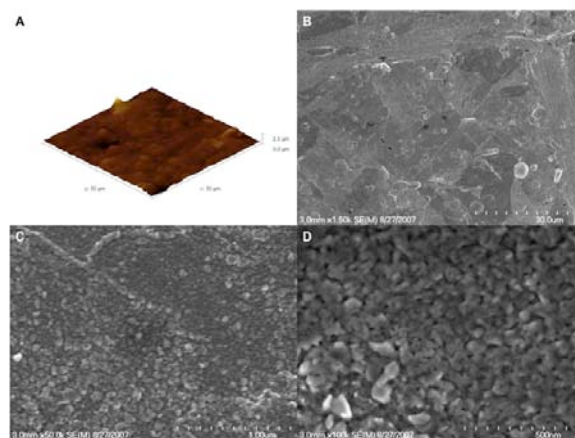


Figure 5 – AFM and SEM evaluation of the Alumina coated implant surface. A- Surface roughness (AFM). B, C and D- SEM images at low and high magnification. At 50,000x and 100,000x magnification the nanofeatures of the surface are evident (C and D).

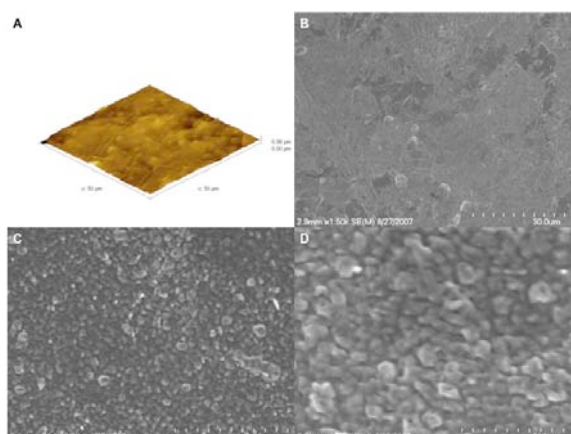


Figure 6 – AFM and SEM evaluation of the Zirconia coated implant surface. A- Surface roughness (AFM). B, C and D- SEM images at low and high magnification. At 50,000x and 100,000x magnification the nanofeatures of the surface are evident (C and D).

Surface roughness parameters were obtained from the AFM analysis and are described in Table 1. The roughness profile is shown in figures 1 to 6. AFM images and resultant values for nanocoated surfaces were comparable to Machined surfaces and resulted from the coating process. At higher resolution, nanoscale features were evident on the coated surfaces.

Table 1 - Surface roughness from optical interferometry analyses. Figures are mean values, standard deviations within parenthesis.

Surfaces	Machined		Acid etched		Anatase		Rutile		Alumina		Zirconia	
	Mean	±SD	Mean	±SD	Mean	±SD	Mean	±SD	Mean	±SD	Mean	±SD
Roughness parameters												
Sa	95.2* ^b	6.9	377.7* ^e	36.3	122.7* ^d	1.2	101.5* ^c	14.9	108.0* ^c	21.0	73.6* ^a	19.4
Sq	124.0	9.6	463.7	26.6	159.3	8.5	133.9	23.4	151.3	32.7	101.7	28.4
Skewness	0.4	0.4	-0.2	0.3	-0.1	0.2	0.4	0.4	0.7	0.5	-0.9	0.2
Kurtosis	1.1	0.0	-0.4	0.4	2.1	2.7	1.4	0.6	4.0	1.5	3.7	0.9

*Means were significantly different at $p \leq 0.05$.

The XPS analysis demonstrated traces of different chemical components on each surface (Table 2 and Figure 7). On the M surface traces of Mg, Zn, Na, Ca, S and Si were probably due to the machining, polishing and cleaning processes. A high-resolution analysis showed presence of Ti metallic and titanium oxide (TiO₂) on this surface. The Ac surface presented traces of Zn, Ca and S. The high-resolution analysis also showed presence of Ti metallic and titanium oxide (TiO₂) on this surface. For the nanostructured surfaces, the high-resolution scanning demonstrated that the titanium on these surfaces were in oxide groups and no traces of titanium metallic was found. They also demonstrated that aluminum or zirconium found on Al and Zr surfaces were in oxide groups. For the Al group, a high level of aluminum was found on this surface, and Zr was observed at a high concentration on Zr

group surfaces. The small amount of Mg, Zn, N, Ca, P and Si found on these surfaces were probably due to the cleaning/coating process. The amount of titanium observed on Al and Zr surfaces also demonstrates that the oxide surface is composed of titanium oxide and aluminum or zirconium oxides, for Al and Zr, respectively.

Table 2 - Ion composition data from XPS analyses.

	Atomic Concentration %												
	Mg 1s	Zn 2p	Na 1s	N 1s	Ca 2p	S 2p	P 2p	Si 2p	Al 2p	Zr 3d	O 1s	C 1s	Ti 2p
Machined	0.7		3.66		0.61	0.59		3.15			54.68	26.61	10.01
Acid etched		0.89			0.3	0.8					56.93	18.33	22.76
Anatase		0.55		0.43	0.28						61.11	13.63	24
Rutile		0.24			0.66		0.93				60.5	18.63	19.05
Alumina	0.48	0.09		1.34	0.48		0.61	1.99	7.7		52.01	25.47	9.84
Zirconia	0.74							1.28		11.61	57.04	21.28	8.05

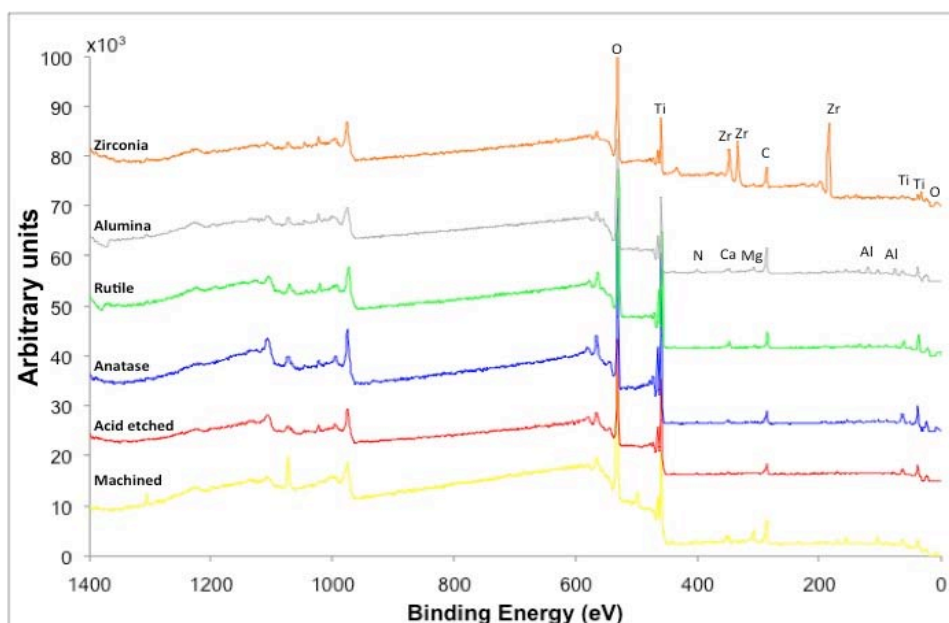


Figure 7 – Representative wide-scan XPS spectra of Machined, Acid etched, Anatase, Rutile, Alumina and Zirconia treated Titanium disks (Arbitrary units).

Cells were successfully grown and expanded on all surfaces. Cell layers were formed in multilayers and retraction from the disks was not observed. From the cultures established with 100,000 cells, there were sufficient numbers of cells present after 3, 7, 14 and 28 days for isolation of total RNA (> 5 µg of total RNA) to perform the arrayed real time PCR reactions.

Initially, all six surfaces were evaluated regarding ALP, BSP, OCN, OPN, OSX and Runx2 gene expression (Figure 8). Subsequently, based on the results of the Al group

compared to the others nanostructured surfaces we performed an 84 genes array comparison of this surface to the M group (Table 3).

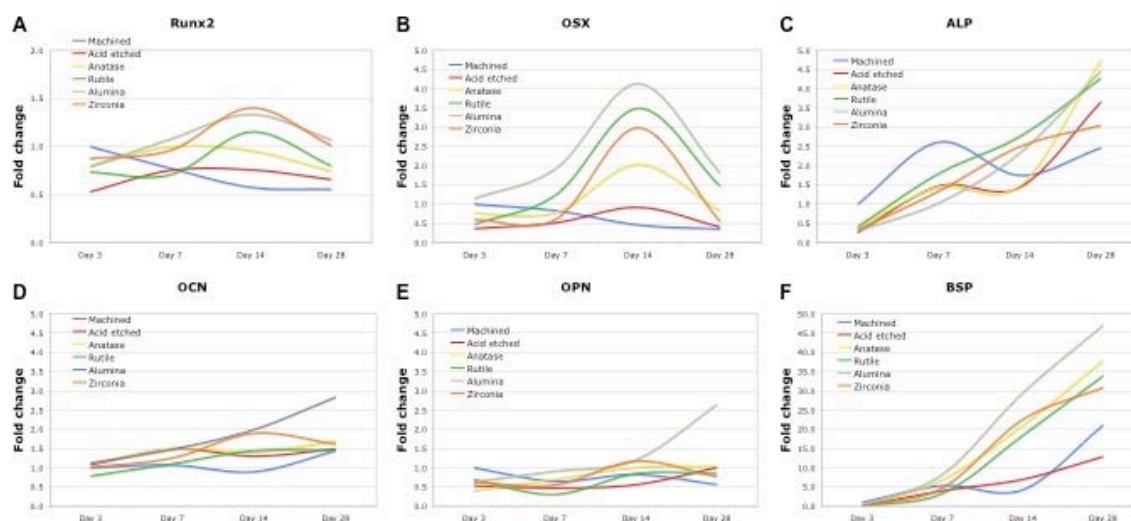


Figure 8 – Adherent hMSCs bone-specific mRNA expression. Total RNA was isolated from cells at 3, 7, 14 and 28 days of culture on Machined, Acid etched, Anatase, Rutile, Alumina and Zirconia treated Titanium disks. Expression levels (fold change) for Runx2, Osterix, Alkaline phosphatase, Osteocalcin, Osteopontin, and Bone sialoprotein are compared for all surfaces. The results are shown as fold change ($2^{-\Delta\Delta Ct}$ method, baseline=day 3 cells on Machined surface).

Surface-specific gene regulation was observed for all studied genes. One general observation was that early differences among the surfaces (day 3 or 7) were often of lower magnitude than differences observed at 14 and 28 days. At day 3 no statistical difference were found among the surfaces. After 14 days the nanostructured surfaces presented a remarkably increase for OSX and BSP compared to M and Ac (Figure 8B and 8F).

The relative expression levels of Runx2 mRNA, a key transcription factor for osteoblast differentiation, did not changed in this study (Figure 8A). However, a slight increase was observed for Al and Zr at day 14. OSX mRNAs (another key transcription factor for osteoblast differentiation) relative expression levels were more than 2-fold up-regulated at day 14 for An (2-fold), Ru (3.5-fold), Al (4-fold) and Zr (3-fold) (Figure 8B). OSX expression levels for M and Ac approximated baseline levels. ALP mRNAs relative levels for An, Al and Zr presented the highest level at day 28 (around 4-fold increase) (Figure 8C). At day 14 and 28 the BSP relative mRNAs expression was significantly up regulated for all nanostructured surfaces (up to 45-fold increase for Al) (Figure 8F). OCN and OPN mRNA levels were constant for all surfaces throughout the 28 days period of the experiment (Figure 8D and 8E). The only exception was for Al that presented an up regulation of 2.5-fold for both genes at day 28.

Table 3 - Up and downregulated genes on Machined and Alumina surfaces at day 3, 7 and 14 (Normalized with Machined day 3 and presented as Fold change). *Significantly different at $p \leq 0.05$. **Significantly different at $p \leq 0.001$.

Symbol	Description	Alumina 3d	Machined 7d	Alumina 7d	Machined 14d	Alumina 14d
Bone Matrix Proteins						
ALPL	Alkaline phosphatase, liver/bone/kidney	-3.0 *	5.4	-1.4	2.3	1.7
BGLAP	Osteocalcin	2.2 *	8.6	2.6 *	1.9	3.3 *
BGN	Biglycan	1.8	1.4	2.2 *	1.7	3.2 *
BMP Superfamily						
BMP2	Bone morphogenetic protein 2	2.4	1.8	4.5 *	1.3	6.5 *
BMP4	Bone morphogenetic protein 4	2.0	1.5	3.3 *	3.1 *	6.4 **
BMP5	Bone morphogenetic protein 5	2.0	1.2	1.9	1.4	4.0
BMP6	Bone morphogenetic protein 6	-2.2	-3.2	-14.2 *	-8.9 *	-5.7
GDF10	Growth differentiation factor 10	2.2	2.2	2.2	1.1	2.1
TGFB1	Transforming growth factor, beta 1	2.9 **	1.7	2.0 *	2.2 *	3.2 *
TGFB2	Transforming growth factor, beta 2	1.9	-1.1	1.1	-1.1	1.3
TGFB3	Transforming growth factor, beta 3	1.2	1.1	-1.4	-2.2 *	-1.7
Receptors						
CD36	CD36 molecule (thrombospondin receptor)	1.6	-1.1	1.3	-1.4	4.0 *
CDH11	Cadherin 11, type 2, OB-cadherin	2.1 *	1.1	2.8 *	1.2	2.7 *
EGFR	Epidermal growth factor receptor	2.3	1.7	2.5 *	2.5 *	3.5 *
FGFR1	Fibroblast growth factor receptor 1	-1.2	1.3	1.5	-1.1	1.3
FGFR2	Fibroblast growth factor receptor 2	1.4	-1.5	1.2	-2.5 *	1.3
FLT1	Fms-related tyrosine kinase 1	1.6	3.8 *	4.2 *	2.3	3.9
ICAM1	Intercellular adhesion molecule 1 (CD54)	-1.8	3.0 *	1.6	4.0 *	1.9
SCARB1	Scavenger receptor class B, member 1	-3.8 *	1.5	-1.2	1.2	-1.6
TGFB1	Transforming growth factor, beta receptor I	1.0	-1.3	-1.3	-1.3	-1.2
TGFB2	Transforming growth factor, beta receptor II	2.8 *	2.5 *	2.7	2.8 *	3.4 *
VCAM1	Vascular cell adhesion molecule 1	1.5	1.6	3.7 **	1.7	2.4 *
VDR	Vitamin D (1,25-dihydroxyvitamin D3) receptor	1.4	-1.1	1.4	-1.2	1.5
IGF1R	Insulin-like growth factor 1 receptor	-1.1	-1.2	-1.6	-1.2	1.5
PHEX	Phosphate regulating endopeptidase homolog, X-linked	1.0	2.0 *	2.4 *	2.2	3.4 *
Growth Factors						
EGF	Epidermal growth factor (beta-urogastrone)	-1.0	-1.6	1.1	-1.0	-1.6
FGF1	Fibroblast growth factor 1 (acidic)	1.6	-1.3	-1.8	1.5	1.1
FGF2	Fibroblast growth factor 2 (basic)	1.6	1.5	-1.3	1.7	1.4
IGF1	Insulin-like growth factor 1 (somatomedin C)	-2.6 *	-1.1	2.1 *	-9.5 *	1.8
IGF2	Insulin-like growth factor 2 (somatomedin A)	-1.9	2.0	2.1	1.2	1.5
PDGFA	Platelet-derived growth factor alpha	3.0 **	2.0 *	2.2	2.9 *	3.4 *
VEGFA	Vascular endothelial growth factor A	2.1	1.1	2.1 **	1.2	1.6
VEGFB	Vascular endothelial growth factor B	-1.7	1.2	1.4	1.1	2.9 *
Integrin Receptors						
ITGA1	Integrin, alpha 1	2.2 *	1.6	1.1	1.6	2.3
ITGA2	Integrin, alpha 2	2.8	-1.1	-1.8	1.3	1.1
ITGA3	Integrin, alpha 3	1.5	3.2 *	2.7 *	3.6 *	3.5 *
ITGB1	Integrin, beta 1	1.2	-1.2	1.0	1.1	1.2
Collagen						
COL10A1	Collagen, type X, alpha 1	-1.5	1.4	1.5	6.7 *	5.5 *
COL11A1	Collagen, type XI, alpha 1	1.7	1.4	2.3 *	1.4	3.1 *
COL12A1	Collagen, type XII, alpha 1	1.6	1.1	1.5	1.0	1.9
COL14A1	Collagen, type XIV, alpha 1	1.5	-1.6	-1.4	-2.5 *	-1.1
COL15A1	Collagen, type XV, alpha 1	2.5 *	-1.9	1.2	2.7 *	2.4 *
COL1A1	Collagen, type I, alpha 1	1.2	-1.1	1.0	-1.1	-1.2
COL1A2	Collagen, type I, alpha 2	2.9 *	1.2	2.8 *	2.2 *	3.1 *
COL2A1	Collagen, type II, alpha 1	1.3	1.0	1.8	-1.2	1.5
COL3A1	Collagen, type III, alpha 1	1.1	1.2	-1.7	-1.3	1.1
COL4A3	Collagen, type IV, alpha 3	-1.2	1.7	1.0	2.8	1.3
COL5A1	Collagen, type V, alpha 1	1.7	-1.1	1.2	1.2	1.3
Cartilage Related Genes						
COMP	Cartilage oligomeric matrix protein	1.9	1.1	2.3 *	1.2	4.1 *
SOX9	SRY (sex determining region Y)-box 9	1.6	-1.5	1.4	-1.8	1.1
Metalloproteinases						
BMP1	Bone morphogenetic protein 1	1.9	1.3	1.8	1.1	3.2 *
MINPP1	Multiple inositol polyphosphate histidine phosphatase, 1	1.1	-1.1	1.2	-1.0	1.2
MMP10	Matrix metalloproteinase 10 (stromelysin 2)	2.0	1.2	-1.2	-2.2	1.5
MMP2	Matrix metalloproteinase 2	1.5	1.2	1.2	1.1	1.7
MMP8	Matrix metalloproteinase 8	-7.1 *	1.3	-2.9 *	-1.0	-5.0 *
MMP9	Matrix metalloproteinase 9	1.7	-1.9	1.7	-1.5	1.3
Transcription Factors						
MSX1	Msh homeobox 1	-5.2	-1.8	-6.3	-12.5	-2.2
NFKB1	Nuclear factor of kappa in B-cells 1 (p105)	1.4	1.2	1.7	1.8	2.1
RUNX2	Runt-related transcription factor 2	1.3	1.2	1.5	-1.2	1.9
SMAD1	SMAD family member 1	1.1	-1.1	1.0	-1.6	1.2
SMAD2	SMAD family member 2	1.6	1.5	1.8	1.4	1.9
SMAD3	SMAD family member 3	1.5	1.9	1.8	1.9	1.8
SMAD4	SMAD family member 4	1.3	-1.2	1.1	-1.3	-1.1
TWIST1	Twist homolog 1	1.7	1.5	-5.5	1.1	1.4
Other genes						
CTSK	Cathepsin K	1.7	1.5	2.8 *	3.0 *	7.3 *
FN1	Fibronectin 1	2.1 *	1.3	1.4	1.7	2.0 *
SERPINH1	heat shock protein 47	2.3 *	1.2	1.8	1.4	1.6
STATH	Statherin	4.3 *	2.4	2.7 *	2.4	4.1 *

To determine the mechanism involved in the regulatory effect of nanostructured aluminum oxide coating on human mesenchymal stem cells, we screened an array of osteogenic-specific genes. These genes were classified in groups of mRNAs according to the known or proposed function of the encoded protein (Table 3). The categories are: growth factors, transcription factors, soluble ligand receptors, integrin receptors, bone matrix proteins, cartilage-related genes, collagen, and TGF/BMP superfamily genes. As shown in Table 3, from day 3 to day 7 an increasing number of genes were up-regulated on nano Al compared to machined. At day 3, 24 genes were up-regulated and six were down-regulated compared to M 3d. At day 7, Al had 26 genes up-regulated and four genes down-regulated, while M at day 7 presented 11 genes up-regulated and one gene down-regulated. At 14 days, 33 genes were up-regulated and three down-regulated on Al, and M had 17 genes up-regulated and 7 genes down-regulated.

Transcription factors

In this study, we did not observe any significant change in Runt-related transcription factor 2 (Runx2) mRNA relative levels on either surface at any time point. However, at day 14 we could observe a slight increase of Runx2 levels for Al. The nuclear factor kappa B (NFkB) encoding mRNA was 2.0-fold increased on Al surfaces, and the expression for Msh homeobox 1 mRNA was decreased at all time points for both surfaces (12.5-fold decreased for M at day 14). In this study we did not observed any change in the expression pattern for the SMAD family genes (SMAD1-4).

TGF/BMP superfamily

For the TGF/BMP superfamily an increasing up regulation for Bone morphogenetic protein 2 (BMP2) mRNA relative expression was observed on adherent hMSCs growing on Al surface, 2.4-, 4.4- and 6.5-fold increase at days 3, 7 and 14, respectively. At the same time points we did not observed any changes on the BMP2 levels on the M surface. The bone morphogenetic protein 5 (BMP5) relative levels were also increased on Al surface but not on M at all time points. Bone morphogenetic protein 4 (BMP4) mRNA levels were increased on Al at day 7 (3.3-fold) and 14 (6.3-fold), and M at day 14 (3.1-fold). We also found an increased mRNA expression level for transforming growth factor b1 (TGFb1) mRNA on Al surfaces for all time points (up to 3.2-fold at day 14) and M at day 14 only (2.2-fold increase).

Growth factors

Colony stimulating factor 2 and 3 (CSF2 and CSF3) were up regulated on AI surfaces at day 3, 2.5- and 2.0-fold increase, respectively. At day 7 we observed an increase expression of CSF2 mRNA only compared to M, and at day 14 an increase expression of CSF2 was observed on adherent hMSCs plated on M disks, however the levels of CSF2 and CSF3 mRNA on AI surface were also increased at day 14. Fibroblast growth factor 3 (FGF3) mRNA was increased at day 3 and 7 on AI surfaces. On the other hand, Insulin-like growth factor 1 (IGF1) mRNA was 9-fold down regulated on M surface at day 14. This same gene (IGF1) mRNA expression was increased on AI surface at day 7. Platelet-derived growth factor alpha polypeptide (PDGFA) and Vascular endothelial growth factor A (VEGFA) mRNA levels were up-regulated at day 3 (3-fold for PDGFA and 2.1-fold for VEGFA) and 7 (2.1-fold for PDGFA and 2-fold for VEGFA) on AI surfaces. We also found a 3.5-fold increase in PDGFA at day 14 on hMSCs adherent to AI disks.

Soluble ligand receptors

The expression level of 15 mRNAs encoding receptor associated with different function during cell differentiation are presented in Table 3. Calcitonin receptor mRNA expression levels was increased on AI surfaces at all time points, specially at day 3 (3.7-fold increase) and day 14 (3.6-fold increase). Fms-related tyrosine kinase 1 (FLT1) mRNA presented an increased expression on AI compared to Machined at days 7 and 14. Epidermal growth factor receptor (EGFR) and Transforming growth factor beta receptor II (TGFBR2) was also up regulated on AI surfaces compared to M surfaces at all time points.

Integrin receptors

The expression pattern of a subfamily of receptors, integrin receptors. Integrin a1 and integrin a2 mRNA levels were increased on adherent cells plated on AI surfaces at the earliest time point, with up to 2.2- and 2.8-fold increase. Integrin b1 mRNA was also evaluated in this study and did not presente any change compared to the control group (M day 3). Integrin a3 mRNA levels were up regulated on both AI and M at day 7 and day 14.

Collagen genes

We found that collagen type I a2 was increased at all time points. It is the major component of the organic part of the extra cellular matrix (ECM) of bone tissue. We also found an increased mRNA expression levels for collagen type XI a1 for AI only at days 7 and 14, and an up regulation at day 14 for collagen type X a1 for both surfaces. Collagen type II a1 mRNA levels, which is the major component of the ECM in cartilage, was not detected on adherent hMSCs on both sufaces at any time point.

Bone matrix proteins

We observed that the levels of biglycan (BGN) was up regulated at day 3, 7 and 14 on AI compared to M at all time points. At day 14 this gene reached the peak of 3.1-fold increase for AI. Osteocalcin mRNA levels were also increase on AI, but on day 7 its levels on M reached up to 8.6-fold increase. In this study, alkaline phosphatase mRNA relative expression was increased on M surface in all time points.

Cartilage-related genes

Two cartilage-related genes were also evaluated in this study. Cartilage oligomeric matrix protein (COMP) mRNA levels was increased on AI at day 7 and 14 (4.0-fold) and had no changes on M surface. The Sox9 mRNA relative expression was not observed in this study.

Other genes

Other genes evaluated in this study were: Cathepsin K (CTSK), Fibronectin 1 (FN1), Heat shock protein 47 (HSP47), Statherin, and Tumor necrosis factor α (TNF α). CTSK mRNA expression levels increased up to 7.3-fold for AI and 3-fold for M at day 14. FN1 expression levels were increased for AI surfaces at day 3 (2-fold) and 14 (2-fold), and TNF α levels were up to 2-fold increase for AI disks at day 3 and 14 and for M day 7.

Discussion

This array analysis performed on titanium disks with different topographies demonstrated that cell behavior may be influenced by nanotopographic cues on the implant surface. In our study we used hMSCs that were differentiated into the osteoblastic lineage, we then evaluated the effects of a nanostructured surface on the gene expression profile of these newly differentiated osteoblasts. Some studies have focused on the effects of topography on MSCs behavior without the addition of osteogenic supplement in the cell media (Leven et al., 2004; Dalby et al., 2007). These studies were able to observe some changes in gene expression related to the different materials. However, we understand that some initial signaling is necessary to commit the MSCs into the osteoblastic pathway and improve the cell response.

The changes in gene expression levels observed in this study are attributed to an enhanced effect of nanostructured surfaces on osteoblast differentiation. Other studies have demonstrated its beneficial effects on osteoblast differentiation and bone accrual around

dental implants in vivo and in vitro (Isa et al., 2006; Mendes et al., 2007; Guo et al., 2007; Mendonça et al., 2008). However, at this point, we could not distinguish whether or not these differences were related to the Nanotopography alone or to the chemical composition of the surface. We also demonstrated that the chemical composition of the surface could be altered, by adding aluminum or zirconium onto the surface. The nanofeatures on the surfaces were around 20-50 nm and did not change significantly the initial roughness of the Machined surface.

After we evaluated osteoblast-specific gene expression using a small number of PCR primers comparing four different nanostructured surfaces up to 28 days we selected the nanostructured surface Al for focusing in a more broad response. At this point we confirmed a positive differentiation of hMSCs into osteoblasts. We evaluated up to 84 genes related to osteoblast differentiation and mineralized tissues formation available in the specific array. For this PCR array, 75 genes were evaluated and 9 were dropped out because it was more related to other mineralized tissues (5 genes) or the expression level was not detectable (4 genes).

According to the classification above, these genes groups pointed out for a better result of nanostructured alumina compared to machined titanium disks. The expression of the cartilage-related gene SOX 9 was not detected on both groups; however the expression of Cartilage oligomeric matrix protein (COMP) was observed. COMP is an important component of endochondral ossification, but it was also demonstrated to be expressed by osteoblasts in embryonic and adult tissues, but not in osteocytes (di Cesare et al., 2000). Collagen type II, which is also characteristic of cartilage formation was not detected during this study, on the other hand, collagen type I $\alpha 2$ (major component of bone tissue) was up regulated on Al surface at all time points, and increased on M only at day 14. BMP1 or procollagen C proteinase, which is an enzyme responsible for removal of the C-terminal procollagen propeptides of the major fibrillar collagen types I-III, is a secreted metalloprotease requiring calcium and needed for cartilage and bone formation (Amano et al., 2000; Palmieri et al., 2008) and it was also upregulated on Al surfaces at 14 days.

Regarding the TGF/BMP superfamily we observed in this study a remarkably increasing in the BMP2 and BMP4 expression for Al surface at all time points. BMP 5 was also highly expressed at days 3 and 14 for Al. For the M surface we only observed an increasing in BMP4 expression at day 14. Ho et al., (2008) suggested that BMP5 are required not only for skeletal patterning during embryonic development, but also for bone response and remodeling to mechanical stimulation, which may be important for the

implant/bone interface withstand the loading. TGF β 1, another important factor for osteoblast differentiation (Macdonald et al., 2007), was also up regulated on AI at all time points, but only at day 14 on M. Although we observed this increase in TGF/BMP superfamily genes, we did not observe any significant changes in the SMAD transcription factor genes, which are the responsible for the BMP signaling inside the cell. However, other mechanisms may be involved in this signaling. Otomo and colleagues (2007), demonstrated that disruption of the FLT1 tyrosine kinase domain gene (FLT1(TK $^{-/-}$)) led to significant decrease in the values of mineralizing surface, mineral apposition rate, and bone formation rate in the trabecular bone of the proximal tibiae of FLT1(TK $^{-/-}$) mice compared with those in FLT1(TK $^{+/+}$) mice. In our study the levels of FLT1 was increased in both surfaces at day 7 and 14, but at day 14 the mRNA expression levels for AI (3.9-fold) was much higher than for M (2.3-fold).

For the genes related to the bone matrix, in our study we observed an increased expression of ALP for M at all time points. This gene is considered a significant marker of osteoblast differentiation especially in lineage specific cells such as MG63 (Olivares-Navarrete et al., 2008) but may not be as significant in hMSCs. Osteocalcin mRNA levels were increased in adherent cells growing on AI surface at all time points, but at day 7 it reached its highest levels on M (8.6-fold). However, according to Kotobuki and colleagues (2008), they suggested that OCN expression at the gene level does not lead to matrix mineralization.

Mayer et al., (2005) evaluated the expression of vascular endothelial growth factor (VEGFA) expression in hMSCs and the role of VEGF signaling in modulation of osteogenic differentiation. The authors found that transcripts for VEGFA were seen to be elevated during osteogenesis and high expression of VEGFA stimulated mineralization using recombinant hMSCs. They suggested that VEGFA acts as autocrine factor for osteoblast differentiation. In our study the levels of VEGFA were increased on AI at day 3 and day 7 and the levels of VEGFB were increased at day 14. No changes were observed for these genes on M surface.

In this study we evaluated the potential differences that occurs during the osseointegration process at nanosctured coated titanium implant surfaces with defined nanometer-scale features versus implants with defined machined and acid etched surfaces devoid of intentionally arrayed nanoscale features. The *in vitro* molecular data, obtained for Al₂O₃, when compared with machined or acid etched cpTitanium implant surfaces supported greater osteoblastic differentiation, osteoblast-specific gene expression. A systematic investigation of how nanoscale topography of a given bulk chemistry affects the processes underscoring the result of osseointegration is indicated. The present data cannot distinguish

between chemical and nanotopographic effects, however other recent studies have shown that the size and characteristics of the features may be more important than chemical composition effects alone (Mendes et al., 2007). We could observe an improved response of all nanostructured surfaces as an increase in the OSX and BSP expression, which means a higher response to differentiate into osteoblasts. Furthermore, we demonstrated that the nanostructured surface coated with aluminum oxide significantly changed the hMSCs gene expression pattern towards an up regulation in osteoblast differentiation. These surfaces may be able to improve the osseointegration response providing a faster and more reliable bone to implant contact.

Capítulo 6 - Tratamento com H₂SO₄ / H₂O₂ Adiciona Nanoestruturas à Superfície de Implantes e Melhora a Expressão Gênica Específica de Osteoblastos

Neste capítulo uma diferente metodologia para a produção de superfícies nanoestruturadas foi utilizado. Um tratamento baseado em um ataque ácido por H₂SO₄ / H₂O₂ foi utilizado para adicionar um padrão nanoestruturado à superfície dos implantes de titânio. Este estudo avaliou a influência destas superfícies de implante na diferenciação de osteoblastos. Foram também utilizadas células-tronco mesenquimais humanas, que foram cultivadas sobre as superfícies nanoestruturadas. Estas superfícies foram caracterizadas fisicamente (Microscopia de força atômica - AFM, microscopia eletrônica de varredura – MEV). Após 3, 7, 14 e 28 dias as células foram removidas para isolar o RNA. O perfil de expressão gênica dos genes relacionados à cascata de diferenciação de osteoblastos foi obtido. Observou-se uma melhor resposta da superfície com tratamento ácido que adicionou as nanoestruturas, quando comparado à superfície controle. Esta superfície também foi apta a alterar o padrão de expressão gênica das células-tronco mesenquimais humanas. Esta superfície provida de nanoestruturas também demonstrou que poderia levar a uma melhor e mais rápida resposta de osseointegração.

Este capítulo foi submetido para publicação com pequenas modificações. Gustavo Mendonça, Daniela Baccelli Silveira Mendonça, Francisco J. L. Aragão, Lyndon F. Cooper.

H₂SO₄ / H₂O₂ treatment imparts nanofeatures to the implant surface and improves osteoblast-specific gene expression

Abstract:

Background: Development of new implant surfaces can improve osseointegration results and help understand osteoblast / implant surface interactions. A H₂SO₄/H₂O₂ treatment imparts nanofeatures to the implant surface and can increase the osteoblast response. The aim of this study was to evaluate the gene expression of human Mesenchymal Stem Cells (hMSCs) cultured on commercial pure Titanium (cpTi) disks and differentiated into osteoblasts. The hypothesis was that a nanostructured surface altered initial osteoinductive responses of cells to increase bone-specific gene expression. **Materials and Methods:** Commercially pure grade IV titanium disks (20.0x1.0 mm) were polished or polished and subsequently treated by grit-blasting or grit-blasting / acid etching with a H₂SO₄/H₂O₂ solution. The surfaces were divided into three groups: smooth (S), grit-blasted (Gb), and nanostructured: grit-blasted/acid etched (Nano). Surfaces were examined by scanning electron microscopy (SEM) and atomic force microscopy (AFM). hMSCs were grown on the disks. The data points analyzed were 3, 7, 14 and 28 days. Real Time PCR was used to measure the mRNA levels of ALP, BSP, Runx2, OCN, OPG, and OSX. The housekeeping gene GAPDH was used as a control. Descriptive statistics were calculated using Microsoft Excel. T-test was performed for comparison of mRNA levels compared to S surfaces (p<0.05). **Results:** All the osteoblast specific genes were regulated differently and most of them were upregulated on the Nano surfaces. Runx2 and OSX mRNAs were more than 3-fold upregulated at day 14 and 28. Higher levels for ALP (38-fold), BSP (76-fold) and OCN (3-fold) were also observed on the Nano surfaces. **Conclusion:** The results demonstrate that a grit-blasted surface imparted with nanofeatures by H₂SO₄/H₂O₂ treatment affected adherent cell bone specific gene expression.

Key words:

Nanotopography; Dental Implant; Surface treatment; Bone regeneration.

Introduction

Implant surface technology has evolved in the last decade and focused in developing new surfaces capable of supporting the osseointegration process even in compromised patients. In the early 1980s, the main clinical advantage of osseointegration was the predictable clinical result that occurred when an osseous interface was reproducibly formed and maintained at the titanium surface of load bearing dental implants (Adell et al., 1990.

These outcome is much more predictable in patients with a more dense bone type (bone type 1-3), and less predictable in poor lamellar bone (type 4) (Neves et al., 2006) and some selected patient populations (e.g. smokers, diabetics) were supported by initial reports (Jaffin; Berman, 1991; Bain, 1996; Fiorellini et al., 2000). The cause of these failures, while not precisely determined, was largely attributed to a failure in bone formation in support of osseointegration. Challenging osseointegration with new protocols such as immediate placement and immediate loading may require further control of bone formation and osseointegration (Morton et al., 2004).

Implant surface plays an important role affecting the rate and extent of osseointegration (Cooper 1998; Nanci et al., 1998; Boyan et al., 1993; Schwartz et al., 1992; Stanford et al., 2006). Many studies have given insight on the osseointegration process, and it is now well described both histologically and at the cellular level (Davies, 2003). The adhesion of a fibrin blood clot and the population of the implant surface by blood-derived cells and mesenchymal stem cells are orchestrated in a manner that results in osteoid formation and its subsequent mineralization (Masuda et al., 1997; Meyer et al., 2004; Berglundh et al., 2003). A seamless progression of changing cell populations and elaboration and modification of the tissue / implant interface eventually results in bone forming in direct contact with the implant surface. Precisely how much of the implant surface directly contacts bone, how rapidly this bone accrual occurs, and the mechanical nature of the bone / implant connection is influenced by the nature of the implant surface itself (Le Guéhennec et al., 2007)

Early investigations revealed the biocompatible nature of the cpTitanium implant (Kasemo, 1983), and the importance of the implant surface was brought into consideration in this complex process of osseointegration in a number of different ways. Several investigations at the cellular and molecular level have contributed to defining cellular responses to titanium as “compatible” and advantageous. Subsequently, experiments with surface topography encouraged new considerations of improvements in bone formation at the implant surface. At this point, in the early 1990s, an important role for surface microtopography was advocated (Buser et al., 1991). More recently several investigations have been pointing out to the nanotopographic level of the implant surface or the combination between micro and nanofeatures to improve the osseointegration process (Webster et al., 2001a; Guo et al., 2007).

Nanotechnology has been defined as “the creation of functional materials, devices and systems through control of matter on the nanometer length scale (1–100nm), and

exploitation of novel phenomena and properties (physical, chemical, biological) at that length scale” (National Aeronautics and Space Administration). Nanotechnology involves materials that have a nano-sized topography in at least one of its significant dimension. These materials have a size range between 1-100nm (10^{-9} m). Materials are also classified according to their form and structure as, nanocrystals, nanocoatings, nanoparticles, and nanofibers (Christenson et al., 2007).

Based on the hypothesis that nanostructured surfaces can modulate initial osteoinductive responses of cells to increase bone-specific gene expression. The aim of this study was to evaluate the gene expression of human Mesenchymal Stem Cells (hMSCs) differentiated into osteoblasts and cultured on commercial pure Titanium (cpTi) disks modified with a combination of micro and nano features.

Materials and Methods

Surfaces preparation

Commercially pure grade IV titanium disks (20.0x1.0 mm) were used. Initially, all the disks were polished using Si carbide papers starting from grade 320, 400 to 600 grits. Subsequently, the disks were grit-blasted with 100 μ m aluminum oxide particles, and sonicated three times in distilled water for 15 min each to clean, followed by immersion in 50/50 v/v % solution of H₂O₂ and H₂SO₄ (Fisher Scientific, Inc., Pittsburgh, PA) for 2 hours. Following treatment with H₂SO₄/H₂O₂ solution, the substrates were sonicated three times in ultrapure deionized (DI) water (resistivity 1/4 8.2MO, pH1/4 6.82, Millipore Inc.), then three times in ethanol, before drying under the hood (samples prepared in this manner are hereafter referred to as “Nano”). Another set of disks was polished only and composed the Smooth (S) group. This disks were sonicated three times in distilled water for 15 min each to clean, and then it was passivated with 30% HNO₃ for 15 min. A third group was composed of disks that after polishing were grit-blasted, cleaned and passivated with 30% HNO₃ for 15 min (this disks composed the Grit-blasted (Gb) group). The sequence for disks preparation are shown in Table 1

Table 1 – Surfaces preparation

	Polishing with Si carbide papers	Grit-blasting with 100 μ m aluminum oxide particles	Passivated with 30% HNO ₃	immersion H ₂ O ₂ /H ₂ SO ₄ solution
Smooth (S)	Yes		Yes	
Grit-blasted (Gb)	Yes	Yes	Yes	
Acid-etched (Nano)	Yes	Yes		Yes

Surfaces analysis

The surface of the disks was examined by a high-resolution scanning electron microscope (Field Emission Scanning Electron Microscope (FEG-SEM), Hitachi S-4700) and atomic force microscopy (Nanoscope IIIA atomic force microscope (Digital Instruments, Santa Barbara, CA, United States)). Observations were made at three different points on the disks surfaces, and average values were calculated. XPS spectra were recorded on a Kratos Axis Ultra spectrometer with a concentric hemispherical analyzer and a delay line detector. Monochromatic Al Ka x-rays were used at 150 W, and the chamber base pressure was less than 10^{-8} torr. Survey spectra were obtained at a pass energy of 80 eV and a step size of 1 eV, while high resolution elemental scans were taken at a pass energy of 20 eV and a step size of 0.1 eV. All spectra were corrected for the adventitious C 1s peak at 284.6eV.

Cell Culture

Human mesenchymal stem cells (hMSCs) P2 were purchased (Lonza) and cultured in accordance with published protocols. Growth media included Dulbecco's modified eagle medium Low glucose (LG-DMEM) (Gibco) supplemented with 10% fetal bovine serum (FBS) and antibiotic/antimycotic (penicillin/streptomycin/amphotericin B, Sigma). Osteogenic media includes LG-DMEM (Gibco, #11885) supplemented with 10% FBS and antibiotic/antimycotic and the osteogenic supplements 10^{-7} M dexamethasone (Sigma), 10mM glycerophosphate (Sigma G9891) and 0.2mM ascorbic acid (Sigma). Passage 2 cells were plated at low density and grown until nearly confluent. Cells were subsequently passaged onto prepared titanium disks using 100,000 cells in 250 μ l of growth media. The formed meniscus was left undisturbed to permit cell attachment over 4 hours and subsequently additional growth media was applied. Following overnight incubation, cultures were carefully rinsed and osteogenic media was placed in culture dishes. This represented the starting time point (T = 0). The osteogenic media was replaced every third day. Disks with adherent cell and forming tissue layers were collected on day 3, 7, 14, and 28.

RNA isolation and analysis

For evaluation of mRNA expression in cells adherent to titanium disks. Titanium disks were removed from the culture dishes and rinsed twice with cold phosphate buffered saline (PBS). Adherent cells on each disk were lysed using Trizol (Invitrogen, Carlsbad, CA) and lysates were collected by pipetting and centrifugation. Total RNA in the cell lysates was isolated using the Trizol according to the manufacturer's protocol and collected by ethanol precipitation. Total RNA was quantified using UV spectrophotometry. From each total RNA sample, cDNA was generated using RT² First Strand Kit reverse transcriptase (Superarray, Frederick, MD) in a standard 20 μ L reaction using 1 μ g of the total RNA. All cDNAs were

subjected to polymerase chain reaction (PCR) for GAPDH mRNA as a test of RNA integrity and cDNA synthesis. Subsequently, equal volumes of cDNA were used to program real time PCR reactions specific for mRNAs encoding ALP, BSP, Runx2, OCN, OPG, and OSX. Reactions were performed using a customized RT² Profiler™ PCR Arrays (CAHP-0398) (Superarray, Frederick, MD) and thermocycling in an ABI 7200 real time thermocycler (Applied Biosystems, Foster City, CA). Relative mRNA abundance was determined by the $2^{-\Delta\Delta Ct}$ method and reported as fold induction. GAPDH abundance was used for normalization. The data points analyzed were 3, 7, 14 and 28 days. Real Time PCR was used to measure the mRNA levels of ALP, BMP6, BSP, Runx2, OCN, OPG, and OSX. The housekeeping gene GAPDH was used as a control.

Statistical analyses

Descriptive statistics were calculated using SPSS. The roughness parameter (Sa) was compared by one-way ANOVA followed by Tukey Test. For the gene expression analysis, descriptive statistics were calculated using Microsoft Excel. T-test was performed for comparison of mRNA levels compared to S surfaces. For all statistical analysis significance level was set at $P < .05$.

Results

Surface analysis

The surfaces in this study presented different characteristics related to the nanoscale level, but also included micro-scale topographic differences (Figures 1-3). At low resolution, scanning electron micrographs suggest the conservation of microfeatures between the two grit-blasted surfaces (GB and Nano) (Figure 2 and 3) and the absence of such microfeatures for the S surfaces (Figure 1). At high resolution, it reveals the presence of discrete 20 – 30nm nanofeatures on the grit-blasted surface treated with H₂SO₄/H₂O₂ (Figure 3). At high resolution, there is little nanotopographic character on the GB surface (Figure 2). When compared to the S surface, there is no evidence of topographic features at the nanoscale level as well (Figure 1).

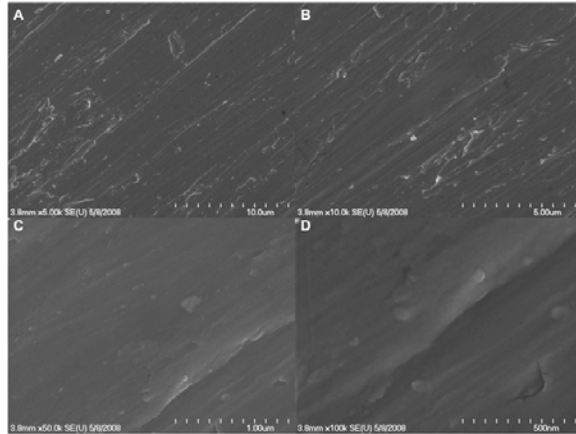


Figure 1 – SEM evaluation of the Machined surfaces at low (A and B) and high magnification (C and D). At 100,000x magnification nanofeatures are not observed.

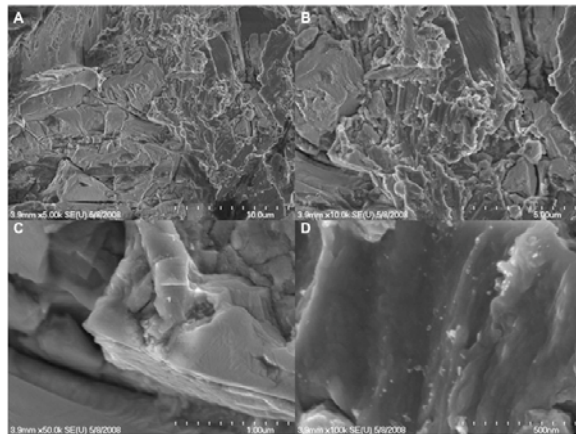


Figure 2 – SEM evaluation of the Grit-blasted surfaces at low (A and B) and high magnification (C and D). At 100,000x magnification nanofeatures are not observed.

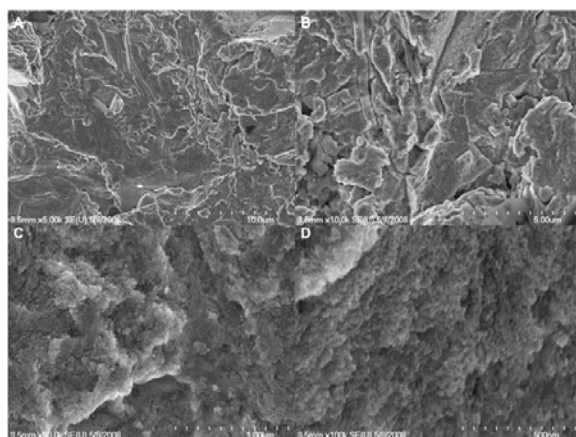


Figure 3 – SEM evaluation of the Nanostructured surfaces at low (A and B) and high magnification (C and D). Images C and D are able to show nanofeatures imparted to the surface due to the acid treatment.

Measurement of surface parameters showed a difference among the three prepared surfaces (Figure 4). The Sa roughness parameter demonstrated a much smoother surface

for the S group which was polished with up to 600grit sandpaper. The GB and Nano groups presented higher Sa values due to the grit-blasting process with 100 μ m alumina particles. This grit-blasting process was held responsible for the Sa values for the GB group which was found to be around 160 μ m. The highest Sa values was found in the Nano group and it was due to the subsequent acid etch treatment following the grit-blasting (Figure 4). The waviness of both GB and Nano surfaces were similar and much higher than the S surface (Figure 4).

Cells were successfully grown and expanded on all surfaces. Cell layers were formed in multilayers and retraction from the disks was not observed. From the cultures established with 100,000 cells, there were sufficient numbers of cells present after 3, 7, 14 and 28 days for isolation of total RNA (> 5 μ g of total RNA) to perform the arrayed real time PCR reactions.

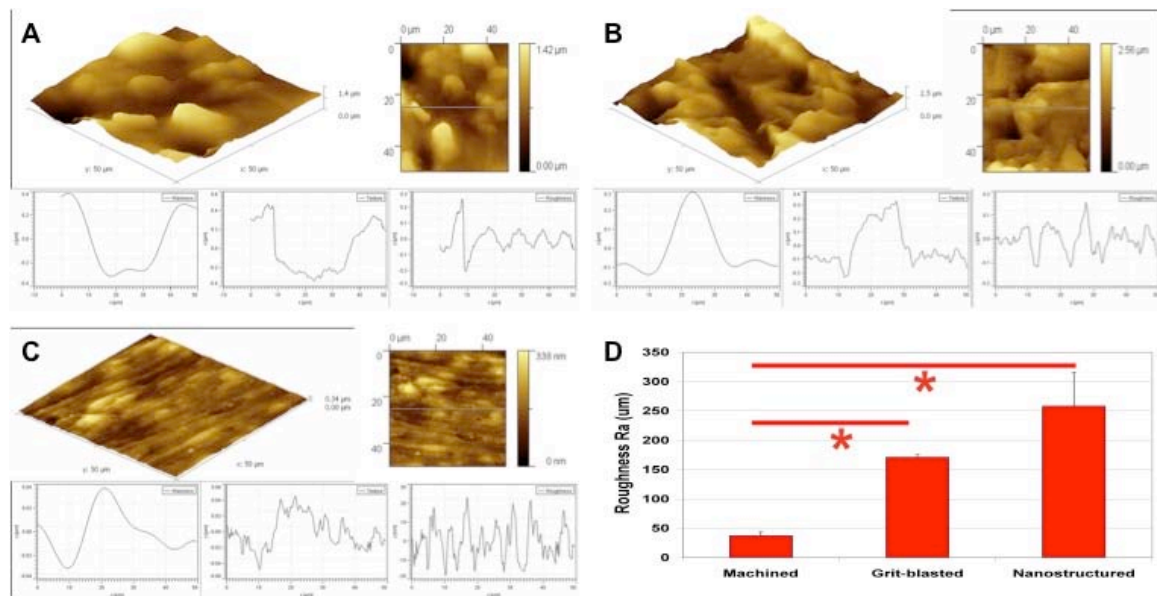


Figure 4 – AFM evaluation of the (A) Machined, (B) Grit-blasted and (C) Nanostructured surfaces. The graph in D depicts the Roughness (Ra) for each surface. * Statistically significant difference ($p < 0.05$).

Figures 5 and 6 show hMSCs growing on S and Nano after 24 hours. At 1,500x magnification cells growing on both surfaces are very similar; however, at 10,000x an increased fillapodia is observed on Nano. At 50,000x and 100,000x the interaction between the cells and the nanofeatures of the surface is evident and the cell seems to blend into the surface.

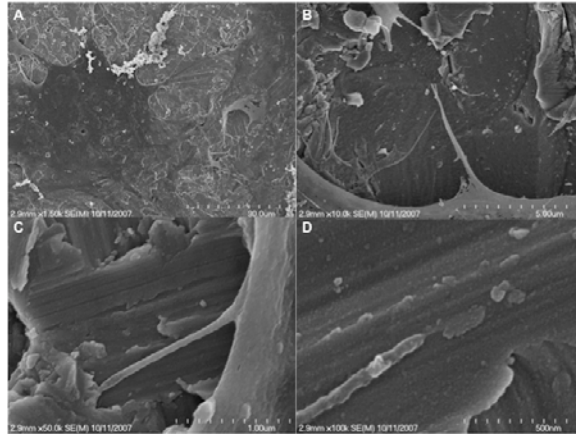


Figure 5 - hMSCs growing on Machined. (A) At 1,500x magnification the surface characteristics can not be distinguished; however, (B) at 10,000x a little fillapodia is observed on Machined. (C) and (D) At 50,000x and 100,000x the interaction between the cells and the surface is weak.

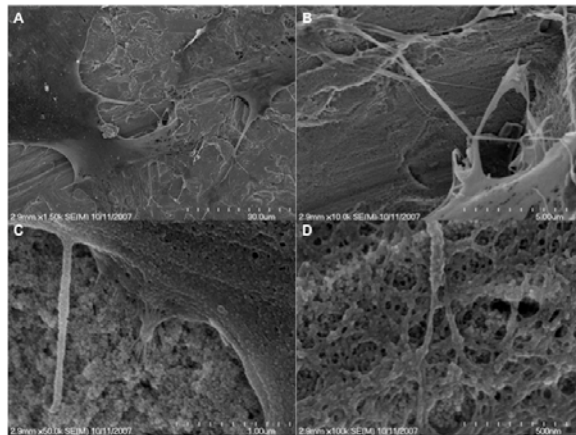


Figure 6 – hMSCs growing on Nano. (A) At 1,500x magnification no changes are observed compared to Figure 5; however, (B) at 10,000x an increased fillapodia is observed on Nano. (C) and (D) At 50,000x and 100,000x the interaction between the cells and the nanofeatures of the surface is shown.

Surface-specific gene regulation was observed for all studied genes. One general observation was that early differences among the surfaces (day 3 or 7) were often of lower magnitude than differences observed at 14 and 28 days. At day 3 no statistical difference were found among the surfaces. Another observation was that the Nano group presented, at day 7, an expression pattern similar to S for all genes. After 14 days Nano presented a marked increase compared to GB and S.

ALP mRNAs relative levels for Nano were slightly down-regulated at day 7. At day 14 and 28 it was 15-fold and 40-fold up-regulated, respectively; compared to a much lower expression for S and GB surfaces (Figure 7). BSP relative mRNAs expression was similarly up regulated for both GB and Nano at day 7 (10-fold increase). At day 14 the expression

levels for Nano, GB and S were 80- 55-, and 25-fold, respectively (Figure 8). OPN mRNA levels were constant for S throughout the 28 days period of the experiment, and behaved very similar for GB and Nano. At day 28 the relative expression level for GB and Nano were up to 58-fold increase for both surfaces (Figure 9).

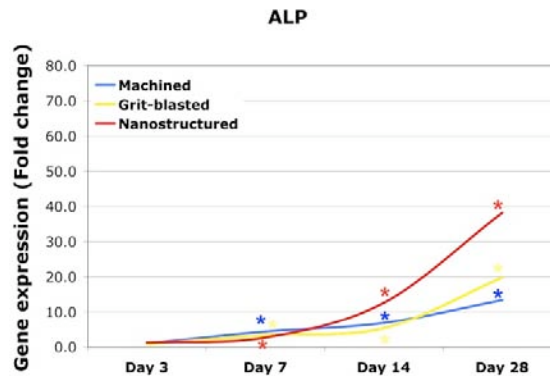


Figure 7 - Adherent hMSCs bone-specific mRNA expression. Expression levels (fold change) for ALP are compared for all surfaces. Total RNA was isolate from cells at 3, 7, 14 and 28 days of culture on Machined, Grit-blasted and Nanostructured Titanium disks. The results are shown as fold change ($2^{-\Delta\Delta Ct}$ method, baseline=day 3 cells on Machined surface). *Statistically significant difference compared to baseline ($p < 0.05$).

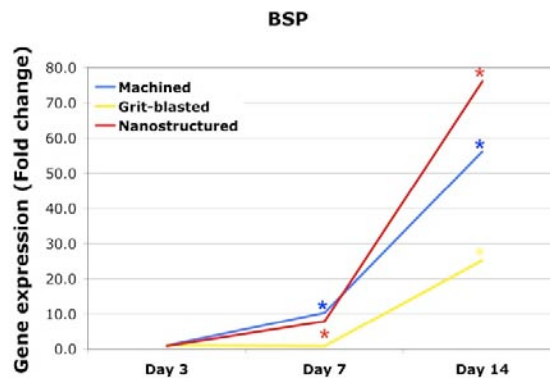


Figure 8 - Adherent hMSCs bone-specific mRNA expression. Expression levels (fold change) for BSP are compared for all surfaces. Total RNA was isolate from cells at 3, 7, and 14 days of culture on Machined, Grit-blasted and Nanostructured Titanium disks. The results are shown as fold change ($2^{-\Delta\Delta Ct}$ method, baseline=day 3 cells on Machined surface). *Statistically significant difference compared to baseline ($p < 0.05$).

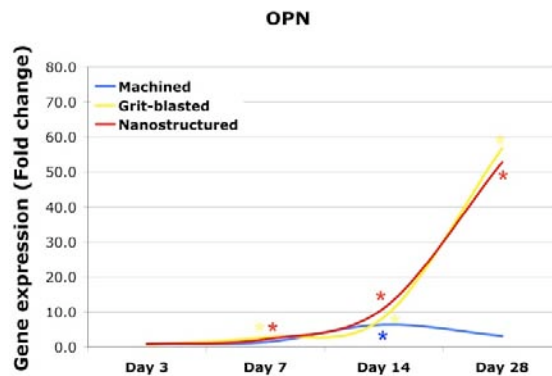


Figure 9 - Adherent hMSCs bone-specific mRNA expression. Expression levels (fold change) for OPN are compared for all surfaces. Total RNA was isolate from cells at 3, 7, 14 and 28 days of culture on Machined, Grit-blasted and Nanostructured Titanium disks. The results are shown as fold change ($2^{-\Delta\Delta C_t}$ method, baseline=day 3 cells on Machined surface). *Statistically significant difference compared to baseline ($p < 0.05$).

The levels of OCN mRNA expression were up to 3-fold increased for S and Nano at day 14 and kept the same rate for Nano at day 28. The levels of OCN mRNA for S dropped close to baseline level at 28 days. For GB, the OCN mRNA relative levels reached 2-fold increase at 7 days and kept constant throughout the experiment (Figure 10).

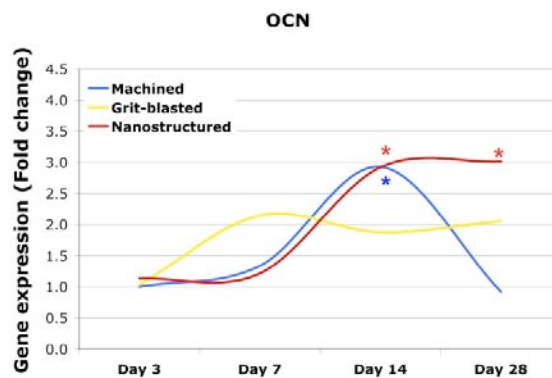


Figure 10 - Adherent hMSCs bone-specific mRNA expression. Expression levels (fold change) for OCN are compared for all surfaces. Total RNA was isolate from cells at 3, 7, 14 and 28 days of culture on Machined, Grit-blasted and Nanostructured Titanium disks. The results are shown as fold change ($2^{-\Delta\Delta C_t}$ method, baseline=day 3 cells on Machined surface). *Statistically significant difference compared to baseline ($p < 0.05$).

OSX mRNAs (key transcription factor for osteoblast differentiation) expression levels were more than 2.5-, 3.5- and 4- fold up-regulated at day 7, 14 and 28 for Nano. OSX expression levels for GB reached up to 4-fold at day 7 and then dropped to baseline levels at day 14 and 28. For the S surface, its level reached 2.5-fold increase at day 7 and then decrease to baseline (Figure 11). The relative expression levels of Runx2 RNA was up to 3.5-fold for Nano at day 14 and 28. For the GB surface, it varied around 2.5-fold for the same

period. The Runx2 expression levels for S surface was up to 2-fold increase at day 14 (Figure 12).

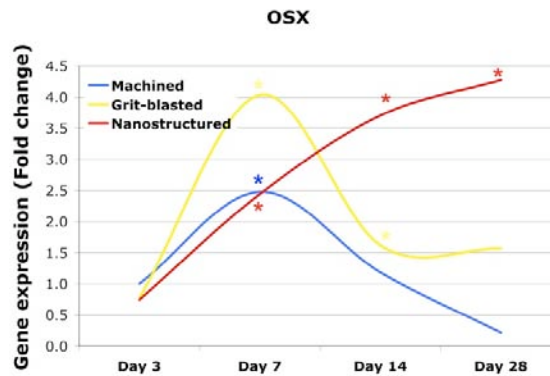


Figure 11 - Adherent hMSCs bone-specific mRNA expression. Expression levels (fold change) for OSX are compared for all surfaces. Total RNA was isolate from cells at 3, 7, 14 and 28 days of culture on Machined, Grit-blasted and Nanostructured Titanium disks. The results are shown as fold change ($2^{-\Delta\Delta C_t}$ method, baseline=day 3 cells on Machined surface). *Statistically significant difference compared to baseline ($p < 0.05$).

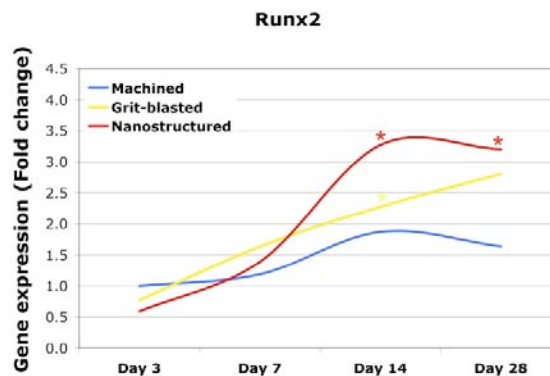


Figure 12 - Adherent hMSCs bone-specific mRNA expression. Expression levels (fold change) for Runx2 are compared for all surfaces. Total RNA was isolate from cells at 3, 7, 14 and 28 days of culture on Machined, Grit-blasted and Nanostructured Titanium disks. The results are shown as fold change ($2^{-\Delta\Delta C_t}$ method, baseline=day 3 cells on Machined surface). *Statistically significant difference compared to baseline ($p < 0.05$).

Discussion

The importance of surface topography has been demonstrated in many studies (Buser et al., 2001; Ogawa; Nishimura, 2003; Ogawa; Nishimura, 2006), but until the late 1990s they had focused on micron-scale modifications (Buser et al., 2001; Ogawa; Nishimura, 2003). More recently, the focus has been shifting to the nano-scale level (Guo et al., 2007; Coelho; Suzuki, 2005; Mendes et al., 2007; Berglundh et al., 2007). The observation that a micron-scale rough surface prepared by grit blasting and subsequent acid

etching was able to impart nanofeatures to the surface and these modifications increased the cellular activity or tissue responses leading to greater osteogenesis on this surface gave opportunity to many investigations and new implant surfaces (Guo et al., 2007; Berglundh et al., 2007). In this study we used 100 μ m aluminum oxide particles to create the microtopography by grit-blasting and subsequently acid-etched with a H₂SO₄/H₂O₂ that is also known to impart nanofeatures to the titanium surface (Nanci et al., 1998; Oliveira; Nanci, 2004). The differences between the treatments were observed by SEM and AFM. The amount of nanofeatures observed on the three surfaces by the SEM is significantly higher on the Nano surface compared to S and Gb.

By observation of the AFM analysis we could see that the changes in the Sa on the three surfaces were related to the grit blasting process and subsequently the acid etching. The waviness of the surface changed considerably from S to Gb due to the grit-blasting with 100 μ m alumina particles and increased the roughness of Gb around 170 μ m. The same grit-blasting step was also applied on the Nano surface, and followed the acid etching the roughness increased to 250 μ m. The waviness of both surfaces, Gb and Nano, are similar and due to the micron preparation (grit-blasting) of these surfaces.

Chemical treatments or acid oxidation, such as Hydrofluoric acid have been used to create nanotopography (Nanci et al., 1998; Wang et al., 2001; Uchida et al., 2002). Different methods can be used to impart nanofeatures to a surface. The chemical treatment is used to expose reactive groups on the material surface and create nanoscale topography. Per example, the use of NaOH-treatment catalyzes the production of titanium nanostructures outward from the titanium surface (Kim et al., 2000), creating a sodium titanate gel layer on the Ti surface. This gel-like layer over the material allows hydroxyapatite deposition. Meanwhile, H₂O₂ treatment produces a titania-gel layer. The use of a mixture of H₂SO₄/H₂O₂ has been used for deoxidation and controlled reoxidation of metals and creates novel nanostructures of amorphous titanium oxide on the implant surface (Nanci et al., 1998) It was found that the treatment of the implant surface with H₂O₂/HCl increased the adsorption of RGD peptides onto the surface followed by passivated surfaces (30% HNO₃) and heat-treated surfaces (Wang et al., 2001). These surface treatments also increased the mineralization in the same order. Treatment with hydrofluoric acid also creates discrete nanostructures on TiO₂ grit blasted surfaces (Ellingsen et al., 2006). Titanium oxide nanotubes chemically treated with NaOH accelerated HA crystal growth in a simulated body fluid (SBF) (Oh et al., 2005). The kinetics of HA formation is significantly accelerated by the presence of the nanostructure associated to the NaOH treatment. In all methods above, both chemical and topography changes are imparted. In this study, this chemical treatment also

eliminated surface contaminants from the grit-blasting process and resulted in consistent and reproducible nanoscale topography over micron topography.

In this *in vitro* study we sought to evaluate an acid-etching treatment that imparted nanostructures to a titanium implant surface and altered cell behavior. These data supports a conclusion that the nanoscale modification of titanium implants increased the osteogenic behavior of cells resulting in an increased stimulus to cell differentiation and mineralization, but does not fully address the role of nanoscale topography in the process of osseointegration. Many authors (Webster et al., 1999; Webster et al., 2000a; Webster et al., 2000b; Price et al., 2003a) have presented data showing the positive effects of nanostructured surfaces when compared to the same materials in micron scale. The present data cannot distinguish between chemical and nanotopographic effects, however other recent studies have shown that the size and characteristics of the features may be more important than chemical composition effects alone (Mendes et al., 2007).

This investigation used human mesenchymal stem cells to model osteoinduction and osteoblastic differentiation in cell culture performed on three different titanium substrates. One surface was a polished smooth surface. The other two surfaces were prepared by grit-blasting, and one of them was subsequently treated by acid-etching to impart nanostructures onto this surface. Under osteoinductive conditions, the mesenchymal stem cells can reproducibly differentiate into osteoblasts when cultured on tissue culture plastic dishes (Jaiswal et al., 1997). Cooper et al (2006), used this model to explore the effect of titanium surface topography on adherent cell osteoblastic differentiation and showed that changes in bone matrix protein expression occur as a function of the titanium surface topography. This confirms previous observations demonstrated in evaluation of the Osseospeed™ surface (Astra Tech AB, Molndal, Sweden) (Guo et al., 2007). Recent studies by Dalby et al (2007, 2008) using hMSCs have demonstrated that nanotopography were able to influence these cells to differentiate even when no osteogenic media was added to the culture. They suggested that human mesenchymal populations are especially sensitive to nanotopography and can use these features for subsequent differentiation into osteoblasts.

The surface-specific gene expression obtained at each time point demonstrated a relative higher mRNA expression level for Runx2 and OSX for Nano at day 14 and 28. Runx2 and OSX are key transcription genes in osteoblast differentiation (Harada et al., 1999; Harada; Rodan, 2003) and an increase in its levels may be related to the effect of different surfaces on hMSCs differentiation and commitment to osteoblast lineage. Increased levels in Runx2 expression have also been demonstrated in other studies (Guo et al., 2007; Isa et al.,

2006). At day 7 the Gb surface presented a higher level of OSX mRNA relative expression that decreased rapidly to baseline levels. On the other hand, the Nano surface was able to increase and keep its level high up to 28 days. Runx2 elevations are related to increasing in the expression of other bone related genes such as Alkaline phosphatase, Collagen type I, Osteocalcin, and Osteopontin.

In a study using a similar surface preparation, Oliveira and Nanci (2004) observed an early and increased expression of OPN and BSP. The same group also observed an increase in bone-to-implant contact when placing implants prepared with H_2SO_4/H_2O_2 solution in dogs mandible (Tavares et al., 2007). One observation from this study was that up to day 7 all surfaces presented a similar pattern in gene expression levels (specially S and Nano). After day 14 the surface with imparted nanofeatures demonstrated an increased capacity in inducing osteoblast specific gene expression, with an increased expression of ALP, BSP, compared to S and Gb. At day 28 the expression levels on Nano were also higher for OCN. ALP, BSP, OCN and OPN are marked genes of osteoblast differentiation and expressed at various time-points related to stage of cell commitment (Cooper, 1998).

A grit-blasted surface imparted with nanofeatures by H_2SO_4/H_2O_2 treatment affected adherent hMSCs improving bone specific gene expression. These nanofeatures (<100nm) were able to increase osteoinductive gene expression in adherent hMSCs.

Capítulo 7 – Discussão Geral

O objetivo deste trabalho foi avaliar o efeito de características nanométricas na superfície de implantes dentários osseointegrados de titânio. Uma ampla revisão da literatura (Capítulo 2) demonstrou uma série de efeitos benéficos quando características nanométricas são adicionadas, de acordo com vários métodos empregados (Tabela 1, Capítulo 2), à superfície dos implantes (Tabelas 2 e 3, Capítulo 2). Estes efeitos foram então investigados a nível molecular e biomecânico em uma série de estudos *in vitro* e *in vivo* (Capítulos 3 a 6). Neste capítulo será feita uma discussão geral relativa aos diferentes métodos e modelos utilizados. A discussão completa dos resultados obtidos em cada capítulo foi feita anteriormente, no contexto de cada capítulo apresentado (Capítulos 3 a 6). Neste trabalho não foi verificada nenhuma complicação referente à utilização destes implantes em animais, nem referentes à utilização de células cultivadas sobre as superfícies dos discos de titânio.

Todas as superfícies utilizadas neste estudo foram caracterizadas física e quimicamente (Microscopia de força atômica - AFM, microscopia eletrônica de varredura – MEV, e espectroscopia de fluorescência – XPS) (Capítulos 3 a 6). As superfícies nanoestruturadas avaliadas neste trabalhos fazem referência às superfícies contendo uma camada nanoestruturada de óxido de titânio, óxido de alumínio, óxido de zircônio e também uma superfície nanoestruturada criada por meio de ataque ácido. Neste trabalho, para os Capítulos 3 e 4, foram selecionados dois grupos controles, um composto por implantes usinados (de superfície lisa) e um composto por implantes de superfície com ataque ácido (superfície rugosa – a nível micrométrico). Para os Capítulos 5 e 6 o grupo controle foi composto por disco de titânio polidos (de superfície lisa) ou jateados e ataque ácido (superfície rugosa – a nível micrométrico). Estes tipos de superfícies usadas como controle são o modelos padrão de superfície utilizados atualmente (Brånemark, 1983; Ellingsen et al., 2004; Buser et al., 2004) e nos permitiu verificar os efeitos das superfícies nanoestruturadas em relação as superfícies controle.

A análise no MEV revelou que as superfícies nanoestruturadas apresentavam características em escala nanométrica que não estavam presentes nas superfícies lisas ou rugosas (a nível micrométrico). Estas características eram compostas por porosidades e acréscimos na superfície em escala menor do que 100nm (geralmente em torno de 20 a 50nm) (Capítulos 3 a 6). A análise no AFM também demonstrou que as superfícies nanoestruturadas apresentaram uma rugosidade semelhante à superfície lisa o que comprova a característica nanométrica do filme utilizado. Entretanto, a superfície

nanoestruturada preparada com ataque ácido apresentou uma rugosidade aumentada, que pode ser tido afetada pelo processo de jateamento feito previamente para esta superfície (utilizando partículas de óxido de alumínio com 100µm de diâmetro). Nesta superfície o ataque ácido (H_2SO_4/H_2O_2) criou características nanométricas na superfície mas a rugosidade foi afetada pelo jateamento com particular micrométricas.

A análise de EDS e XPS demonstrou claramente que as superfícies nanoestruturadas de óxido de titânio, óxido de alumínio e óxido de zircônio tiveram a sua composição química alterada (Capítulos 3 a 5). Nas superfícies preparadas a partir de alumínio e zircônio, estes materiais foram encontrados recobrando amplamente as respectivas superfícies (Tabela 2 e Figura 7, Capítulo 5). Esta análise também comprovou que estes materiais estavam na sua forma oxidada, o que os torna mais estáveis no meio biológico. Para as duas superfícies contendo óxido de titânio, também foi observado a presença de titânio na forma de óxido de titânio e não titânio metálico (reativo). Para as superfícies lisa e rugosa foi observado a presença de titânio tanto na forma de óxido (TiO_2) quanto na forma de íons metálicos (reativos quimicamente). A literatura cita amplamente os benefícios do titânio como sendo biocompatível baseados na presença da camada de óxidos presente na superfície dos implantes (Linder et al., 1983; Branemark et al., 1985; Le Guéhennec et al., 2007).

Os métodos para obtenção de superfícies nanoestruturadas variam amplamente na literatura (Tabela 1, Capítulo 2). Neste trabalho foram utilizados dois métodos diferentes, um baseado na tecnologia de filmes finos, no qual uma camada de espessura nanométrica é adicionada a superfície dos implantes ou discos de titânio (Ben-Nissan; Choi, 2006; Choi; Ben-Nissan, 2007). Neste método, diferentes materiais podem ser utilizados e adicionados à superfície como uma maneira de otimizar a superfície para o contato com o tecido ósseo (Pechini, 1967). Um segundo método foi baseado na subtração química da superfície, no qual um tratamento químico remove parte da superfície deixando a superfície com características nanoestruturadas (devido a utilização de H_2O_2) e modificando quimicamente esta superfície (Puleo; Nanci, 1999; Oliveira; Nanci, 2004). Neste método, o controle da composição química da superfície passa a ser mais limitado, mas ainda assim ocorre uma mudança estrutural e química que otimiza essa superfície para favorecer a adsorção de proteínas e adesão de células (Wang et al., 2001; Wang et al., 2002; Uchida et al., 2002; Oliveira; Nanci, 2004; Oliveira et al., 2007).

Inicialmente buscou-se investigar os efeitos das superfícies nanoestruturadas em relação a sua composição química e características nanométricas. Nos Capítulos 3 e 4,

implantes de titânio recobertos com um filme nanométrico composto por óxido de titânio, óxido de alumínio ou óxido de zircônio foi avaliado quanto aos efeitos celulares (a nível molecular) e aos efeitos biomecânicos (torque de remoção) e histológicos (análise histométrica). Nestes primeiros trabalhos utilizou-se um modelo animal (*Ratus norvegicus*) para obter estes resultados (Abron et al., 2001). Nestes estudos todos os resultados foram obtidos em triplicata. Este modelo animal foi escolhido por sua facilidade de manuseio e permitir a utilização de implantes de tamanho reduzido, o que facilitou o desenvolvimento desta pesquisa. No entanto, o uso de um animal de pequeno porte dificultou algumas análises mecânicas e histométricas, pois o tamanho reduzido do implante limitou estes valores (Meirelles et al., 2008a; Meirelles et al., 2008b). Todavia, os resultados obtidos nos Capítulos 3 e 4 permitiram verificar uma tendência a favor de todas as superfícies nanoestruturadas avaliadas neste trabalho. Os valores do torque de remoção e histométricos, mesmo reduzidos, foram comparáveis a outros estudos encontrados na literatura (Narai; Nagahata, 2003).

Nos Capítulos 5 e 6, investigou-se os efeitos das superfícies nanoestruturadas *in vitro*. Nestes trabalhos foram utilizadas células tronco mesenquimais humanas (hMSCs) compradas e expandidas em laboratório a partir da passagem 2 (Lonza, EUA). Este tipo de célula é apta a se diferenciar em células do tecido ósseo, cartilaginoso ou adiposo, quando devidamente estimulada para uma destas três vias. Nestes trabalhos, após um período de expansão, estas células foram colocadas sobre os discos e diferenciadas na via osteogênica (esta diferenciação foi comprovada via PCR). Este modelo *in vitro* permite avaliar os efeitos das superfícies na expressão gênica e na diferenciação destas células na linhagem de escolha (osteogênica).

No Capítulo 5 as mesmas seis superfícies utilizadas nos Capítulos 3 e 4 foram inicialmente avaliadas. Nesta etapa inicial as seis superfícies foram caracterizadas física e quimicamente (Microscopia de força atômica - AFM, microscopia eletrônica de varredura - MEV, e espectroscopia de fluorescência - XPS). Células tronco mesenquimais humanas (hMSCs) foram cultivadas sobre estas superfícies, e a partir do RNA isolado, foi obtido o cDNA utilizando uma enzima de transcriptase reversa e PCR em tempo real (Real-time RT-PCR). Um painel inicial da expressão de seis genes foi obtido para estas seis superfícies, para quatro diferentes períodos (3, 7, 14 e 28 dias). Estes genes são específicos da cascata de diferenciação e mineralização de osteoblastos (Cooper et al., 2006; Guo et al., 2007). Baseado nestes resultados, verificou-se que todas as superfícies nanoestruturadas apresentaram-se novamente superiores as superfícies lisa e rugosa. Das superfícies nanoestruturadas, a superfície de óxido de alumínio apresentou melhores resultados que as

demais. Baseados nestes resultados, uma segunda etapa deste Capítulo avaliou os efeitos desta superfície na expressão de 84 genes relacionados à cascata de diferenciação de tecidos mineralizados em três diferentes períodos (3, 7 e 14 dias).

A metodologia utilizada nos Capítulos 5 e 6 empregam o uso de real-time RT-PCR, entretanto, foram adquiridas placas de 96 poços preparadas com “primers” específicos dos genes de interesse (PCR array technology, Superarray, Frederick, MD, USA). Posteriormente o cDNA é diluído em ddH₂O e misturado com o “master mix” que contém a enzima para a reação de PCR. Na primeira parte do Capítulo 5 e também para o Capítulo 6 uma placa foi “customizada” contendo sete genes de interesse (ALP, BMP6, BSP, OCN, OPN, OSX e Runx2) mais um controle endógeno (GADPH) distribuídos nas doze colunas de cada placa de 96 poços (doze replicatas de oito genes) (CAPH-0398, Superarray, Frederick, MD, USA). Para a segunda etapa do Capítulo 5 uma placa (96 poços) de estoque contendo 84 genes relacionados ao processo de osteogênese foi adquirida (PAHS-0026A, Superarray, Frederick, MD, USA). Além destes 84 genes esta placa também contém seis diferentes genes endógenos que podem ser utilizados para a normalização dos dados, além de controles positivos e negativos da reação de PCR e contaminação da amostra com DNA genômico. Neste experimento cada placa era preenchida com o cDNA diluído de uma única amostra. Este experimento nos permitiu obter um painel da expressão de genes da diferenciação de osteoblastos comparando a superfície de óxido de alumínio à superfície lisa.

No Capítulo 6, uma diferente metodologia de fabricação foi empregada, utilizando um ataque ácido a base de H₂SO₄ e H₂O₂. Este método está amplamente citado na literatura (Wang et al., 2001; Wang et al., 2002; Uchida et al., 2002; Oliveira; Nanci, 2004; Oliveira et al., 2007), e foi escolhido para também poder verificar os efeitos das superfícies nanoestruturadas em relação ao controle. Foi possível também verificar o papel da superimposição das nanoestruturas à micro-textura da superfície. A diferença deste artigo para os demais entretanto, é que previamente ao tratamento ácido foi feito um jateamento da superfície (partículas de óxido de alumínio com 100µm de diâmetro), resultando em uma superfície com características a nível micrométrico e nanométrico. Trabalhos prévios têm demonstrado que a utilização de diferentes substâncias no tratamento químico de superfícies são capazes de criar diferentes padrões nestas superfícies (Oliveira; Nanci, 2004; Cooper et al., 2006; Oliveira et al., 2007; Berglundh et al., 2007; Guo et al., 2007). Por exemplo, a utilização de ácido hidrofúorídrico (HF) ou a mistura de H₂SO₄ / H₂O₂ é capaz de criar nanoestruturas na superfície do titânio (Oliveira; Nanci, 2004; Guo et al., 2007), entretanto a utilização de ácido clorídrico (HCl) ou ácido sulfúrico isoladamente (H₂SO₄) não produzem o mesmo efeito. Neste artigo, os resultados da superimposição de nanoestruturas sobre uma superfície previamente jateada com partículas de óxido de

alumínio aumentou a expressão gênica das hMSCs, favorecendo a diferenciação para a linhagem osteoblástica. Resultado similar ao que foi obtido com a utilização do recobrimento das amostras com os filmes finos de óxidos de titânio, alumínio e zircônio.

Conclusões Gerais

Nestes trabalhos foi possível avaliar inicialmente os efeitos de superfícies nanoestruturadas de implantes osseointegrados com relação a diferenciação de osteoblastos. O desenvolvimento deste trabalho permitiu o aprofundamento do conhecimento atual com relação ao mecanismo que leva ao processo de osseointegração e fornece novos horizontes para o desenvolvimento de futuras pesquisas para compreender ainda melhor este mecanismo.

- As superfícies nanoestruturadas foram caracterizadas física e quimicamente e foi possível observar a presença de características nanométricas presentes na superfície. Estas características foram criadas utilizando diferentes metodologias que também permitem a adição de diferentes elementos químicos à superfície dos implantes.
- As superfícies nanoestruturadas levaram a um aumento da expressão de genes relacionados à cascata de diferenciação de osteoblastos tanto no modelo animal utilizado (*Rattus norvegicus*), quanto em células tronco mesenquimais humanas e murinas.
- As superfícies nanoestruturadas levaram a uma maior contato osso-implante e a um aumento no torque de remoção após a inserção destes implantes em tibia de *Rattus norvegicus*.
- A superfície nanoestruturada de óxido de alumínio levou a um aumento significativo da expressão de genes relacionados à cascata de diferenciação de osteoblastos baseado em um PCR array avaliado, indicando que esta superfície induz uma maior diferenciação de osteoblastos.

Perspectivas futuras

Baseado nos resultados desta pesquisa, é necessário no futuro, avaliar os efeitos destas superfícies nanoestruturadas em estudos a longo prazo, para comprovar seus efeitos benéficos não somente nas etapas iniciais de osseointegração, mas também na sobrevida destes implantes, tanto em casos de colocação e carga imediata como em situações convencionais (instalação de implantes em leito ósseo cicatrizado e aguardar osseointegração para confeccionar a prótese). É também necessário que se busque compreender melhor o mecanismo que está envolvido neste aumento da expressão gênica observado nas superfícies nanoestruturadas para que esta metodologia possa ser aplicada

em outros processos que envolvam a regeneração e reparação do tecido ósseo. E também que se avalie separadamente os efeitos da composição química e das características nanoestruturadas nestas superfícies para poder entender melhor os mecanismo de atuação destas superfícies e expandir o emprego destes materiais na área de biologia e saúde humana. Outro efeito a ser estudado é a interação destas superfícies nanoestruturadas na área de contato entre pilares e os tecidos moles.

Referências Bibliográficas

1. Abron A, Hopfensperger M, Thompson J, Cooper LF. Evaluation of a predictive model for implant surface topography effects on early osseointegration in the rat tibia model. *J Prosthet Dent* 2001;85:40-46.
2. Adell R, Eriksson B, Lekholm U, Branemark PI, Jemt T. Long-term follow-up study of osseointegrated implants in the treatment of totally edentulous jaws. *Int J Oral Maxillofac Implants* 1990;5:347-59.
3. Adell R, Lekholm U, Rockler B, Branemark PI. A 15-year study of osseointegrated implants in the treatment of the edentulous jaw. *Int J Oral Surg* 1981;10:387-416.
4. Advincula MC, Rahemtulla FG, Advincula RC, Ada ET, Lemons JE, Bellis SL. Osteoblast adhesion and matrix mineralization on sol-gel-derived titanium oxide. *Biomaterials* 2006;27:2201-12.
5. Albrektsson T, Dahl E, Enbom L, Engevall S, Engquist B, Eriksson AR, Feldmann G, Freiberg N, Glantz PO, Kjellman O, et al. Osseointegrated oral implants. A Swedish multicenter study of 8139 consecutively inserted Nobelpharma implants. *J Periodontol* 1988;59:287-96.
6. Albrektsson T, Sennerby L. Direct bone anchorage of oral implants: clinical and experimental considerations of the concept of osseointegration. *Int J Prosthodont* 1990;3:30-41.
7. Albrektsson T, Wennerberg A. Oral implant surfaces: Part 1--review focusing on topographic and chemical properties of different surfaces and in vivo responses to them. *Int J Prosthodont* 2004;17:536-43a.
8. Albrektsson T, Wennerberg A. Oral implant surfaces: Part 2--review focusing on clinical knowledge of different surfaces. *Int J Prosthodont* 2004;17:544-64b.
9. Albrektsson T, Zarb G, Worthington P, Eriksson AR. The long-term efficacy of currently used dental implants: a review and proposed criteria of success. *Int J Oral Maxillofac Implants* 1986;1:11-25.
10. Alsberg E, Feinstein E, Joy MP, Prentiss M, Ingber DE. Magnetically-guided self-assembly of fibrin matrices with ordered nano-scale structure for tissue engineering. *Tissue Eng* 2006;12:3247-56.
11. Amano S, Scott IC, Takahara K, Koch M, Champlaud MF, Gerecke DR, Keene DR, Hudson DL, Nishiyama T, Lee S, Greenspan DS, Burgeson RE. Bone morphogenetic protein 1 is an extracellular processing enzyme of the laminin 5 gamma 2 chain. *J Biol Chem* 2000 28;275:22728-35.

12. Andersson AS, Bäckhed F, von Euler A, Richter-Dahlfors A, Sutherland D, Kasemo B. Nanoscale features influence epithelial cell morphology and cytokine production. *Biomaterials* 2003;24:3427-36.
13. Araújo MG, Sukekava F, Wennström JL, Lindhe J. Ridge alterations following implant placement in fresh extraction sockets: an experimental study in the dog. *J Clin Periodontol J Clin Periodontol* 2005;32:645-52.
14. Arias JL, Mayor MB, Pou J, Leng Y, León B, Pérez-Amor M. Micro- and nano-testing of calcium phosphate coatings produced by pulsed laser deposition. *Biomaterials* 2003;24:3403-8.
15. Arima Y, Iwata H. Effect of wettability and surface functional groups on protein adsorption and cell adhesion using well-defined mixed self-assembled monolayers. *Biomaterials* 2007;28:3074-82.
16. Ayad S, Boot-Handford R, Humphries MJ, Kadler KE, Shuttleworth A. *The Extracellular Matrix Factsbook*, Academic Press Inc., San Diego, CA (1994), p. 29.
17. Bain CA. Smoking and implant failure--benefits of a smoking cessation protocol. *Int J Oral Maxillofac Implants* 1996;11:756-9.
18. Balasundaram G, Sato M, Webster TJ. Using hydroxyapatite nanoparticles and decreased crystallinity to promote osteoblast adhesion similar to functionalizing with RGD. *Biomaterials* 2006;27:2798-805.
19. Baraton MI, Chen X, Gonsalves KE. FTIR study of nanostructured alumina nitride powder surface: determination of the acidic/basic sites by CO, CO₂, and acetic acid adsorptions. *Nanostruct Mater* 1997;8:435.
20. Becker J, Kirsch A, Schwarz F, Chatzinikolaidou M, Rothamel D, Lekovic V, Laub M, Jennissen HP. Bone apposition to titanium implants biocoated with recombinant human bone morphogenetic protein-2 (rhBMP-2). A pilot study in dogs. *Clin Oral Investig* 2006;10:217-24.
21. Ben-Nissan B, Choi AH. Sol-gel production of bioactive nanocoatings for medical applications. Part 1: an introduction. *Nanomed* 2006;1:311-9.
22. Berglundh T, Abrahamsson I, Albouy JP, Lindhe J. Bone healing at implants with a fluoride-modified surface: an experimental study in dogs. *Clin Oral Implants Res* 2007;18:147-52.
23. Berglundh T, Abrahamsson I, Lang NP, Lindhe J. De novo alveolar bone formation adjacent to endosseous implants. *Clin Oral Implants Res* 2003;14:251-62.
24. Berry CC, Dalby MJ, Oreffo RO, McCloy D, Affrosman S. The interaction of human bone marrow cells with nanotopographical features in three dimensional constructs. *J Biomed Mater Res A* 2006;79:431-9.

25. Bigi A, Nicoli-Aldini N, Bracci B, Zavan B, Boanini E, Sbaiz F, Panzavolta S, Zorzato G, Giardino R, Facchini A, Abatangelo G, Cortivo R. In vitro culture of mesenchymal cells onto nanocrystalline hydroxyapatite-coated Ti13Nb13Zr alloy. *J Biomed Mater Res A* 2007;82:213-21.
26. Boyan BD, Schwartz Z, Hambleton JC. Response of bone and cartilage cells to biomaterials in vivo and in vitro. *J Oral Implantol* 1993;19:116-22;
27. Branemark PI, Adell R, Breine U, Hansson BO, Lindström J, Ohlsson A. Intra-osseous anchorage of dental prostheses. I. Experimental studies. *Scand J Plast Reconstr Surg* 1969;3:81-100
28. Branemark PI, Zarb GA, Albrektsson T. Introduction in osseointegration. IN:_____, Tissue-integrated prostheses. Osseointegration in clinical dentistry. Chicago, Quintessence Books, 1985. Cap.1.
29. Branemark PI. Osseointegration and its experimental background. *J Prosthet Dent* 1983;50:399-410.
30. Briggs EP, Walpole AR, Wilshaw PR, Karlsson M, Palsgard E. Formation of highly adherent nano-porous alumina on Ti-based substrates: a novel bone implant coating. *J Mater Sci Mater Med* 2004;15:1021-9.
31. Brody S, Anilkumar T, Liliensiek S, Last JA, Murphy CJ, Pandit A. Characterizing nanoscale topography of the aortic heart valve basement membrane for tissue engineering heart valve scaffold design. *Tissue Eng* 2006;12:413-21.
32. Brunette DM. The effects of implant surface topography on the behavior of cells. *Int J Oral Maxillofac Implants* 1988;3:231-4
33. Burger EH, Klein-Nulend J. Mechanotransduction in bone--role of the lacuno-canalicular network. *FASEB J* 1999;13 Suppl:S101-12.
34. Buser D, Brogini N, Wieland M, Schenk RK, Denzer AJ, Cochran DL, Hoffmann B, Lussi A, Steinemann SG. Enhanced bone apposition to a chemically modified SLA titanium surface. *J Dent Res* 2004;83:529-33.
35. Buser D, Schenk RK, Steinemann S, Fiorellini JP, Fox CH, Stich H. Influence of surface characteristics on bone integration of titanium implants. A histomorphometric study in miniature pigs. *J Biomed Mater Res* 1991;25:889-902.
36. Cai K, Bossert J, Jandt KD. Does the nanometre scale topography of titanium influence protein adsorption and cell proliferation? *Colloids Surf B Biointerfaces* 2006;49:136-44.
37. Callan DP, O'Mahony A, Cobb CM. Loss of crestal bone around dental implants: a retrospective study. *Implant Dent* 1998;7:258-66.

38. Canabarro A, Diniz MG, Paciornik S, Carvalho L, Sampaio EM, Beloti MM, Rosa AL, Fischer RG. High concentration of residual aluminum oxide on titanium surface inhibits extracellular matrix mineralization. *J Biomed Mater Res A* 2008;87:588-97.
39. Cavalcanti-Adam EA, Volberg T, Micoulet A, Kessler H, Geiger B, Spatz JP. Cell spreading and focal adhesion dynamics are regulated by spacing of integrin ligands. *Biophys J* 2007;92:2964-74.
40. Chiesa R, Giavaresi G, Fini M, Sandrini E, Giordano C, Bianchi A, Giardino R. In vitro and in vivo performance of a novel surface treatment to enhance osseointegration of endosseous implants. *Oral Surg Oral Med Oral Pathol Oral Radiol Endod* 2007;103:745-56.
41. Choi AH, Ben-Nissan B. Sol-gel production of bioactive nanocoatings for medical applications. Part II: current research and development. *Nanomed* 2007;2:51-61.
42. Christenson EM, Anseth KS, van den Beucken JJ, Chan CK, Ercan B, Jansen JA, Laurencin CT, Li WJ, Murugan R, Nair LS, Ramakrishna S, Tuan RS, Webster TJ, Mikos AG. Nanobiomaterial applications in orthopedics. *J Orthop Res* 2007;25:11-22.
43. Chun AL, Moralez JG, Webster TJ, Fenniri H. Helical rosette nanotubes: a biomimetic coating for orthopedics? *Biomaterials* 2005;26:7304-9.
44. Cochran DL. A comparison of endosseous dental implant surfaces. *J Periodontol* 1999;70:1523-39.
45. Coelho PG, Suzuki M. Evaluation of an ibad thin-film process as an alternative method for surface incorporation of bioceramics on dental implants. A study in dogs. *J Appl Oral Sci* 2005;13:87-92.
46. Colon G, Ward BC, Webster TJ. Increased osteoblast and decreased *Staphylococcus epidermidis* functions on nanophase ZnO and TiO₂. *J Biomed Mater Res A* 2006;78:595-604.
47. Cooper LF, De Kok IJ, Rojas-Vizcaya F, Pungpapong P, Chang SH. The immediate loading of dental implants. *Compend Contin Educ Dent* 2007;28:216-25.
48. Cooper LF, Yliheikkila PK, Felton DA, Whitson SW. Spatiotemporal assessment of fetal bovine osteoblast culture differentiation indicates a role for BSP in promoting differentiation. *J Bone Miner Res* 1998;13:620-632.
49. Cooper LF, Zhou Y, Takebe J, Guo J, Abron A, Holmen A, Ellingsen JE. Fluoride modification effects on osteoblast behavior and bone formation at TiO₂ gritblasted c.p. titanium endosseous implants. *Biomaterials* 2006;27:926-936.
50. Cooper LF. Biologic determinants of bone formation for osseointegration: clues for future clinical improvements. *J Prosthet Dent* 1998;80:439-49.

51. Dalby MJ, Andar A, Nag A, Affrossman S, Tare R, McFarlane S, Oreffo RO. Genomic expression of mesenchymal stem cells to altered nanoscale topographies. *J R Soc Interface*. 2008;5:1055-65.
52. Dalby MJ, Gadegaard N, Tare R, Andar A, Riehle MO, Herzyk P, Wilkinson CD, Oreffo RO. The control of human mesenchymal cell differentiation using nanoscale symmetry and disorder. *Nat Mater* 2007;6:997-1003.
53. Dalby MJ, McCloy D, Robertson M, Wilkinson CD, Oreffo RO. Osteoprogenitor response to defined topographies with nanoscale depths. *Biomaterials* 2006;27:1306-15.
54. Davies JE. Bone bonding at natural and biomaterial surfaces. *Biomaterials* 2007;28:5058-5067.
55. Davies JE. Understanding peri-implant endosseous healing. *J Dent Educ* 2003;67:932-49.
56. Di Cesare PE, Fang C, Leslie MP, Tulli H, Perris R, Carlson CS. Expression of cartilage oligomeric matrix protein (COMP) by embryonic and adult osteoblasts. *J Orthop Res* 2000;18:713-20.
57. Dike LE, Chen CS, Mrksich M, Tien J, Whitesides GM, Ingber DE. Geometric control of switching between growth, apoptosis, and differentiation during angiogenesis using micropatterned substrates. *In Vitro Cell Dev Biol Anim* 1999;35:441-8.
58. Donath K, Breuner G. A method for the study of undecalcified bones and teeth with attached soft tissues. The Säge-Schliff (sawing and grinding) technique. *J Oral Pathol*. 1982;11:318-26.
59. Dong W, Zhang T, Epstein J, Cooney L, Wang H, Li Y, Jiang YB, Cogbill A, Varadan V, Tian ZR. Multifunctional Nanowire Bioscaffolds on Titanium. *Chem. Mater* 2007;19:4454-4459.
60. Donlay T, Gillett WB. Titanium endosseous implant-soft tissue interface: a literature review. *J Periodontol* 1991;2:153-160.
61. Eisenbarth E, Velten D, Breme J. Biomimetic implant coatings. *Biomol Eng* 2007;24:27-32.
62. Elias KL, Price RL, Webster TJ. Enhanced functions of osteoblasts on nanometer diameter carbon fibers. *Biomaterials*. 2002;23:3279-87.
63. Ellingsen JE, Johansson CB, Wennerberg A, Holmen A. Improved retention and bone-to-implant contact with fluoride-modified titanium implants. *Int J Oral Maxillofac Implants* 2004;19:659-66.

64. Ellingsen JE, Lyngstadaas SP. Increasing Biocompatibility by Chemical Modification of Titanium Surfaces. In: Ellingsen JE, Lyngstadaas PS, editors. *Bio-Implant Interface; Improving Biomaterials and Tissue Reactions*. Boca Raton, Florida: CRC Press LLC; 2003. p. 323-40.
65. Ellingsen JE, Thomsen P, Lyngstadaas SP. Advances in dental implant materials and tissue regeneration. *Periodontol 2000* 2006;41:136-56.
66. Ellingsen JE. On the Properties of Surface-modified Titanium. In: Davies JE, editor. *Bone Engineering*. Toronto: em squared inc. Toronto, Canada; 2000. p.183-88.
67. Ergun C, Liu H, Halloran JW, Webster TJ. Increased osteoblast adhesion on nanograined hydroxyapatite and tricalcium phosphate containing calcium titanate. *J Biomed Mater Res A* 2007;80:990-7.
68. Fath, K., Edgell, C., and Burrige, K. The distribution of distinct integrins in focal contacts is determined by the substratum composition. *J Cell Sci* 1989;92:67-75.
69. Fiorellini JP, Chen PK, Nevins M, Nevins ML. A retrospective study of dental implants in diabetic patients. *Int J Periodontics Restorative Dent* 2000;20:366-73.
70. Gahlert M, Gudehus T, Eichhorn S, Steinhauser E, Kniha H, Erhardt W. Biomechanical and histomorphometric comparison between zirconia implants with varying surface textures and a titanium implant in the maxilla of miniature pigs. *Clin Oral Implants Res*. 2007;18:662-8
71. García AJ, Reyes CD. Bio-adhesive surfaces to promote osteoblast differentiation and bone formation. *J Dent Res* 2005;84:407-13.
72. Germanier Y, Tosatti S, Broggin N, Textor M, Buser D. Enhanced bone apposition around biofunctionalized sandblasted and acid-etched titanium implant surfaces. A histomorphometric study in miniature pigs. *Clin Oral Implants Res* 2006;17:251-7.
73. Goené RJ, Testori T, Trisi P. Influence of a nanometer-scale surface enhancement on de novo bone formation on titanium implants: a histomorphometric study in human maxillae. *Int J Periodontics Restorative Dent* 2007;27:211-9.
74. Goodacre CJ, Kan JY, Rungcharassaeng K. Clinical complications of osseointegrated implants. *J Prosthet Dent* 1999;81:537-52.
75. Gottfredsen K, Hjorting-Hansen E, Budtz-Jørgensen E. Clinical and radiographic evaluation of submerged and nonsubmerged implants in monkeys. *Int J Prosthodont* 1990;3:463-9.
76. Guo J, Padilla RJ, Ambrose W, De Kok IJ, Cooper LF. Modification of TiO₂ grit blasted titanium implants by hydrofluoric acid treatment alters adherent osteoblast gene expression in vitro and in vivo. *Biomaterials* 2007;28:5418-25.

77. Gutwein LG, Webster TJ. Increased viable osteoblast density in the presence of nanophase compared to conventional alumina and titania particles. *Biomaterials* 2004;25:4175-83.
78. Hansen JC, Lim JY, Xu LC, Siedlecki CA, Mauger DT, Donahue HJ. Effect of surface nanoscale topography on elastic modulus of individual osteoblastic cells as determined by atomic force microscopy. *J Biomech* 2007;40:2865-71.
79. Hansson S, Norton M. The relation between surface roughness and interfacial shear strength for bone-anchored implants. A mathematical model. *J Biomech* 1999;32:829-36.
80. Hansson S. The dental implant meets bone – a clash of two paradigms. *Applied Osseointegration Research* 2006;1:15–17
81. Harada H, Tagashira S, Fujiwara M, Ogawa S, Katsumata T, Yamaguchi A, Komori T, Nakatsuka M. Cbfa1 isoforms exert functional differences in osteoblast differentiation. *J Biol Chem* 1999 12;274:6972-6978.
82. Harada S, Rodan GA. Control of osteoblast function and regulation of bone mass. *Nature* 2003;423:349-55.
83. Hart A, Gadegaard N, Wilkinson CDW, Oreffo ROC, Dalby MJ. Filapodial Sensing of Nanotopography in Osteoprogenitor Cells. *European Cells and Materials* Vol. 10. Suppl. 2, 2005 p. 65.
84. Hart A, Gadegaard N, Wilkinson CDW, Oreffo ROC, Dalby MJ. Osteoprogenitor response to low-adhesion nanotopographies originally fabricated by electron beam lithography. *J Mater Sci: Mater Med* 2007;18:1211–1218.
85. Ho AM, Marker PC, Peng H, Quintero AJ, Kingsley DM, Huard J. Dominant negative Bmp5 mutation reveals key role of BMPs in skeletal response to mechanical stimulation. *BMC Dev Biol.* 2008;8:35.
86. Isa ZM, Schneider GB, Zaharias R, Seabold D, Stanford CM. Effects of fluoridemodified titanium surfaces on osteoblast proliferation and gene expression. *Int J Oral Maxillofac Implants* 2006;21:203-211.
87. Jaffin RA, Berman CL. The excessive loss of Branemark fixtures in type IV bone: a 5-year analysis. *J Periodontol* 1991;62:2-4.
88. Jaiswal N, Haynesworth SE, Caplan AI, Bruder SP. Osteogenic differentiation of purified, culture-expanded human mesenchymal stem cells in vitro. *J Cell Biochem.* 1997;64:295-312.
89. Johansson CB, Albrektsson T. A removal torque and histomorphometric study of commercially pure niobium and titanium implants in rabbit bone. *Clin Oral Implants Res* 1991;2:24-9.

90. Jung YC, Han CH, Lee IS, Kim HE. Effects of ion beam-assisted deposition of hydroxyapatite on the osseointegration of endosseous implants in rabbit tibiae. *Int J Oral Maxillofac Implants* 2001;16:809-18.
91. Kallus T, Bessing C. Loose gold screws frequently occur in full-arch fixed prostheses supported by osseointegrated implants after 5 years. *Int J Oral Maxillofac Implants* 1994;9:169-78.
92. Kapur KK. Veterans administration cooperative dental implant study- comparisons between fixed partial dentures supported by blade-vent implants and removable partial dentures. Part II: comparisons of success rates and periodontal health between two treatment modalities. *J Prosthet Dent* 1989;62:685-703.
93. Kapur KK. Veterans administration cooperative dental implant study-comparisons between fixed partial dentures supported by blade-vent implants and removable partial dentures. Part IV: comparisons of patient satisfaction between two treatment modalities. *J Prosthet Dent* 1991;66:517-530.
94. Kasemo B. Biocompatibility of titanium implants: surface science aspects. *J Prosthet Dent* 1983;49:832-7.
95. Kay S, Thapa A, Haberstroh KM, Webster TJ. Nanostructured polymer/nanophase ceramic composites enhance osteoblast and chondrocyte adhesion. *Tissue Eng* 2002;8:753-61.
96. Kim HM, Kokubo T, Fujibayashi S, Nishiguchi S, Nakamura T. Bioactive macroporous titanium surface layer on titanium substrate. *J Biomed Mater Res* 2000 5;52:553-7.
97. Kim HW, Koh YH, Li LH, Lee S, Kim HE. Hydroxyapatite coating on titanium substrate with titania buffer layer processed by sol-gel method. *Biomaterials* 2004;25:2533-8.
98. Klabunde KJ, Strak J, Koper O, Mohs C, Park D, Decker S, Jiang Y, Lagadic I, and Zhang D. Nanocrystals as stoichiometric reagents with unique surface chemistry. *J Phys Chem* 1996;100:12141,.
99. Kotobuki N, Matsushima A, Kato Y, Kubo Y, Hirose M, Ohgushi H. Small interfering RNA of alkaline phosphatase inhibits matrix mineralization. *Cell Tissue Res* 2008;332:279-88.
100. Kubota S, Johkura K, Asanuma K, Okouchi Y, Ogiwara N, Sasaki K, Kasuga T. Titanium oxide nanotubes for bone regeneration. *J Mater Sci Mater Med* 2004;15:1031-5.
101. Le Guéhennec L, Soueidan A, Layrolle P, Amouriq Y. Surface treatments of titanium dental implants for rapid osseointegration. *Dent Mater* 2007;23:844-54.
102. Lee SH, Kim HW, Lee EJ, Li LH, Kim HE. Hydroxyapatite-TiO₂ hybrid coating on Ti implants. *J Biomater Appl* 2006;20:195-208.

103. Leven RM, Viridi AS, Sumner DR. Patterns of gene expression in rat bone marrow stromal cells cultured on titanium alloy discs of different roughness. *J Biomed Mater Res A* 2004;70:391-401.
104. Lickorish D, Guan L, Davies JE. A three-phase, fully resorbable, polyester/calcium phosphate scaffold for bone tissue engineering: Evolution of scaffold design. *Biomaterials* 2007;28:1495-502.
105. Lim JY, Dreiss AD, Zhou Z, Hansen JC, Siedlecki CA, Hengstebeck RW, Cheng J, Winograd N, Donahue HJ. The regulation of integrin-mediated osteoblast focal adhesion and focal adhesion kinase expression by nanoscale topography. *Biomaterials* 2007;28:1787-97
106. Lim JY, Hansen JC, Siedlecki CA, Runt J, Donahue HJ. Human foetal osteoblastic cell response to polymer-demixed nanotopographic interfaces. *J R Soc Interface* 2005;2:97-108.
107. Linder L, Albrektsson T, Brånemark PI, Hansson HA, Ivarsson B, Jönsson U, Lundström I. Electron microscopic analysis of the bone-titanium interface. *Acta Orthop Scand* 1983;54:45-52.
108. Liu DM, Troczynski T, Tseng WJ. Water-based sol-gel synthesis of hydroxyapatite: process development. *Biomaterials* 2001;22:1721-30.
109. Liu H, Slamovich EB, Webster TJ. Increased osteoblast functions among nanophase titania/poly(lactide-co-glycolide) composites of the highest nanometer surface roughness. *J Biomed Mater Res A* 2006;78:798-807.
110. Macdonald KK, Cheung CY, Anseth KS. Cellular delivery of TGFbeta1 promotes osteoinductive signalling for bone regeneration. *J Tissue Eng Regen Med* 2007;1:314-7.
111. Mante FK, Little K, Mante MO, Rawle C, Baran GR. Oxidation of titanium, RGD peptide attachment, and matrix mineralization rat bone marrow stromal cells. *J Oral Implantol* 2004;30:343-9.
112. Masuda T, Salvi GE, Offenbacher S, Felton DA, Cooper LF. Cell and matrix reactions at titanium implants in surgically prepared rat tibiae. *Int J Oral Maxillofac Implants* 1997;12:472-485.
113. Mayer H, Bertram H, Lindenmaier W, Korff T, Weber H, Weich H. Vascular endothelial growth factor (VEGF-A) expression in human mesenchymal stem cells: autocrine and paracrine role on osteoblastic and endothelial differentiation. *J Cell Biochem* 2005;95:827-39.
114. McManus AJ, Doremus RH, Siegel RW, Bizios R. Evaluation of cytocompatibility and bending modulus of nanoceramic/polymer composites. *J Biomed Mater Res A* 2005;72:98-106.
115. Meirelles L, Arvidsson A, Albrektsson T, Wennerberg A. Increased bone formation to unstable nano rough titanium implants. *Clin Oral Implants Res* 2007;18:326-32.

116. Meirelles L, Arvidsson A, Andersson M, Kjellin P, Albrektsson T, Wennerberg A. Nano hydroxyapatite structures influence early bone formation. *J Biomed Mater Res A* 2008;87:299-307b.
117. Meirelles L, Currie F, Jacobsson M, Albrektsson T, Wennerberg A. The effect of chemical and nanotopographical modifications on the early stages of osseointegration. *Int J Oral Maxillofac Implants* 2008;23:641-7a.
118. Meirelles L. On nano size structures for enhanced early bone formation [PhD]. Gothenburg: Gothenburg University; 2007.
119. Mendes VC, Moineddin R, Davies JE. The effect of discrete calcium phosphate nanocrystals on bone-bonding to titanium surfaces. *Biomaterials* 2007;28:4748-55.
120. Mendonça G, Mendonça DB, Aragão FJ, Cooper LF. Advancing dental implant surface technology--from micron- to nanotopography. *Biomaterials* 2008;29:3822-35.
121. Mendonça G, Neves FD, Fernandes Neto AJ, Lira T. Avaliação longitudinal de próteses sobre implantes enfatizando dificuldades e insucessos – Controle de um ano. *BCI* 2001;8:228-235.
122. Meyer U, Joos U, Mythili J, Stamm T, Hohoff A, Fillies T, Stratmann U, Wiesmann HP. Ultrastructural characterization of the implant/bone interface of immediately loaded dental implants. *Biomaterials* 2004;25:1959-67.
123. Monsees TK, Barth K, Tippelt S, Heidel K, Gorbunov A, Pompe W, Funk RH. Effects of different titanium alloys and nanosize surface patterning on adhesion, differentiation, and orientation of osteoblast-like cells. *Cells Tissues Organs* 2005;180:81-95.
124. Morton D, Jaffin R, Weber HP. Immediate restoration and loading of dental implants: clinical considerations and protocols. *Int J Oral Maxillofac Implants* 2004;19 Suppl:103-8.
125. Murphy SB, Ecker TM, Tannast M. Two- to 9-year clinical results of alumina ceramic-on-ceramic THA. *Clin Orthop Relat Res* 2006;453:97-102.
126. Nanci A, Wuest JD, Peru L, Brunet P, Sharma V, Zalzal S, McKee MD. Chemical modification of titanium surfaces for covalent attachment of biological molecules. *J Biomed Mater Res* 1998;40:324-35.
127. Narai S, Nagahata S. Effects of alendronate on the removal torque of implants in rats with induced osteoporosis. *Int J Oral Maxillofac Implants* 2003;18:218-23.
128. Neves FD, Fones D, Bernardes SR, Prado CJ, Neto AJ. Short implants--an analysis of longitudinal studies. *Int J Oral Maxillofac Implants* 2006;21:86-93.

129. Nishimura I, Huang Y, Butz F, Ogawa T, Lin L, JakeWang C. Discrete deposition of hidroxyapatite nanoparticles on a titanium implant with predisposing substrate microtopography accelerated osseointegration. *Nanotechnology* 18 (2007) 245101 (9pp).
130. Ogawa T, Nishimura I. Different bone integration profiles of turned and acid-etched implants associated with modulated expression of extracellular matrix genes. *Int J Oral Maxillofac Implants* 2003;18:200-10.
131. Ogawa T, Nishimura I. Genes differentially expressed in titanium implant healing. *J Dent Res* 2006;85:566-70.
132. Oh SH, Finones RR, Daraio C, Chen LH, Jin S. Growth of nano-scale hydroxyapatite using chemically treated titanium oxide nanotubes. *Biomaterials* 2005;26:4938-43.
133. Oliva J, Oliva X, Oliva JD. One-year follow-up of first consecutive 100 zirconia dental implants in humans: a comparison of 2 different rough surfaces. *Int J Oral Maxillofac Implants* 2007;22:430-5.
134. Olivares-Navarrete R, Raz P, Zhao G, Chen J, Wieland M, Cochran DL, Chaudhri RA, Ornoy A, Boyan BD, Schwartz Z. Integrin alpha2beta1 plays a critical role in osteoblast response to micron-scale surface structure and surface energy of titanium substrates. *Proc Natl Acad Sci USA*. 2008;105:15767-72.
135. Oliveira PT, Nanci A. Nanotexturing of titanium-based surfaces upregulates expression of bone sialoprotein and osteopontin by cultured osteogenic cells. *Biomaterials* 2004;25:403-13.
136. Oliveira PT, Zalzal SF, Beloti MM, Rosa AL, Nanci A. Enhancement of in vitro osteogenesis on titanium by chemically produced nanotopography. *J Biomed Mater Res A* 2007;80:554-64.
137. Orsini G, Piattelli M, Scarano A, Petrone G, Kenealy J, Piattelli A, Caputi S. Randomized, controlled histologic and histomorphometric evaluation of implants with nanometer-scale calcium phosphate added to the dual acid-etched surface in the human posterior maxilla. *J Periodontol* 2007;78:209-18.
138. Otomo H, Sakai A, Uchida S, Tanaka S, Watanuki M, Moriwaki S, Niida S, Nakamura T. Flt-1 tyrosine kinase-deficient homozygous mice result in decreased trabecular bone volume with reduced osteogenic potential. *Bone* 2007;40:1494-501.
139. Oxby G, Lindqvist J, Nilsson P. Early Loading of Astra Tech OsseoSpeed Implants Placed in Thin Alveolar Ridges and Fresh Extraction Sockets. *Applied Osseointegration Research* 2006;5:68-72.
140. Palin E, Liu H, Webster TJ. Mimicking the nanofeatures of bone increases bone-forming cell adhesion and proliferation. *Nanotechnology* 2005;16:1828–1835.

141. Palmieri A, Pezzetti F, Brunelli G, Zollino I, Lo Muzio L, Martinelli M, Scapoli L, Arlotti M, Masiero E, Carinci F. Zirconium oxide regulates RNA interfering of osteoblast-like cells. *J Mater Sci Mater Med* 2008;19:2471-6.
142. Park GE, Webster TJ. A Review of Nanotechnology for the Development of Better Orthopedic Implants. *J Biomed Nanotechnol* 2005;1:18-29.
143. Park JY, Gemmell CH, Davies JE. Platelet interactions with titanium: modulation of platelet activity by surface topography. *Biomaterials* 2001;22:2671-82.
144. Park YS, Yi KY, Lee IS, Han CH, Jung YC. The effects of ion beam-assisted deposition of hydroxyapatite on the grit-blasted surface of endosseous implants in rabbit tibiae. *Int J Oral Maxillofac Implants* 2005;20:31-8.
145. Pechini M. U.S. Patent; 3,300,697; 1967.
146. Piattelli A, Degidi M, Paolantonio M, Mangano C, Scarano A. Residual aluminum oxide on the surface of titanium implants has no effect on osseointegration. *Biomaterials* 2003;24:4081-9.
147. Piveteau LD, Gasser B, Schlapbach L. Evaluating mechanical adhesion of sol-gel titanium dioxide coatings containing calcium phosphate for metal implant application. *Biomaterials* 2000;21:2193-201.
148. Popat KC, Chatvanichkul KI, Barnes GL, Latempa TJ Jr, Grimes CA, Desai TA. Osteogenic differentiation of marrow stromal cells cultured on nanoporous alumina surfaces. *J Biomed Mater Res A* 2007;80:955-64a.
149. Popat KC, Leoni L, Grimes CA, Desai TA. Influence of engineered titania nanotubular surfaces on bone cells. *Biomaterials* 2007;28:3188-97b.
150. Price RL, Ellison K, Haberstroh KM, Webster TJ. Nanometer surface roughness increases select osteoblast adhesion on carbon nanofiber compacts. *J Biomed Mater Res A* 2004;70:129-38.
151. Price RL, Gutwein LG, Kaledin L, Tepper F, Webster TJ. Osteoblast function on nanophase alumina materials: Influence of chemistry, phase, and topography. *J Biomed Mater Res A* 2003;67:1284-93a.
152. Price RL, Waid MC, Haberstroh KM, Webster TJ. Selective bone cell adhesion on formulations containing carbon nanofibers. *Biomaterials* 2003;24:1877-87b.
153. Price RL, Haberstroh KM, Webster TJ. Enhanced functions of osteoblasts on nanostructured surfaces of carbon and alumina. *Med Biol Eng Comput* 2003;41:372-5.
154. Puleo DA, Nanci A. Understanding and controlling the bone-implant interface. *Biomaterials* 1999;20:2311-2321.

155. Ricci JL, Charvet J, Frenkel SR, Chang R, Nadkarni P, Turner J, Alexander H. Bone Response to Laser Microtextured Surfaces in: Bone Engineering, ed; JE Davies, 2000, Em2 Inc., Toronto Chapter 25 pp8-9.
156. Ricci JL, Grew JC, Alexander H. Connective-tissue responses to defined biomaterial surfaces. I. Growth of rat fibroblast and bone marrow cell colonies on microgrooved substrates. *J Biomed Mater Res A* 2008;85:313-25.
157. Rodrigues SN, Goncalves IC, Martins MC, Barbosa MA, Ratner BD. Fibrinogen adsorption, platelet adhesion and activation on mixed hydroxyl-/methyl-terminated self-assembled monolayers. *Biomaterials* 2006;27:5357-67.
158. Schliephake H, Aref A, Scharnweber D, Bierbaum S, Roessler S, Sewing A. Effect of immobilized bone morphogenic protein 2 coating of titanium implants on peri-implant bone formation. *Clin Oral Implants Res* 2005;16:563-9.
159. Schneider GB, Perinpanayagam H, Clegg M, Zaharias R, Seabold D, Keller J, Stanford C. Implant surface roughness affects osteoblast gene expression. *J Dent Res* 2003;82:372-6.
160. Schwartz Z, Lohmann CH, Oefinger J, Bonewald LF, Dean DD, Boyan BD. Implant surface characteristics modulate differentiation behavior of cells in the osteoblastic lineage. *Adv Dent Res* 1999;13:38-48.
161. Schwartz Z, Nasazky E, Boyan BD. Surface microtopography regulates osteointegration: the role of implant surface microtopography in osteointegration. *Alpha Omegan* 2005;98:9-19.
162. Schwartz Z, Swain LD, Marshall T, Sela J, Gross U, Amir D, Muller-Mai C, Boyan BD. Modulation of matrix vesicle enzyme activity and phosphatidylserine content by ceramic implant materials during endosteal bone healing. *Calcif Tissue Int* 1992;51:429-37.
163. Scotchford CA, Gilmore CP, Cooper E, Leggett GJ, Downes S. Protein adsorption and human osteoblast-like cell attachment and growth on alkylthiol on gold self-assembled monolayers. *J Biomed Mater Res* 2002;59:84-99.
164. Shalabi MM, Gortemaker A, Van't Hof MA, Jansen JA, Creugers NH. Implant surface roughness and bone healing: a systematic review *J Dent Res*. 2006;85:496-500
165. Shishido T, Clarke IC, Williams P, Boehler M, Asano T, Shoji H, Masaoka T, Yamamoto K, Imakiire A. Clinical and simulator wear study of alumina ceramic THR to 17 years and beyond. *J Biomed Mater Res B Appl Biomater* 2003 15;67:638-47.
166. Sinha RK, Tuan RS. Regulation of human osteoblast integrin expression by orthopedic implant materials. *Bone* 1996;18:451-7.
167. Smith DE, Zarb GA. Criteria for success of osseointegrated endosseous implants. *J Prosthet Dent* 1989;62:567-572.

168. Stanford CM, Johnson GK, Fakhry A, Gratton D, Mellonig JT, Wanger W. Outcomes of a fluoride modified implant one year after loading in the posterior-maxilla when placed with the osteotome surgical technique. *Applied Osseointegration Research* 2006;5:50-55.
169. Suska F, Gretzer C, Esposito M, Emanuelsson L, Wennerberg A, Tengvall P, Thomsen P. In vivo cytokine secretion and NF-kappaB activation around titanium and copper implants. *Biomaterials* 2005;26:519-27.
170. Tan J, Saltzman WM. Biomaterials with hierarchically defined micro- and nanoscale structure. *Biomaterials* 2004;25:3593-601.
171. Tasker LH, Sparey-Taylor GJ, Nokes LD. Applications of nanotechnology in orthopaedics. *Clin Orthop Relat Res* 2007;456:243-9.
172. Tavares MG, de Oliveira PT, Nanci A, Hawthorne AC, Rosa AL, Xavier SP. Treatment of a commercial, machined surface titanium implant with H₂SO₄/H₂O₂ enhances contact osteogenesis. *Clin Oral Implants Res* 2007;18:452-8.
173. Teixeira AI, Abrams GA, Bertics PJ, Murphy CJ, Nealey PF. Epithelial contact guidance on well-defined micro- and nanostructured substrates. *J Cell Sci* 2003 15;116:1881-92.
174. Teixeira AI, McKie GA, Foley JD, Bertics PJ, Nealey PF, Murphy CJ. The effect of environmental factors on the response of human corneal epithelial cells to nanoscale substrate topography. *Biomaterials* 2006;27:3945-54.
175. Tolstunov L. Dental implant success-failure analysis: a concept of implant vulnerability. *Implant Dent* 2006;15:341-6.
176. Tosatti S, Schwartz Z, Campbell C, Cochran DL, VandeVondele S, Hubbell JA, Denzer A, Simpson J, Wieland M, Lohmann CH, Textor M, Boyan BD. RGD-containing peptide GCRGYGRGDSPG reduces enhancement of osteoblast differentiation by poly(L-lysine)-graft-poly(ethylene glycol)-coated titanium surfaces. *J Biomed Mater Res A* 2004;68:458-72.
177. Trisi P, Lazzara R, Rebaudi A, Rao W, Testori T, Porter SS. Bone-implant contact on machined and dual acid-etched surfaces after 2 months of healing in the human maxilla. *J Periodontol* 2003;74:945-56.
178. Uchida M, Kim HM, Miyaji F, Kokubo T, Nakamura T. Apatite formation on zirconium metal treated with aqueous NaOH. *Biomaterials* 2002;23:313-7.
179. Wan Y, Wang Y, Liu Z, Qu X, Han B, Bei J, Wang S. Adhesion and proliferation of OCT-1 osteoblast-like cells on micro- and nano-scale topography structured poly(L-lactide). *Biomaterials* 2005;26:4453-9.
180. Wang L, Zhao G, Olivares-Navarrete R, Bell BF, Wieland M, Cochran DL, Schwartz Z, Boyan BD. Integrin beta1 silencing in osteoblasts alters substrate-dependent responses to 1,25-dihydroxy vitamin D₃. *Biomaterials* 2006;27:3716-25.

181. Wang XX, Hayakawa S, Tsuru K, Osaka A. A comparative study of in vitro apatite deposition on heat-, H₂O₂-, and NaOH-treated titanium surfaces. *J Biomed Mater Res* 2001;54:172-8.
182. Wang XX, Hayakawa S, Tsuru K, Osaka A. Bioactive titania-gel layers formed by chemical treatment of Ti substrate with a H₂O₂/HCl solution. *Biomaterials* 2002;23:1353-7.
183. Ward BC, Webster TJ. The effect of nanotopography on calcium and phosphorus deposition on metallic materials in vitro. *Biomaterials* 2006;27:3064-3074.
184. Washburn NR, Yamada KM, Simon CG Jr, Kennedy SB, Amis EJ. High-throughput investigation of osteoblast response to polymer crystallinity: influence of nanometer-scale roughness on proliferation. *Biomaterials* 2004;25:1215-24.
185. Webster TJ, Ejiogor JU. Increased osteoblast adhesion on nanophase metals: Ti, Ti6Al4V, and CoCrMo. *Biomaterials* 2004;25:4731-9.
186. Webster TJ, Ergun C, Doremus RH, Lanford WA. Increased osteoblast adhesion on titanium-coated hydroxylapatite that forms CaTiO₃. *J Biomed Mater Res A* 2003;67:975-80.
187. Webster TJ, Ergun C, Doremus RH, Siegel RW, Bizios R. Enhanced functions of osteoblasts on nanophase ceramics. *Biomaterials* 2000;21:1803-10a.
188. Webster TJ, Ergun C, Doremus RH, Siegel RW, Bizios R. Specific proteins mediate enhanced osteoblast adhesion on nanophase ceramics. *J Biomed Mater Res* 2000;51:475-83b.
189. Webster TJ, Schadler LS, Siegel RW, Bizios R. Mechanisms of enhanced osteoblast adhesion on nanophase alumina involve vitronectin. *Tissue Eng* 2001;7:291-301a.
190. Webster TJ, Ergun C, Doremus RH, Siegel RW, Bizios R. Enhanced functions of osteoclast-like cells on nanophase ceramics. *Biomaterials* 2001;22:1327-1333b.
191. Webster TJ, Hellenmeyer EL, Price RL. Increased osteoblast functions on theta + delta nanofiber alumina. *Biomaterials* 2005;26:953-60.
192. Webster TJ, Siegel RW, Bizios R. Osteoblast adhesion on nanophase ceramics. *Biomaterials* 1999;20:1221-7.
193. Webster TJ, Smith TA. Increased osteoblast function on PLGA composites containing nanophase titania. *J Biomed Mater Res A* 2005;74:677-86.
194. Wennerberg A, Albrektsson T. Suggested Guidelines for the Topographic Evaluation of Implant Surfaces. *Int J Oral Maxillofac Implants* 2000;15:331-344.

195. Wennerberg A, Ektessabi A, Albrektsson T, Johansson C, Andersson B. A 1-year follow-up of implants of differing surface roughness placed in rabbit bone. *Int J Oral Maxillofac Implants* 1997;12:486-94.
196. Wenz HJ, Bartsch J, Wolfart S, Kern M. Osseointegration and clinical success of zirconia dental implants: a systematic review. *Int J Prosthodont*. 2008 Jan-Feb;21(1):27-36.
197. Wong M, Eulenberger J, Schenk R, Hunziker E. Effect of surface topology on the osseointegration of implant materials in trabecular bone. *J Biomed Mater Res* 1995;29:1567-75.
198. Wu SJ, DeJong LC, Rahaman MN. Sintering of nanophase γ -Al₂O₃ powder. *J Am Ceram Soc* 1996;79:2207.
199. Zarb GA, Schmitt A. The longitudinal clinical effectiveness of osseointegrated dental implants: the Toronto study. Part III: Problems and complications encountered. *J Prosthet Dent* 1990;64:185-94.
200. Zhao G, Schwartz Z, Wieland M, Rupp F, Geis-Gerstorfer J, Cochran DI, Boyan BD. High surface energy enhances cell response to titanium substrate microstructure. *J Biomed Mater Res A* 2005;74:49-58.
201. Zhao G, Zinger O, Schwartz Z, Wieland M, Landolt D, Boyan BD. Osteoblast-like cells are sensitive to submicron-scale surface structure. *Clin Oral Implants Res* 2006;17:258-64.
202. Zhou J, Chang C, Zhang R, Zhang L. Hydrogels prepared from unsubstituted cellulose in NaOH/urea aqueous solution. *Macromol Biosci* 2007;7:804-9.
203. Zhu B, Lu Q, Yin J, Hu J, Wang Z. Alignment of osteoblast-like cells and cell-produced collagen matrix induced by nanogrooves. *Tissue Eng* 2005;11:825-34.
204. Zreiqat H, Valenzuela SM, Nissan BB, Roest R, Knabe C, Radlanski RJ, Renz H, Evans PJ. The effect of surface chemistry modification of titanium alloy on signalling pathways in human osteoblasts. *Biomaterials* 2005;26:7579-86.

Livros Grátis

(<http://www.livrosgratis.com.br>)

Milhares de Livros para Download:

[Baixar livros de Administração](#)

[Baixar livros de Agronomia](#)

[Baixar livros de Arquitetura](#)

[Baixar livros de Artes](#)

[Baixar livros de Astronomia](#)

[Baixar livros de Biologia Geral](#)

[Baixar livros de Ciência da Computação](#)

[Baixar livros de Ciência da Informação](#)

[Baixar livros de Ciência Política](#)

[Baixar livros de Ciências da Saúde](#)

[Baixar livros de Comunicação](#)

[Baixar livros do Conselho Nacional de Educação - CNE](#)

[Baixar livros de Defesa civil](#)

[Baixar livros de Direito](#)

[Baixar livros de Direitos humanos](#)

[Baixar livros de Economia](#)

[Baixar livros de Economia Doméstica](#)

[Baixar livros de Educação](#)

[Baixar livros de Educação - Trânsito](#)

[Baixar livros de Educação Física](#)

[Baixar livros de Engenharia Aeroespacial](#)

[Baixar livros de Farmácia](#)

[Baixar livros de Filosofia](#)

[Baixar livros de Física](#)

[Baixar livros de Geociências](#)

[Baixar livros de Geografia](#)

[Baixar livros de História](#)

[Baixar livros de Línguas](#)

[Baixar livros de Literatura](#)
[Baixar livros de Literatura de Cordel](#)
[Baixar livros de Literatura Infantil](#)
[Baixar livros de Matemática](#)
[Baixar livros de Medicina](#)
[Baixar livros de Medicina Veterinária](#)
[Baixar livros de Meio Ambiente](#)
[Baixar livros de Meteorologia](#)
[Baixar Monografias e TCC](#)
[Baixar livros Multidisciplinar](#)
[Baixar livros de Música](#)
[Baixar livros de Psicologia](#)
[Baixar livros de Química](#)
[Baixar livros de Saúde Coletiva](#)
[Baixar livros de Serviço Social](#)
[Baixar livros de Sociologia](#)
[Baixar livros de Teologia](#)
[Baixar livros de Trabalho](#)
[Baixar livros de Turismo](#)